AFRL-AFOSR-JP-TR-2022-0022

Introducing the superconducting Saddle-Point qubit

Stace, Tom
QUEENSLAND UNIVERSITY OF TECHNOLOGY
2 GEORGE ST
BRISBANE, , 4000
AUS

05/06/2022
Final Technical Report

Air Force Research Laboratory
Air Force Office of Scientific Research
Asian Office of Aerospace Research and Development
Unit 45002, APO AP 96338-5002

REPORT DOCUMENTATION PAGE

PLEASE DO NOT RETURN YOUR FORM TO THE ABOVE ORGANIZATION.

1. REPORT DATE	**2. REPORT TYPE**	**3. DATES COVERED**	
20220506	Final	**START DATE** 20200228	**END DATE** 20220227

4. TITLE AND SUBTITLE
Introducing the superconducting Saddle-Point qubit

5a. CONTRACT NUMBER	**5b. GRANT NUMBER**	**5c. PROGRAM ELEMENT NUMBER**
	FA2386-20-1-4006	61102F
5d. PROJECT NUMBER	**5e. TASK NUMBER**	**5f. WORK UNIT NUMBER**

6. AUTHOR(S)
Tom Stace

7. PERFORMING ORGANIZATION NAME(S) AND ADDRESS(ES)
QUEENSLAND UNIVERSITY OF TECHNOLOGY
2 GEORGE ST
BRISBANE 4000
AUS

8. PERFORMING ORGANIZATION REPORT NUMBER

9. SPONSORING/MONITORING AGENCY NAME(S) AND ADDRESS(ES)	**10. SPONSOR/MONITOR'S ACRONYM(S)**	**11. SPONSOR/MONITOR'S REPORT NUMBER(S)**
AOARD UNIT 45002 APO AP 96338-5002	AFRL/AFOSR IOA	AFRL-AFOSR-JP-TR-2022-0022

12. DISTRIBUTION/AVAILABILITY STATEMENT
A Distribution Unlimited: PB Public Release

13. SUPPLEMENTARY NOTES

14. ABSTRACT
Two final report documents - one a summary slide for use in internal reports and presentations, and the other with a brief summary of the work completed and two journal papers that resulted from this work. The high quality of this works represents a successful grant which will encourage a follow-on effort,

15. SUBJECT TERMS

16. SECURITY CLASSIFICATION OF:			**17. LIMITATION OF ABSTRACT**	**18. NUMBER OF PAGES**
a. REPORT	**b. ABSTRACT**	**c. THIS PAGE**		
U	U	U	SAR	1

19a. NAME OF RESPONSIBLE PERSON	**19b. PHONE NUMBER** *(Include area code)*
GEOFFREY ANDERSEN	

Final Report for SOARD Grant FA2386-20-1-4006

"Introducing the superconducting Saddle-Point qubit"

Date: 28 March 2022

Name of Principal Investigators (PI and Co-PIs):

- e-mail address : stace@physics.uq.edu.au
- Institution : University of Queensland
- Mailing Address : St Lucia, Brisbane, QLD, 4072
- Phone : +61 7 3365 1868

Period of Performance: 2019 – February 27, 2022 (End date of "No Cost Extension")

Abstract: Quantum devices are extremely sensitive to noise, which presents the major challenge in developing robust quantum technologies.

In contrast, digital technologies rest on the existence of stable states of matter that retain classical information over long times. Fundamentally, this is because stable classical states of matter physically embody an error correcting code. Magnetic memory exemplifies this principle by energetically implementing a repetition code amongst many coupled electronic spins.

Is there an analogously stable quantum phase of matter that retains quantum information robustly?

This is a long-standing open problem in quantum physics. This project will pursue a new direction in this search by introducing and analysing a new kind of solid-state quantum bit (qubit), which physically embodies a quantum error correcting code known as the Gottesman-Kitaev-Preskill code. This new system, which we call the "saddle-point" qubit, is based on the conjunction of two superconducting circuit elements: the Josephson junction and the Quantum Phase Slip device.

Introduction: This project aimed to develop the theory around the highly nonlinear "saddle point" qubit. The proposed device has been named a "dualmon" in the literature, and this nomenclature has been adopted by other practitioners in the field. The aims of this project were to
1. Develop realistic saddle-point qubit models to assess performance against classical noise.

2. Extend the model to include open quantum systems dynamics, to assess performance against quantum noise.

3. Analyse state preparation protocols to measure and produce arbitrary single qubit states.

4. Develop feedback protocols to implement active error correction.

5. Develop protocols for coupling two saddle-point qubits.

Br: The theoretical research program has largely completed aims 1-3, reported in publications [1] and [2]. Aims 4 and 5 are still

Publications from this research program:

This grant has supported salary for a postdoctoral research fellow, Dr Deniz Steigmann, undertaking detailed "microscopic" modelling of aim 5. This work has been based on understanding . This work was heavily impacted by COVID over the reporting period (resulting in a no cost extension), and so work has slowed substantially.

Since the start of this project, two papers have been completed or are near completion:
1. Dat Thanh Le, Arne Grimsmo, Clemens Müller, and T. M. Stace, "Doubly nonlinear superconducting qubit", Phys. Rev. A **100**, 062321 (December 2019)

2. Dat Thanh Le, Jared H. Cole, and T. M. Stace, "Building a bigger Hilbert space for superconducting devices, one Bloch state at a time" Phys. Rev. Research **2**, 013245 (March 2020)

Ongoing work: The early results above paved the way for the research program, and this work is

ongoing.

Stace and Steigmann have been developing a comprehensive theory of gates focused on achieving aim 5 of the proposed research program. This has focused on building a theoretical model of a Majorana junction, that coupled arrays of semiconductor quantum dots hybridized with a superconducting substrate with a "weak link" tunnel barrier in the quantum dot array. This system has been described in the literature as a 4-pi periodic device, which was discussed phenomenologically in [2] as a device suitable for creating quantum gates acting the saddle-point qubit.

This work has taken longer than expected, largely due to unanticipated complexity in developing these models. This has emerged from a realization that a full understanding of the processes required to implement gates on superconducting devices will depend on a more detailed microscopic model of hybrid superconducting – semiconducting systems, which has been the focus of Steigmann's approach. I have attached a PDF document of Steigmann's research covering 2021 to date. This will form the basis of an extended research publication, but is not yet fully complete.

List of Publications and any Significant Collaborations that resulted from your AOARD supported project:

a) papers published in peer-reviewed journals,

[1] and [2] above, attached.

b) papers published in peer-reviewed conference proceedings,

--

d) conference presentations without papers,

COVID has prevented conference engagement on this work.

e) manuscripts submitted but not yet published, and

--

f) other: 1 manuscript in preparation, see PDF attached.

g) provide a list any interactions with industry or with Air Force Research Laboratory scientists or significant collaborations that resulted from this work.

Unfortunately it was not possible to engage with AFRL personnel during the past two years.

Attachments: Publications a) and document f) listed above.

Doubly nonlinear superconducting qubit

Dat Thanh Le,[1,2,*] Arne Grimsmo,[3] Clemens Müller,[1,4] and T. M. Stace[1,†]

[1]*ARC Centre for Engineered Quantum System, Department of Physics, University of Queensland, Brisbane, Queensland 4072, Australia*

[2]*Thang Long Institute of Mathematics and Applied Sciences (TIMAS), Thang Long University, Nghiem Xuan Yem, Hoang Mai, Hanoi 10000, Vietnam*

[3]*ARC Centre for Engineered Quantum Systems, School of Physics, The University of Sydney, Sydney, New South Wales 2006, Australia*

[4]*IBM Research Zurich, 8803 Rüschlikon, Switzerland*

(Received 3 April 2019; published 17 December 2019)

We describe a superconducting circuit consisting of a Josephson junction in parallel with a quantum phase slip wire, which implements a Hamiltonian that is periodic in both charge and flux. This Hamiltonian is exactly diagonalizable in a double-Bloch band, and the eigenstates are shown to be code states of the Gottesman-Kitaev-Preskill quantum error correcting code. The eigenspectrum has several critical points, where the linear sensitivity to external charge and flux noise vanishes. The states at these critical points thus hold promise as qubit states that are insensitive to common external noise sources.

DOI: 10.1103/PhysRevA.100.062321

I. INTRODUCTION

Quantum devices are typically sensitive to noise, which presents the major challenge in developing robust quantum technologies. In contrast, digital technologies rest on the existence of stable states of matter that retain classical information over long times. Fundamentally, this is because stable classical states of matter embody an error correcting code. For example, ferromagnet domains in hard disks energetically implement a repetition code among many coupled electronic spins. By analogy, it is desirable to engineer quantum systems whose Hamiltonians encode a quantum error correcting code.

One approach to developing robust quantum devices is to design a "symmetry protected" logical space of nearly degenerate ground states $\{|\bar{0}\rangle, |\bar{1}\rangle\}$ [1], such as the proposed 0-π qubit [2–6], which rejects charge and flux noise. Here we instead introduce and analyze a simple superconducting circuit with a set of eigenstates that are robust against noise, without relying on ground state degeneracy. This device is built from a Josephson junction (JJ) [7] and a quantum phase slip (QPS) wire [8–11], making its Hamiltonian periodic in both charge and flux. The two junctions in this circuit are dual to each other, by which we name the device the dualmon. We show that the dualmon Hamiltonian is exactly diagonalizable, where there are two quantum numbers each associated to one canonical coordinate, and that typical noise processes commute with the Hamiltonian, affording some symmetry protection to the device.

The energy eigenbasis of the dualmon circuit includes the codewords of the Gottesman-Kitaev-Preskill (GKP) error correcting code [12,13] which occur at four critical points in the eigenspectrum: one minimum (ground state), one maximum, and two saddle points. At these critical points, we find that the device is insensitive (at linear order) to fluctuations in both charge and flux, making the critical points promising candidates for robust quantum information storage. We also show that these results hold when the circuit includes realistic parasitic inductance and capacitance.

The paper is structured as follows. In Sec. II, we analyze the characteristics of the elementary dualmon circuit and its robustness to classical noise. Section III takes into account the effect of wire inductance and junction capacitance, which are always present in a realistic circuit. We compute the energy bands of this circuit both analytically and numerically to assess the influence of external flux and charge noise. We also discuss on other possible noise sources in the realistic dualmon circuit. In Sec. IV, we couple the circuit to a waveguide to implement spectroscopy. The resulting transmission spectrum shows that the interband transition is dependent upon the system state, based on which we propose a means for state initialization. The waveguide coupling additionally gives rise to a quantum noise model; however, it is found that the dualmon remains resilient against the induced quantum noise. Afterwards, in Sec. V we compare the dualmon with several previously investigated superconducting qubit designs. We conclude the paper in Sec. VI. Several appendices are attached, providing details of calculations described in the main text.

II. THE ELEMENTARY CIRCUIT

Figure 1(a) illustrates the elementary dualmon circuit in which an ideal QPS is in parallel with an ideal JJ, so that there is no parasitic capacitance or inductance. The QPS and JJ are dual circuit elements, with constitutive relations $V_Q = V_c \sin[2\pi Q/(2e)]$ and $I_J = I_c \sin(2\pi\Phi/\Phi_0)$ respectively, where V_Q is the QPS voltage which depends on the charge Q that has flowed through the QPS, I_J is the JJ current which depends on the flux Φ linked by the JJ, and $\Phi_0 = h/(2e)$ is the magnetic flux quantum. The QPS and JJ

*thanhdat.le@uq.net.au

†stace@physics.uq.edu.au

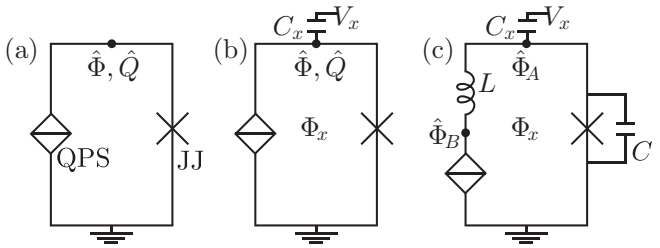

FIG. 1. (a) The elementary dualmon circuit of a quantum phase slip (QPS) wire in parallel with a Josephson junction (JJ). (b) Including coupling to external flux Φ_x and voltage bias V_x. (c) The realistic dualmon circuit including self inductance L and parasitic capacitance C.

elements are characterized by their critical voltage V_c and critical current I_c respectively.

The quantized circuit is described by the flux $\hat{\Phi}$ and the conjugate charge $\hat{Q}$. The Hamiltonian for the system is given by

$$\hat{H} = -E_Q \cos(2\pi\hat{n}) - E_J \cos(\hat{\phi}), \tag{1}$$

where $\hat{n} = \hat{Q}/(2e)$ and $\hat{\phi} = 2\pi\hat{\Phi}/\Phi_0$ satisfy $[\hat{\phi}, \hat{n}] = i$, $E_Q = 2eV_c/(2\pi)$, and $E_J = \Phi_0 I_c/(2\pi)$. The Hamiltonian is periodic in both charge and flux, and since $[e^{\pm i\hat{\phi}}, e^{\pm i2\pi\hat{n}}] = 0$, we find that $[\cos(2\pi\hat{n}), \cos(\hat{\phi})] = 0$. The eigenstates of the system $|k, \varphi\rangle$ are therefore characterised by Bloch quantum numbers $k \in (-1/2, 1/2]$ and $\varphi \in (-\pi, \pi]$, and satisfy dual Bloch relations $\langle k, \varphi|\phi + 2\pi\rangle_{\bar{\phi}} = e^{i2\pi k} \langle k, \varphi|\phi\rangle_{\bar{\phi}}$ [14] and $\langle k, \varphi|n + 1\rangle_{\bar{n}} = e^{i\varphi} \langle k, \varphi|n\rangle_{\bar{n}}$, where the subscripts $\bar{\phi}$ and $\bar{n}$ distinguish the phase and number bases respectively. The basis $\{|k, \varphi\rangle\}$ was introduced and analyzed in the work by Zak [15]; we will subsequently call it the Zak basis.

The eigenenergies of $\hat{H}$ are

$$E_{k,\varphi} = -E_Q \cos(2\pi k) - E_J \cos(\varphi). \tag{2}$$

This spectrum, as shown in Figs. 2(a) and 2(b), has four critical eigenstates,

$$\{|0, 0\rangle, |0, \pi\rangle, |1/2, 0\rangle, |1/2, \pi\rangle\},$$

where $\nabla E_{k,\varphi} = (\partial_k E_{k,\varphi}, \partial_\varphi E_{k,\varphi}) = 0$, which are the ground state, two saddle points, and the maximally excited state respectively. Notably, the saddle points can be made degenerate when $E_Q = E_J$. We will show that the sensitivity to charge and flux noise vanishes at these critical points to linear order.

Expanding the eigenstates in the phase or number bases,

$$|k, \varphi\rangle = \sum_{j=-\infty}^{\infty} e^{i2\pi jk} |\varphi - 2\pi j\rangle_{\bar{\phi}} = \frac{e^{ik\varphi}}{\sqrt{2\pi}} \sum_{j=-\infty}^{\infty} e^{-ij\varphi} |j - k\rangle_{\bar{n}}, \tag{3}$$

makes it apparent that the GKP codewords are eigenstates of the circuit. Particularly, following the definitions from Ref. [12] we can see $|\bar{0}_{\mathrm{GKP}}\rangle = |0, 0\rangle$ and $|\bar{1}_{\mathrm{GKP}}\rangle = |0, \pi\rangle$. The double-Bloch eigenstates in Eq. (3) satisfy the normalisation $\langle k, \varphi\,|k', \varphi'\rangle = \delta(k - k')\delta(\varphi - \varphi')$, and the generalized periodic boundary identities $|-1/2, \varphi\rangle = |1/2, \varphi\rangle$ and $|k, -\pi\rangle = e^{-i2\pi k} |k, \pi\rangle$.

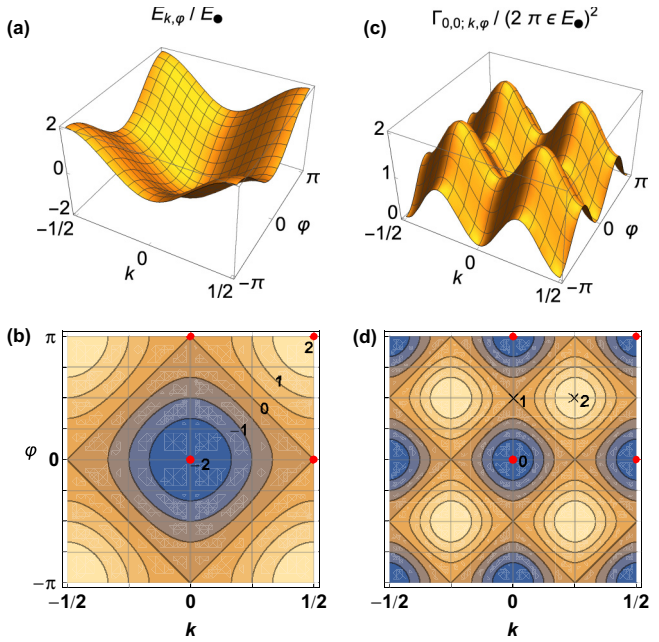

FIG. 2. (a) and (b) Three-dimensional and contour plots of the elementary dualmon circuit energy spectrum, $E_{k,\varphi}$, Eq. (2). The four critical points, where the gradient vanishes, are indicated by red circles. The saddle points are only degenerate if $E_Q = E_J$, but the locations of the critical points are fixed. (c) and (d) The pure dephasing rate $\Gamma_{0,0;k,\varphi}$ of superpositions of the dualmon ground state $|0, 0\rangle$ with other eigenstates $|k, \varphi\rangle$, Eq. (11), due to fluctuations in both external bias charge and flux. The dephasing rate vanishes at the critical points $|k, \varphi\rangle \in \{|0, \pi\rangle, |1/2, 0\rangle, |1/2, \pi\rangle\}$. For illustrative purpose, we have chosen $E_Q = E_J \equiv E_\bullet$ and uniform noise $\epsilon_n = \epsilon_\phi \equiv \epsilon$. Selected function contour and extremal values are marked.

A. Perturbative charge and flux noise in the elementary circuit

We include the effect of external voltage and flux noise, as shown in Fig. 1(b), with an external gate voltage $V_x(t)$ coupled capacitively via a parasitic capacitor C_x and an external flux $\Phi_x(t)$ through the circuit loop [16]. In Appendix A, we show that for small C_x the Hamiltonian of the circuit becomes

$$\hat{H}'(t) = -E_Q \cos\left(2\pi[\hat{n} + n_x(t)]\right) - E_J \cos[\hat{\phi} + \phi_x(t)]. \tag{4}$$

where $n_x(t) = C_x V_x(t)/(2e)$ and $\phi_x(t) = 2\pi\Phi_x(t)/\Phi_0$.

For fixed values of the biases, the eigenenergies are $\bar{E}_{k,\varphi}(n_x, \phi_x) = -E_Q \cos[2\pi(k + n_x)] - E_J \cos(\varphi + \phi_x)$. In linear response, the sensitivity of the system to small variation in bias is therefore given by

$$\left(\partial_{n_x} \bar{E}_{k,\varphi}, \partial_{\phi_x} \bar{E}_{k,\varphi}\right)\big|_{n_x=\phi_x=0} = \nabla E_{k,\varphi}. \tag{5}$$

For time-dependent noise in the bias parameters, this result implies that the noise sensitivity is determined by $\nabla E_{k,\varphi}$, so that the noise sensitivity vanishes at the critical points, at linear order.

For small-amplitude noise, we expand the Hamiltonian to linear order in the noise terms, so

$$\hat{H}'(t) \simeq \hat{H} + n_x(t)\hat{A}_n + \phi_x(t)\hat{A}_\phi, \tag{6}$$

where

$$\hat{A}_n = 2\pi E_Q \sin(2\pi\hat{n}), \tag{7a}$$

$$\hat{A}_\phi = E_J \sin(\hat{\phi}). \tag{7b}$$

Since $[\hat{H}, \hat{A}_n] = [\hat{H}, \hat{A}_\phi] = 0$, flux and charge noise do not induce transitions between eigenstates. Further, the critical states are null vectors of $\hat{A}_{n,\phi}$, so they are immune to charge and flux noise to first order.

We illustrate the general noise insensitivity using the example of uncorrelated charge and flux noise, for which

$$\langle n_x(t) n_x(t')\rangle = \epsilon_n^2 \delta(t-t'), \tag{8a}$$

$$\langle \phi_x(t) \phi_x(t')\rangle = (2\pi\epsilon_\phi)^2 \delta(t-t'), \tag{8b}$$

$$\langle n_x(t) \phi_x(t')\rangle = 0, \tag{8c}$$

where ϵ_n and ϵ_ϕ are noise amplitudes. With this white noise model, the evolution of the system density matrix, ρ, is given by the master equation [17,18]

$$\dot{\rho}(t) = -\frac{i}{\hbar}[\hat{H}, \rho(t)] + 2\epsilon_n^2 \mathcal{D}[\hat{A}_n]\rho(t) + 2(2\pi\epsilon_\phi)^2 \mathcal{D}[\hat{A}_\phi]\rho(t), \tag{9}$$

where $\mathcal{D}[A]\rho = A\rho A^\dagger - (\rho A^\dagger A + A^\dagger A \rho)/2$.

To calculate the decoherence rate between superpositions of eigenstates, we suppose that the system is initially in a pure state $|\psi\rangle = \mu\,|k,\varphi\rangle + \mu'\,|k',\varphi'\rangle$, so that $\rho(0) = |\psi\rangle\langle\psi|$. Off diagonal elements are right eigenoperators of the Lindblad superoperators, but generally with nonzero eigenvalues (i.e., dephasing rates),

$$\mathcal{D}[\hat{A}_n]\,|k,\varphi\rangle\,\langle k',\varphi'| = -\tfrac{1}{2}(2\pi E_Q)^2 \gamma_{2\pi k, 2\pi k'}\,|k,\varphi\rangle\,\langle k',\varphi'|,$$

$$\mathcal{D}[\hat{A}_\phi]\,|k,\varphi\rangle\,\langle k',\varphi'| = -\tfrac{1}{2}E_J^2 \gamma_{\varphi,\varphi'}\,|k,\varphi\rangle\,\langle k',\varphi'|,$$

where

$$\gamma_{y,y'} = [\sin(y) - \sin(y')]^2. \tag{10}$$

The pure dephasing rate is therefore given by

$$\Gamma_{k,\varphi;k',\varphi'} = (2\pi\epsilon_n E_Q)^2 \gamma_{2\pi k, 2\pi k'} + (2\pi\epsilon_\phi E_J)^2 \gamma_{\varphi,\varphi'}. \tag{11}$$

For any choice of k, there are values of k' for which $\gamma_{2\pi k, 2\pi k'} = 0$, and similarly for φ and φ'. Of particular interest is the fact that for superpositions of the critical eigenstates both Lindblad superoperators vanish, $\gamma_{2\pi k, 2\pi k'} = \gamma_{\varphi,\varphi'} = 0$, so that $\Gamma_{k,\varphi;k',\varphi'} = 0$ when $|k,\varphi\rangle$, $|k',\varphi'\rangle \in \{|0,0\rangle, |0,\pi\rangle, |1/2,0\rangle, |1/2,\pi\rangle\}$. We plot $\Gamma_{0,0;k,\varphi}$ in Figs. 2(c) and 2(d), showing that the dephasing rates from fluctuations in both external bias charge and flux vanish at the critical points. This property makes these states intriguing candidates for robustly storing quantum information.

III. REALISTIC CIRCUIT ELEMENTS

Realistically, the dualmon circuit will have some linear inductance L in the ring and capacitance C across the JJ [19]. We therefore extend the model to account for the effects of these parasitic elements, and we show that the noise insensitivity of the elementary circuit is retained under certain assumptions for the circuit parameters.

The resulting lumped-element model, shown in Fig. 1(c), has an additional circuit node, and the Hamiltonian for the realistic circuit is

$$\hat{\mathcal{H}}_{\rm sys} = E_C \hat{n}_A^2 + E_L(\hat{\phi}_A - \hat{\phi}_B)^2 - E_Q \cos(2\pi\hat{n}_B) - E_J \cos(\hat{\phi}_A), \tag{12}$$

where $E_C = (2e)^2/(2C)$, $E_L = \Phi_0^2/(8\pi^2 L)$, and the modes labeled A and B refer to the circuit nodes indicated in Fig. 1(c). We note that models of this form have been studied in Ref. [20].

A. Energy bands

We assume that L and C are small, so that $E_L, E_C \gg E_Q, E_J$. In this case, the high-frequency dynamics of the associated LC oscillator will dominate, so it is convenient to transform to new conjugate coordinates

$$\hat{\phi}_1 = \hat{\phi}_A - \hat{\phi}_B,\ \hat{n}_1 = \hat{n}_A, \quad \hat{\phi}_2 = \hat{\phi}_B,\ \hat{n}_2 = \hat{n}_A + \hat{n}_B. \tag{13}$$

In these coordinates we have

$$\hat{\mathcal{H}}_{\rm sys} = \hat{H}_{\rm HO} + \hat{\mathcal{V}}, \tag{14}$$

where

$$\hat{H}_{\rm HO} = E_C \hat{n}_1^2 + E_L \hat{\phi}_1^2, \tag{15}$$

$$\hat{\mathcal{V}} = -E_Q \cos[2\pi(\hat{n}_1 - \hat{n}_2)] - E_J \cos(\hat{\phi}_1 + \hat{\phi}_2). \tag{16}$$

$\hat{\mathcal{H}}_{\rm sys}$ commutes with $\cos(2\pi\hat{n}_2)$ and $\cos(\hat{\phi}_2)$, so eigenstates of $\hat{\mathcal{H}}_{\rm sys}$ will be simultaneous eigenstates of these operators, which are the Zak basis states $|k,\varphi\rangle_2$.[1] Thus, the eigenstates of $\hat{\mathcal{H}}_{\rm sys}$ take the form

$$|\Psi_{m;k,\varphi}\rangle_{1,2} = |\psi_m(k,\varphi)\rangle_1\,|k,\varphi\rangle_2, \tag{17}$$

where $|\psi_m(k,\varphi)\rangle_1$ are the eigenstates of the reduced Hamiltonian acting on mode 1,

$$\hat{H}_1(k,\varphi) = \hat{H}_{\rm HO} + \hat{V}(k,\varphi), \tag{18}$$

with

$$\hat{V}(k,\varphi) = -E_Q \cos[2\pi(\hat{n}_1 - k)] - E_J \cos(\hat{\phi}_1 + \varphi). \tag{19}$$

The eigenenergies $E_{m;k,\varphi}$ of the two-mode Hamiltonian $\hat{\mathcal{H}}_{\rm sys}$, markedly, coincide with those of the mode-1 Hamiltonian $\hat{H}_1(k,\varphi)$.

We are concerned with the limit $E_L, E_C \gg E_Q, E_J$, in which $\hat{H}_1(k,\varphi)$ describes a weakly nonlinear oscillator (i.e., mode 1) that depends parametrically on the quantum numbers k and φ associated to mode 2. We treat $\hat{V}(k,\varphi)$ perturbatively, and so we denote the eigenstates of $\hat{H}_{\rm HO}$ as $|\psi_m^{(0)}\rangle_1$ with eigenenergies $E_m^{(0)} = (m+1/2)\hbar\Omega$, where

$$\hbar\Omega = 2\sqrt{E_C E_L}. \tag{20}$$

Within the oscillator ground state manifold, $m = 0$, the first-order perturbative correction to the energy is

$$E^{(1)}_{m=0;k,\varphi} = {}_1\langle\psi_0^{(0)}|\hat{V}(k,\varphi)|\psi_0^{(0)}\rangle_1 = -E'_Q \cos(2\pi k) - E'_J \cos(\varphi), \tag{21}$$

[1]Here the subscript $i = 1, 2$ indicates states associated to mode i.

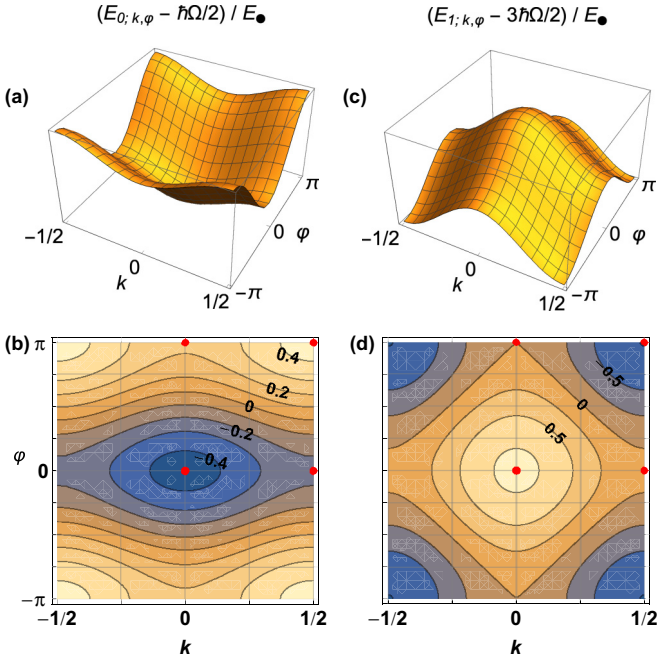

FIG. 3. (a) and (b) The ground state band energy, $E_{m=0;k,\varphi}$, of the realistic dualmon circuit relative to the unperturbed harmonic oscillator ground state energy $E^{(0)}_{m=0}$. (c) and (d) The first excited state band energy, $E_{m=1;k,\varphi}$. Plots are generated by numerically solving the eigenvalue problem (see Appendix B). On this scale, the difference between the numerical values and the perturbative result in Sec. III A is less than 0.005 across the band. For illustrative purposes, plots are drawn with $E_Q = E_J \equiv E_\bullet$, $E_C/E_J = 200$, and $E_L/E_J = 10$. For these parameter values, $z = \sqrt{20}$, $E'_Q = 0.11E_\bullet$, $E'_J = 0.33E_\bullet$, $E''_Q = -0.38E_\bullet$, and $E''_J = -0.40E_\bullet$.

where $E'_Q = e^{-\pi^2/z}E_Q$ and $E'_J = e^{-z/4}E_J$ are renormalized QPS and JJ parameters arising from zero-point motion of mode 1, and $z = \sqrt{E_C/E_L} = \sqrt{L/C}\,(2e)^2/\hbar$ is a dimensionless oscillator impedance. Equation (21) shows that within the oscillator ground state manifold, mode 2 is governed by the elementary Hamiltonian $\hat{H}$ in Eq. (1), with renormalized QPS and JJ energies. Significantly, the critical points remain at the same locations in the double-Bloch band.

To verify the perturbative arguments above, we numerically solve for $|\psi_m(k,\varphi)\rangle_1$ and eigenenergies $E_{m;k,\varphi}$ nonperturbatively in the Zak basis for mode 1, as described in Appendix B. Figures 3(a) and 3(b) show the oscillator ground state manifold energy band $E_{m=0;k,\varphi}$ relative to the unperturbed harmonic oscillator ground state energy, for $E_L, E_C \gg E_Q = E_J$. The nonlinear energies $E_{J,Q}$ are renormalized to $E'_{J,Q}$, but the band structure is otherwise qualitatively the same as the elementary case, and with the same critical eigenstates. We show below that the noise sensitivity vanishes at the critical eigenstates, as for the elementary circuit.

Figures 3(c) and 3(d) also demonstrate the first excited manifold, $E_{m=1;k,\varphi}$, relative to the unperturbed harmonic oscillator first excited state energy. In this manifold, the renormalized nonlinear energies are $E''_Q = (1 - 2\pi^2/z)E'_Q$ and $E''_J = (1 - z/2)E'_J$, so that the first excited band may be inverted relative to the ground state manifold (i.e., the locations of minima and maxima are exchanged). It follows that the interband transition energies at the critical points can be made nondegenerate, facilitating spectroscopic addressability of the critical states. This addressability provides an avenue to state preparation: spectroscopic measurements of a given accuracy will localize the system in a narrow range of k and φ near the observed transition energy. This will be discussed in more detail in Sec. IV.

B. Perturbative charge and flux noise in the realistic circuit

We introduce charge and flux noise in the same manner as for the elementary circuit [21]. The Hamiltonian is then

$$\hat{\mathcal{H}}'_{\rm sys} = E_{C_\Sigma}[\hat{n}_A + n_x(t)]^2 + E_L[\hat{\phi}_A - \hat{\phi}_B - \phi_x(t)]^2 - E_Q\cos(2\pi\hat{n}_B) - E_J\cos(\hat{\phi}_A), \quad (22)$$

where $E_{C_\Sigma} = (2e)^2/(2C_\Sigma)$ with $C_\Sigma = C + C_x$, and n_x and ϕ_x are external bias terms, as discussed earlier. In what follows, we assume that $C_x \ll C$, and take $E_{C_\Sigma} = E_C$ for simplicity.

Constant charge and flux bias can be transformed away by suitable gauge choice [22,23], so we again consider the effect of zero-mean, white noise. As before, we make the coordinate transformation given by Eq. (13), and expand the Hamiltonian to linear order in the noise terms, so

$$\hat{\mathcal{H}}'_{\rm sys} \simeq \hat{\mathcal{H}}_{\rm sys} + n_x(t)\hat{\mathcal{A}}_n + \phi_x(t)\hat{\mathcal{A}}_\phi, \quad (23)$$

where

$$\hat{\mathcal{A}}_n = 2E_C\hat{n}_1, \quad (24a)$$

$$\hat{\mathcal{A}}_\phi = -2E_L\hat{\phi}_1. \quad (24b)$$

The master equation for the noisy system is then

$$\dot{\varrho} = -\frac{i}{\hbar}[\hat{\mathcal{H}}_{\rm sys}, \varrho] + 2\epsilon_n^2\mathcal{D}[\hat{\mathcal{A}}_n]\varrho + 2(2\pi\epsilon_\phi)^2\mathcal{D}[\hat{\mathcal{A}}_\phi]\varrho, \quad (25)$$

where ϱ is the joint density operator for modes 1 and 2.

Since $\hat{\mathcal{A}}_n$ and $\hat{\mathcal{A}}_\phi$ have action on the Hilbert space associated with mode 1 only, they are diagonal within any oscillator manifolds. Using the first-order perturbative correction to the oscillator modes, we compute matrix elements of these dissipators in the ground state manifold (see Appendix C for more detail), and find that

$$_{1,2}\langle\Psi_{0;k\varphi}|\,\hat{\mathcal{A}}_n\,|\Psi_{0;k'\varphi'}\rangle_{1,2} = 2\pi E'_Q\sin(2\pi k)\delta(k-k')\delta(\varphi-\varphi'), \quad (26a)$$

$$_{1,2}\langle\Psi_{0;k\varphi}|\,\hat{\mathcal{A}}_\phi\,|\Psi_{0;k'\varphi'}\rangle_{1,2} = E'_J\sin(\varphi)\delta(k-k')\delta(\varphi-\varphi'), \quad (26b)$$

which implies

$$\Pi_0\hat{\mathcal{A}}_n\Pi_0 = 2\pi E'_Q\sin(2\pi\hat{n}_2), \quad (27a)$$

$$\Pi_0\hat{\mathcal{A}}_\phi\Pi_0 = E'_J\sin(\hat{\phi}_2), \quad (27b)$$

where $\Pi_0 = \int_{-1/2}^{1/2}dk\int_{-\pi}^{\pi}d\varphi\,|\Psi_{0;k,\varphi}\rangle_{1,2}\langle\Psi_{0;k,\varphi}|$ is the projection onto the ground state manifold. Equations (27a) and (27b) are of the same form as the dissipators for the elementary circuit, Eqs. (7a) and (7b), and so lead to dephasing rates of the same form. That is, a superposition of two eigenstates in the ground state manifold, $\mu\,|\Psi_{0;k,\varphi}\rangle + \mu'\,|\Psi_{0;k',\varphi'}\rangle$, will dephase at a rate also given by $\Gamma_{k,\varphi;k',\varphi'}$ in Eq. (11), with

the replacements $E_{Q,J} \to E'_{Q,J}$. As for the elementary circuit, the dephasing rate vanishes for superpositions of the critical states.

C. Parametric and nonperturbative noise sources in the realistic circuit

The Aharonov-Casher interference [24] of phase slips, dependent on charge distribution, could be detrimental to QPS devices. Indeed, phase slips exhibit along a strongly disordered superconducting nanowire [10]; interference of phase slips at different points may cause fluctuations in the phase slip energy E_Q [11,25] and result in dephasing of coherent superpositions. Phase slip interference on JJ chains (i.e., a granular model of superconducting nanowires [19]) has also been observed experimentally [26] and shown to be a decoherence source in the Josephson-junction-chain based fluxonium qubit [27,28]. To mitigate such undesirable effect, a possible approach is to fabricate QPS nanowires in the form of short weak links [29,30], by which phase slips are limited to take place at the narrowest point, thus improving stability of the QPS energy.

The time-dependent charge noise considered in Sec. III B was perturbative, in which the standard-deviation in the charge was small, $\sigma_{n_x} \ll 1/2$. However, localised, two-level charge traps near the circuit can lead to a random-telegraph charge fluctuation with $\sigma_{n_x} \sim 1/2$, which is no longer perturbative. This gives rise to quantum state diffusion, i.e., shifting of the system state in the charge space. However, as long as the noise magnitude is smaller than one electron worth of charge, we speculate that the errors could be correctable by means of active GKP quantum error correction [12], for which GKP codes were originally designed. A short discussion on specific implementation of such active correction is included in Appendix D.

IV. COUPLING TO A WAVEGUIDE

Realistic devices will need to couple to waveguides with which one can initialize, control, and perform readout on the system. Here we couple the dualmon circuit capacitively to a waveguide and analyze spectroscopy on the device. We then propose a spectroscopic procedure for state preparation.

The waveguide coupling also introduces quantum and thermal noise to the system, so we analyze the additional noise arising from this coupling. As for classical charge and flux noise, we show that superpositions of the critical states are robust with respect to the induced quantum noise, for essentially the same reason, i.e., the band gradient vanishes at the critical points.

A. Transmission spectrum

Figure 4 illustrates a circuit where the dualmon is capacitively coupled to a waveguide. A detailed Hamiltonian derivation for this circuit is given in Appendix E. The Hamiltonian for the dualmon system coupled to the waveguide is

$$\hat{\mathcal{H}}_{\rm tot} = \hat{\mathcal{H}}_{\rm sys} + \hat{\mathcal{H}}_{\rm wg} + \hat{\mathcal{H}}_{\rm coup}, \tag{28}$$

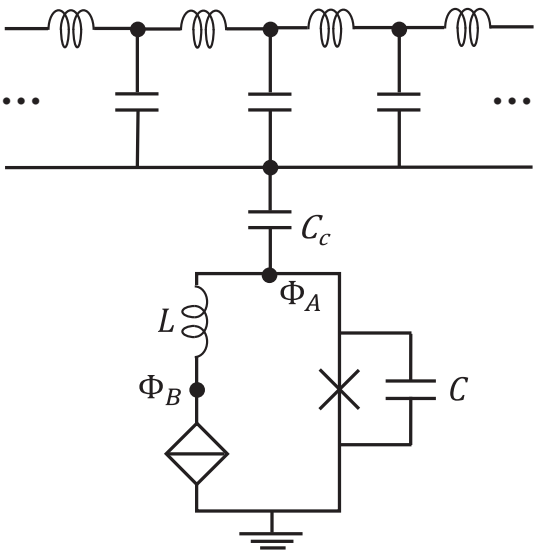

FIG. 4. Lumped-element representation of the capacitive coupling between the realistic dualmon circuit and a waveguide.

where $\hat{\mathcal{H}}_{\rm sys}$ is the dualmon Hamiltonian defined in Eq. (14),

$$\hat{\mathcal{H}}_{\rm wg} = \int d\omega\, \hbar\omega \hat{a}^\dagger(\omega)\hat{a}(\omega), \tag{29}$$

is the waveguide Hamiltonian describing a continuum of modes, and

$$\hat{\mathcal{H}}_{\rm coup} = \int d\omega\, g(\omega)[\hat{a}^\dagger(\omega) + \hat{a}(\omega)]\hat{n}_1, \tag{30}$$

is the interaction with $g(\omega)$ the coupling strength.

We make use of the input-output formalism [31,32] to calculate the transmission spectrum; relevant calculations are presented in more detail in Appendix F. In particular, the dynamics of the dualmon system coupled to the waveguide and driven by a coherent field of amplitude α is governed by

$$\dot{\varrho} = -\frac{i}{\hbar}[\hat{\mathcal{H}}_{\rm drive}, \varrho] + \mathcal{D}[\hat{b}]\varrho, \tag{31}$$

where

$$\hat{\mathcal{H}}_{\rm drive} = \hat{\mathcal{H}}_{\rm sys} - \frac{i\hbar}{2}\sqrt{\gamma}(\alpha e^{-i\omega_D t}\hat{n}_1^+ - \alpha e^{i\omega_D t}\hat{n}_1^-), \tag{32}$$

$$\hat{b} = \sqrt{\gamma}\hat{n}_1^- + \alpha e^{-i\omega_D t}\mathbb{1}. \tag{33}$$

Here $\hat{n}_1^+$ ($\hat{n}_1^-$) is the lower (upper) triangularized version of $\hat{n}_1$, ω_D is the drive frequency, and $\sqrt{\gamma}$ is proportional to $g(\omega_D)$ determining bandwidth of the spectrum. The transmission is defined as

$$T = |\langle\hat{b}\rangle/\alpha|^2, \tag{34}$$

where $\langle\hat{b}\rangle = {\rm Tr}(\hat{b}\varrho)$. We solve the master equation (31), use the obtained results to calculate $\langle\hat{b}\rangle$, and then get the transmission T.

The transmission spectrum, assuming the circuit to be initialized in either one of two critical states $|\Psi_{0;k=0,\varphi=0}\rangle_{1,2}$ and $|\Psi_{0;k=0,\varphi=\pi}\rangle_{1,2}$, is displayed in Fig. 5. For illustrative purpose, the transmission has been plotted in dependence on the detuning of the drive frequency ω_D from the transition

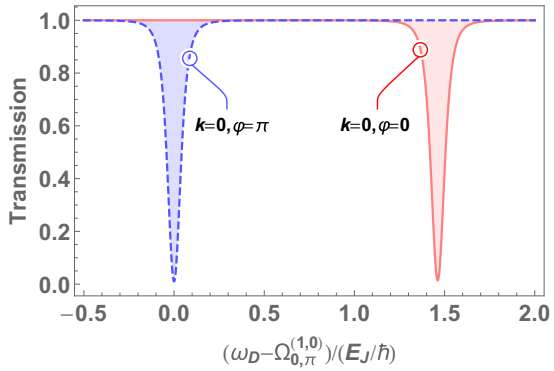

FIG. 5. Transmission spectrum T defined in Eq. (34) with respect to the detuning of the drive frequency ω_D from the transition frequency $\Omega^{(1,0)}_{0,\pi}$ for two critical points, $(k=0,\varphi=0)$ and $(k=0,\varphi=\pi)$. Here $\Omega^{(1,0)}_{0,\pi}$ denotes the interband transition between the ground and first excited bands at the critical point $(k=0,\varphi=\pi)$. Relevant parameters for plotting are chosen as $E_Q=E_J$, $\hbar\Omega=40\sqrt{5}\,E_J$, $z=\sqrt{20}$, $\gamma=0.01\,\omega_D$, and $\hbar\alpha^2=0.1\,E_J$.

between the lowest (i.e., ground) and first excited bands for the critical point $(k=0,\ \varphi=\pi)$, denoted as $\Omega^{(1,0)}_{0,\pi}$.[2] It can be seen from Fig. 5 that resonance depends on the system state. This is consistent with the observation made in Sec. III A, that is, the interband transition frequency is dependent on the state of the device, with the distinguishability of different $|k,\varphi\rangle$ states set by the difference in the interband transition frequency.

B. Qubit initialization by spectroscopy

The spectroscopic measurement described in the preceding subsection moreover gives a route to state preparation. Since the interband transition frequency between the lowest and first excited bands of the dualmon is (k,φ) dependent, transmission at a given frequency $\Omega^{(1,0)}_{k,\varphi}$ will localise the system around the corresponding value of (k,φ).[3] As shown in Appendix G, scanning over transition frequency is equivalent to scanning over the two biases $n_x\in[-1/2,1/2)$ and $\phi_x\in[-\pi,\pi)$; one can thus localise the state to some value of (k,φ) starting from a generic state such as a thermal state. Once the value of (k,φ) has been localized, one can adjust (n_x,φ_x) to move the origin of the band in Fig. 3 such that the state becomes localized at any desired point, e.g., the ground state $(k=0,\ \varphi=0)$.

Choosing, e.g., $(k=0,\ \varphi=0)$ and $(k=0,\ \varphi=\pi)$ as the two operating points for the dualmon, logical basis state preparation corresponds to preparing a state highly localized around one of these two values. The exact form of the distributions over (k,φ) is not particularly important, nor is it crucial that the states are pure, as long as they are sufficiently well localized. This, perhaps counter intuitive, can be understood by making an analogy with approximate GKP codewords [12]. Two approximate qubit codewords for the dualmon can be defined as

$$|i_L\rangle=\int dk\,d\varphi\,\psi_i(k,\varphi)|k,\varphi\rangle, \tag{35}$$

with $\psi_i(k,\varphi)$ some localized distribution around $(k=0,\varphi=0)$ for $i=0$ and $(k=0,\ \varphi=\pi)$ for $i=1$. A well-localized but mixed state can be viewed as an approximate qubit codeword with a set of small (approximately) correctable errors. In other words, we can think of the well-localized mixed state as the codeword $|i_L\rangle$ sent through an error channel with the "size" of the errors bounded by the measurement resolution of the spectroscopic measurement. This is thus analogous to noisy preparation of GKP codewords. In a universal scheme for quantum computing, which we will not discuss here, it is also crucial that the logical operations do not amplify errors too badly, i.e., turning small errors into large ones. Provided that this is true, the two distributions will remain well localized throughout the computation, and can in principle be distinguished with high fidelity in a final measurement.

We have argued that it should be possible to prepare states well-localized around a single value of (k,φ) using spectroscopic measurements, and furthermore such states can be thought of as imperfect, yet high-quality, qubit codewords. It is, however, a far more challenging task to prepare superposition states, such as $|+_L\rangle=\frac{1}{\sqrt{2}}(|0_L\rangle+|1_L\rangle)$, with a similar guarantee of "small errors." Preliminary results suggest that introducing symmetry-breaking terms to the Hamiltonian, e.g., breaking the 2π periodicity of $\hat{\phi}_2$, can be used to prepare states of the form $|+_L\rangle$. The quality of such operations, as well as the possibility of universal control, will be the subject of future work.

C. Pure dephasing from thermal and quantum noise in the waveguide

The capacitive coupling to the waveguide, in addition to allowing performing spectroscopy and state initialization, opens a channel for noise to appear in the dualmon circuit. The induced noise is manifest via the coupling operator $\hat{n}_1$, which is diagonal within each manifold while coupling states among different manifolds. As we are interested in encoding the dualmon in the ground state manifold, say in a superposition of eigenstates $\mu\,|\Psi_{0;k,\varphi}\rangle_{1,2}+\mu'\,|\Psi_{0;k',\varphi'}\rangle_{1,2}$, the relevant decoherence source is either pure dephasing within the encoded manifold or transitions to other manifolds. The master equation for the dualmon density operator when considering only pure dephasing in the ground state manifold is [33]

$$\dot{\varrho}_g=-\frac{i}{\hbar}[\hat{\mathcal{H}}_{\mathrm{sys},g},\varrho_g]+2\pi\lim_{\omega\to 0}(J(\omega)[2N(\omega)+1])\mathcal{D}[\hat{n}_{1,g}]\varrho_g, \tag{36}$$

where ϱ_g, $\hat{\mathcal{H}}_{\mathrm{sys},g}$, and $\hat{n}_{1,g}$ are all projections onto the ground state manifold, $J(\omega)=1/\hbar^2\int d\omega' g^2(\omega)\delta(\omega'-\omega)$ is the spectral density, and $N(\omega)$ is the thermal distribution at frequency ω. $\hat{n}_{1,g}$ can be straightforwardly computed from Eqs. (24a) and (27a). The pure dephasing rate of the superposition of interest

[2] We define $\Omega^{(m,n)}_{k,\varphi}\equiv(E_{m;k,\varphi}-E_{n;k,\varphi})/\hbar$ as the transition frequency from the n^{th} band to the m^{th} band at a fixed pair of (k,φ).

[3] Note that the mapping between interband frequencies $\Omega^{(1,0)}_{k,\varphi}$ and values of (k,φ) is in general not unique, except for at the ground state $(k=0,\varphi=0)$, and the maximally exited state $(k=1/2,\varphi=\pi)$ (see Fig. 8 in Appendix F). Resolving states with similar transition frequencies can however be done by adjusting n_x and ϕ_x while performing spectroscopy at a given frequency.

in the ground state manifold is then found to be

$$\Gamma_{k;k'} = \frac{\pi^2 E_Q'}{E_C} \lim_{\omega\to 0} (J(\omega)[2N(\omega)+1])\gamma_{2\pi k,2\pi k'}, \tag{37}$$

where the function $\gamma_{y,y'}$ has been defined in Eq. (10). In general this is not zero, due to thermal and vacuum fluctuations in the waveguide. However, similar to the case of classical noise in Sec. III B, we have $\gamma_{2\pi k,2\pi k'} = 0$ for superpositions of the critical states, so that dephasing from waveguide fluctuations is completely suppressed.

D. Decoherence from thermal waveguide excitation

Another decoherence source stemming from the waveguide coupling is thermal transitions among different manifolds. We show below that provided the harmonic oscillator gap is much larger than $k_B T$ the thermal induced dephasing rate is very small. For this purpose, we express the coupling operator $\hat{n}_1$ in the form

$$\hat{n}_1 = \int_{-1/2}^{1/2} dl \int_{-\pi}^{\pi} d\theta \sum_{m,n=0}^{\infty} \hat{n}_{1;l,\theta}^{(m,n)}, \tag{38}$$

where $\hat{n}_{1;l,\theta}^{(m,n)} = {}_{1,2}\langle\Psi_{m;l,\theta}|\hat{n}_1|\Psi_{n;l,\theta}\rangle_{1,2}\,|\Psi_{m;l,\theta}\rangle_{1,2}\,\langle\Psi_{n;l,\theta}|$ are eigenoperators of $\hat{\mathcal{H}}_{\rm sys}$ satisfying the commutation relations $[\hat{\mathcal{H}}_{\rm sys}, \hat{n}_{1;l,\theta}^{(m,n)}] = \hbar\Omega_{l,\theta}^{(m,n)}\hat{n}_{1;l,\theta}^{(m,n)}$. The master equation for the dualmon density operator, that accounts for the transitions between manifolds, is then given by [33]

$$\begin{aligned}\dot{\varrho} = &-\frac{i}{\hbar}[\hat{\mathcal{H}}_{\rm sys}, \varrho] \\ &+ \iint dl\, d\theta \sum_{m<n} \pi J\big(\Omega_{l,\theta}^{(n,m)}\big)\big[N\big(\Omega_{l,\theta}^{(n,m)}\big)+1\big]\mathcal{D}\big[\hat{n}_{1;l,\theta}^{(m,n)}\big]\varrho \\ &+ \iint dl\, d\theta \sum_{m>n} \pi J\big(\Omega_{l,\theta}^{(m,n)}\big)N\big(\Omega_{l,\theta}^{(m,n)}\big)\mathcal{D}\big[\hat{n}_{1;l,\theta}^{(m,n)}\big]\varrho. \end{aligned} \tag{39}$$

In Eq. (39), the second and third lines respectively represent relaxations to lower manifolds and excitations to higher manifolds; notably, the two quantum numbers l and θ are conserved, implying the absence of transitions within each manifold. As is well known from the standard two-level-system encoding, either relaxation or excitation dephases coherent superpositions. However, as the dualmon is encoded in superpositions of two eigenstates in the ground state manifold and there are no transitions between these two states, the dephasing rate for the dualmon is determined by excitations out of the ground state manifold only. In Appendix H, we include several calculations comparing dephasing rates of the ordinary two-level-system encoding and ground-state-manifold one. The relevant dephasing rate, from Eq. (39), is proportional to $J(\Omega_{l,\theta}^{(m>0,0)})N(\Omega_{l,\theta}^{(m>0,0)})$. The waveguide (the bath) is assumed to be in thermal state, i.e., $N(\omega) = 1/[\exp(\hbar\omega/k_B T) - 1]$ and as shown in Appendix E $J(\omega) = \nu\hbar\omega$ with ν a constant, so

$$J(\omega)N(\omega) = \nu\hbar\omega/[\exp(\hbar\omega/k_B T) - 1], \tag{40}$$

which is very small for large $\hbar\omega/k_B T$. Hence, thermal dephasing is very weak as long as $\hbar\Omega_{k,\varphi}^{(1,0)} \gg k_B T$. This condition is inherently satisfied with superconducting circuits, since the working temperature is typically very low.

V. COMPARISONS WITH RELATED SUPERCONDUCTING QUBITS

It is instructive to point out the differences between the proposed circuit and other superconducting qubit devices previously discussed in the literature, namely, the 0-π qubit [2–6], the fluxonium [22,23], and the Aharonov-Casher device [34]. Specifically, the 0-π qubit uses two nearly degenerate eigenstates with nearly disjoint support in coordinate space [5], which affords its noise-rejecting properties. Realization of the 0-π qubit would require implementing the π-periodic Josephson junction [2,3,35–38]. In comparison, the robustness of the critical states of the dualmon device arises from the fact that the noise operators associated with weak external charge and flux noise commute with the eigenstates suppressing decay, and the gradient of the energy landscape vanishes at the critical states suppressing dephasing.

The lumped circuit of the imperfect fluxonium [22,23], where phase slip is included at its superinductor [27,28], is remarkably identical to the realistic dualmon circuit shown in Fig. 1(c). However, the essential difference between the two devices lies at the energy scales. In particular, the fluxonium employs a superinductor [22,23,39] to make the inductive energy very small; QPS on the superinductor is treated as an undesired noisy source [27]. The JJ present in the fluxonium circuit generally works in the regime of large E_J/E_C. These are in contrast to the dualmon energy scales, which ideally would be $E_L, E_C \gg E_Q, E_J$ (see Sec. III A). The difference at energy scales then results in the differences in the physics of the two devices. Indeed, fluxon tunneling is the primary process in the fluxonium [27], whereas the dual QPS and JJ elements in the dualmon allow tunneling of both fluxon and Cooper pair. The fluxonium wave function in flux space is localized within the wells of the Josephson cosine potential and in charge space is well localized within the range of a Cooper pair [23]. The dualmon, instead, is completely delocalized in both flux and charge spaces [see Zak states in Eq. (3)]. Finally, the Aharonov-Casher device proposed in Ref. [34] is realized basically as a single JJ shunted by a superinductor, and thus closely resembles the fluxonium design; therefore, the above arguments also hold when comparing such device to the dualmon circuit. Furthermore, in that device the Aharonov-Casher interference effect is ultilized to suppress single fluxon tunneling while making pair tunneling dominant. This is different from the dualmon circuit, where only single fluxon tunneling is considered.

We comment briefly on plausible experimental parameters for the dualmon circuit. Josephson and QPS energies can be routinely engineered to be $E_J \sim E_Q \sim h \times 5$ GHz [11,25,40,41]. Parasitic capacitance and self-inductances of order $C \sim 1$ fF and $L \sim 10$ nH are feasible [8,25,40] corresponding to parameters for the dualmon circuit of $z \sim 3$ and $\hbar\Omega \sim h \times 50$ GHz $\gg E_J, E_Q$, which is well within the validity range of the approximations employed in this work.

VI. CONCLUSIONS

We have shown that the dualmon circuit, encoded in superpositions of the critical points, is resilient against both classical and quantum white noise. The device nonetheless

could suffer from other noise sources, including the charge-dependent Aharonov-Casher effect in QPS devices that lowers the phase slip energy and large temporal charge fluctuations causing diffusion of quantum states. Possibly, the former could be reduced by designing QPS elements in a weak-link form [29,30], while the later might be dealt with via active error correction of the GKP code [12].

Any pair of the critical points could be chosen to represent a qubit; the nearly degenerate saddle points might be a convenient choice. As discussed qualitatively in Sec. IV B, state preparation could be performed by interband spectroscopic measurements. The quality with which we can prepare states near the critical points then depends on the spectral resolution of such a measurement.

Relative phase shifts between the critical states may be achieved using tunable JJ and QPS circuit elements, or by using high frequency drive pulses to access excited states of the oscillator mode. Tuning of JJ and QPS energies leaves the critical states unchanged, thus retaining the protected working space of the qubit; introducing tunable elements, however, opens the qubit to new dephasing channels. More general control requires additional symmetry breaking terms in the Hamiltonian. For example, a shunt inductor switched transiently across the JJ breaks the discrete charge translation symmetry of the Hamiltonian, so it will couple the Zak eigenstates of the original circuit. Detailed analysis of control of the state space for one and multiple devices will be the subject of future work.

We conclude that the dualmon circuit considered here offers a promising avenue for robustly storing quantum information, worthy of further study. In particular, it hosts several critical eigenstates, superpositions of which are insensitive to both charge and flux noise at linear order. This result holds even when the circuit includes parasitic capacitance and inductance. Interestingly, the critical states are physical embodiments of the codewords of the GKP error correcting code. Active fault-tolerant preparation of such states in harmonic oscillators is extremely hard, so the dualmon circuit could possibly offers an alternative path towards accessing these states.

ACKNOWLEDGMENTS

This research was supported by the Australian Research Council Centre of Excellence for Engineered Quantum Systems (EQUS, CE170100009) and a Discovery Early Career Research Award (DE190100380) as well as the Swiss National Science Foundation through the NCCR Quantum Science and Technology. T.M.S. acknowledges visitor support from the Pauli Center for Theoretical Studies, ETH Zurich. We thank J. Cole and V. V. Albert for useful discussions.

APPENDIX A: DERIVATION OF THE BIASED HAMILTONIAN $\hat{H}'(t)$

Here we derive the Hamiltonian $\hat{H}'(t)$ in Eq. (4). Applying the spanning tree model in Ref. [16] for the circuit in Fig. 1(b), we choose the fluxes across the QPS and JJ to be $\Phi_Q = \Phi$ and $\Phi_J = \Phi + \Phi_x$, respectively. The Kirchhoff current conservation law at the active node of the circuit is

$$\dot{Q}_Q + \dot{Q}_{C_x} + \dot{Q}_J = 0. \tag{A1}$$

From the constitutive laws for circuit elements, we know that the charge that has flowed through the QPS is

$$Q_Q(\dot{\Phi}) \equiv \frac{2e}{2\pi}\arcsin(\dot{\Phi}/V_c), \tag{A2}$$

the charge across the bias capacitor is $Q_{C_x} = C_x(\dot{\Phi} - V_x)$, and the current through the Josephson junction is $\dot{Q}_J \equiv I_J = I_c \sin(2\pi(\Phi + \Phi_x)/\Phi_0)$. We thus find that the equation of motion for the circuit is

$$\frac{d}{dt}[Q_Q(\dot{\Phi}) + C_x(\dot{\Phi} - V_x)] + I_c \sin\left[\frac{2\pi}{\Phi_0}(\Phi + \Phi_x)\right] = 0. \tag{A3}$$

We identify terms above with the Euler-Lagrange equation of motion, $\frac{d}{dt}Q - \partial_\Phi L = 0$, where $Q = \partial_{\dot{\Phi}} L$ is the charge conjugate to Φ, which implies

$$Q = \partial L/\partial\dot{\Phi} = Q_Q(\dot{\Phi}) + C_x\dot{\Phi} - Q_x, \tag{A4}$$

$$\partial L/\partial\Phi = -I_c \sin\left[\frac{2\pi}{\Phi_0}(\Phi + \Phi_x)\right], \tag{A5}$$

where $Q_x = C_x V_x$. The Lagrangian is then given by

$$L = \dot{\Phi}\, Q_Q(\dot{\Phi}) + \frac{2eV_c}{2\pi}\cos\left[\frac{2\pi}{2e}Q_Q(\dot{\Phi})\right] + \frac{C_x}{2}(\dot{\Phi} - V_x)^2 + \frac{I_c\Phi_0}{2\pi}\cos\left[\frac{2\pi}{\Phi_0}(\Phi + \Phi_x)\right]. \tag{A6}$$

The Hamiltonian, $H(\Phi, \dot{\Phi}) = \dot{\Phi}Q - L$, is

$$H(\Phi, \dot{\Phi}) = \frac{C_x}{2}\dot{\Phi}^2 - E_Q\cos\left[\frac{2\pi}{2e}Q_Q(\dot{\Phi})\right] - E_J\cos\left[\frac{2\pi}{\Phi_0}(\Phi + \Phi_x)\right], \tag{A7}$$

where $E_Q = 2eV_c/(2\pi)$, $E_J = I_c\Phi_0/(2\pi)$. To compute $H(\Phi, Q)$ we need to invert Eq. (A4) to find $\dot{\Phi} = \dot{\Phi}(Q)$. Implicitly, we have

$$\dot{\Phi} = V_c \sin\left(\frac{2\pi}{2e}(Q - C_x\dot{\Phi} + Q_x)\right). \tag{A8}$$

We cannot solve this analytically for $\dot{\Phi}$; however, if $C_x\dot{\Phi} \ll Q$ we expand the right-hand side of Eq. (A8) in powers of C_x and solve for $\dot{\Phi}$. We find

$$\dot{\Phi} = V_c \sin\left(\frac{2\pi}{2e}(Q + Q_x)\right) \times\left[1 - \frac{2\pi}{2e}C_xV_c\cos\left(\frac{2\pi}{2e}(Q + Q_x)\right)\right] + O(C_x^2). \tag{A9}$$

Substituting this result into Eq. (A7), we obtain

$$H = -E_Q\cos\left(\frac{2\pi}{2e}(Q + Q_x)\right) - E_J\cos\left(\frac{2\pi}{\Phi_0}(\Phi + \Phi_x)\right) + E_{C_x}\cos\left(\frac{4\pi}{2e}(Q + Q_x)\right) + O(C_x^2), \tag{A10}$$

where $E_{C_x} = C_xV_c^2/4$. Quantizing the charge and flux operators, and defining $\hat{n} = \hat{Q}/(2e)$ and $\hat{\phi} = 2\pi\hat{\Phi}/\Phi_0$, the Hamiltonian operator is then

$$\hat{H}' = -E_Q\cos[2\pi(\hat{n} + n_x)] - E_J\cos(\hat{\phi} + \phi_x) + E_{C_x}\cos[4\pi(\hat{n} + n_x)], \tag{A11}$$

where $n_x = Q_x/(2e)$ and $\phi_x = 2\pi\Phi_x/\Phi_0$. If the external capacitance is sufficiently small then $E_{C_x} \ll E_Q, E_J$. Since $[\hat{H}, \cos(4\pi(\hat{n}+n_x))] = 0$, this term does not change the eigenstates, and preserves the critical points. We therefore take $E_{C_x} = 0$ for simplicity, yielding Eq. (4).

APPENDIX B: EIGENVALUE PROBLEM FOR MODE 1

In the Zak basis, we have the useful operator representations [15,20]

$$\langle k,\varphi|\,\hat{n}\,|\psi\rangle = -i\frac{\partial}{\partial\varphi}\langle k,\varphi|\psi\rangle, \tag{B1}$$

$$\langle k,\varphi|\,\hat{\phi}\,|\psi\rangle = \left(-i\frac{\partial}{\partial k}+\varphi\right)\langle k,\varphi|\psi\rangle. \tag{B2}$$

We express eigenstates of the reduced Hamiltonian $\hat{H}_1(k,\varphi)$ in the Zak basis for mode 1, $\{|l,\theta\rangle_1\}$, and we find that $\psi_m(l,\theta;k,\varphi) \equiv {}_1\langle l,\theta\,|\psi_m(k,\varphi)\rangle_1$ are eigenfunctions of the differential operator

$$H_1(k,\varphi) = E_C\left(-i\frac{\partial}{\partial\theta}\right)^2 + E_L\left(-i\frac{\partial}{\partial l}+\theta\right)^2 - E_J\cos(\theta+\varphi) - E_Q\cos[2\pi(l-k)], \tag{B3}$$

where $\psi_m(l,\theta;k,\varphi)$ satisfies generalized periodic boundary conditions

$$\psi_m(-1/2,\theta;k,\varphi) = \psi_m(1/2,\theta;k,\varphi),$$
$$\psi_m(l,-\pi;k,\varphi) = e^{2\pi li}\psi_m(l,\pi;k,\varphi).$$

In this representation, it is straightforward to compute the eigensystem of mode 1 numerically.

It is illustrative to evaluate the well-known *LC* harmonic oscillator ground states in the Zak basis, $\hat{H}_{\rm HO}$. In the phase basis, $\psi_0^{(0)}(\phi) = (\pi z)^{-\frac{1}{4}}e^{-\frac{\phi^2}{2z}}$, where $z = \sqrt{E_C/E_L}$. In the Zak basis, we find that

$$\psi_0^{(0)}(k,\varphi) = \sum_{j=-\infty}^{\infty} e^{-2\pi jki}\psi_0^{(0)}(\varphi-2\pi j) = (\pi z)^{-\frac{1}{4}}e^{-\frac{\varphi^2}{2z}}\vartheta_3\left(\pi k + i\pi\varphi/z, e^{-\frac{2\pi^2}{z}}\right), \tag{B4}$$

where $\vartheta_3(u,q) \equiv 1 + 2\sum_{j=1}^{\infty} q^{j^2}\cos(2uj)$ is an elliptic theta function. The Zak basis highlights the relative localisation of the ground state in k or φ. We plot this function for $z = \pi$, 2π, and 4π in Fig. 6. When the energy scales for the kinetic and potential terms are balanced, at $z = 2\pi$, the ground state is equally delocalized in each coordinate. At this point, the JJ and QPS renormalisation scale factors are equal, i.e., $E_J'/E_J = E_Q'/E_Q$.

APPENDIX C: EVALUATING $\hat{\mathcal{A}}_n$ IN THE GROUND STATE EIGENBASIS MANIFOLD $\{|\Psi_{0;k,\varphi}\rangle_{1,2}\}$

Here we compute ${}_{1,2}\langle\Psi_{0;k,\varphi}|\,\hat{\mathcal{A}}_n\,|\Psi_{0;k',\varphi'}\rangle_{1,2}$:

$${}_{1,2}\langle\Psi_{0;k,\varphi}|\,\hat{\mathcal{A}}_n\,|\Psi_{0;k',\varphi'}\rangle_{1,2} = 2E_{C1}\langle\psi_0(k,\varphi)|\,\hat{n}_1\,|\psi_0(k,\varphi)\rangle_1\delta(k-k')\delta(\varphi-\varphi'). \tag{C1}$$

We expand $|\psi_m(k,\varphi)\rangle_1$ to first order in perturbation theory, and for notational convenience we define the matrix element $[\![\hat{B}]\!]_{jm} = {}_1\langle\psi_j^{(0)}|\,\hat{B}\,|\psi_m^{(0)}\rangle_1$ for an operator $\hat{B}$, so

$$|\psi_m(k,\varphi)\rangle_1 = \left|\psi_m^{(0)}\right\rangle_1 + \sum_{j\neq m}\frac{[\![\hat{V}(k,\varphi)]\!]_{jm}}{\Delta E_{mj}^{(0)}}\left|\psi_j^{(0)}\right\rangle_1, \tag{C2}$$

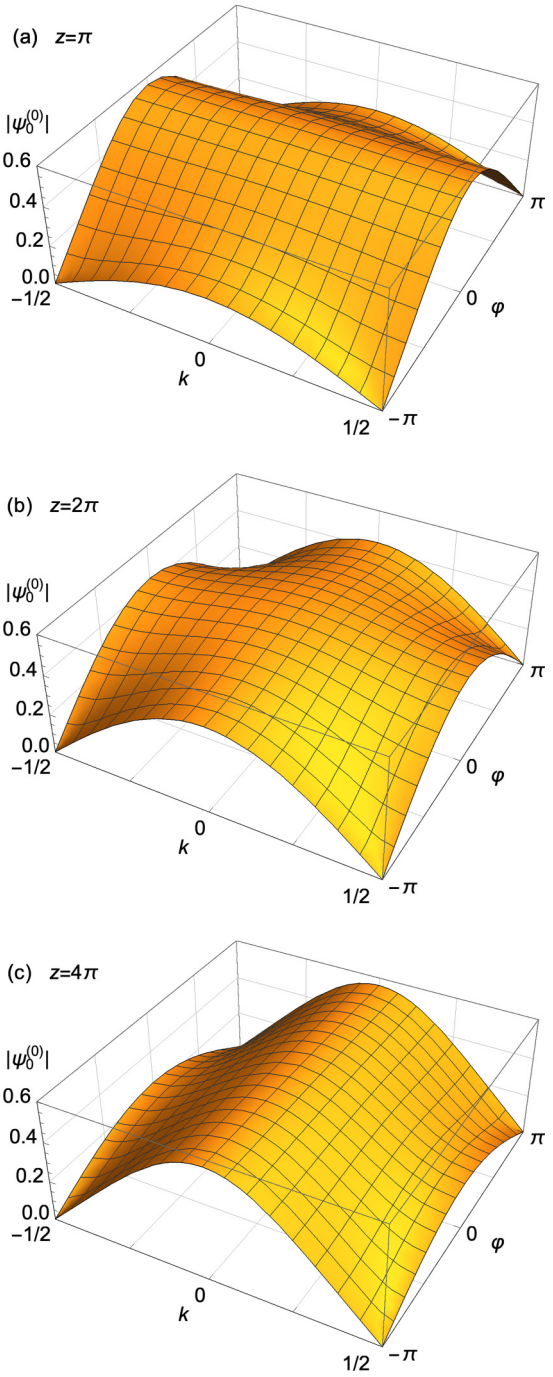

FIG. 6. The harmonic oscillator eigenstates in the Zak basis, $|\langle k,\varphi\,|\psi_0^{(0)}\rangle\,|$, for different values of $z = \sqrt{E_C/E_L}$. (a) For $z < 2\pi$, $\psi_0^{(0)}(k,\varphi)$ is somewhat localized in the modular phase (alternatively, the quasiflux) coordinate, φ, but delocalized in k. (b) For $z = 2\pi$, $\psi_0^{(0)}(k,\varphi)$ is equally delocalized in both coordinates. (c) For $z > 2\pi$, $\psi_0^{(0)}(k,\varphi)$ is somewhat localized in the modular number coordinate (alternatively, the quasicharge [14]), k, but delocalized in φ.

where $\Delta E^{(0)}_{mj} = E^{(0)}_m - E^{(0)}_j = \hbar\Omega(m-j)$. Then,

$$
\begin{aligned}
&{}_1\langle\psi_0(k,\varphi)|\,\hat{n}_1\,|\psi_0(k,\varphi)\rangle_1 \\
&= [\![\hat{n}_1]\!]_{00} + 2\sum_{m\neq 0}\mathrm{Re}\left(\frac{[\![\hat{n}_1]\!]_{0m}[\![\hat{V}(k,\varphi)]\!]_{m0}}{\Delta E^{(0)}_{0m}}\right) + O\left(\left|\frac{V}{\Delta E}\right|^2\right).
\end{aligned}
\tag{C3}
$$

We write the coordinate $\hat{n}_1$ in terms of creation and annihilation operators $\hat{a}_1^\dagger$ and $\hat{a}_1$, i.e., $\hat{n}_1 = i(\hat{a}_1^\dagger - \hat{a}_1)/\sqrt{2z}$. Since $\hat{a}_1^\dagger$ and $\hat{a}_1$ are off-diagonal in the harmonic oscillator eigenbasis, we find $[\![\hat{n}_1]\!]_{0m} = -i\,\delta_{m,1}/\sqrt{2z}$. Ignoring terms $O(|\frac{V}{\Delta E}|^2)$ and higher, we find

$$
{}_1\langle\psi_0(k,\varphi)|\,\hat{n}_1\,|\psi_0(k,\varphi)\rangle_1 = 2\,\mathrm{Re}\left(\frac{[\![\hat{n}_1]\!]_{01}[\![\hat{V}(k,\varphi)]\!]_{10}}{\Delta E^{(0)}_{01}}\right).
\tag{C4}
$$

Evaluating the matrix element for $\hat{V}(k,\varphi)$ gives

$$
\begin{aligned}
[\![\hat{V}(k,\varphi)]\!]_{10} &= -E_Q\,{}_1\langle\psi_1^{(0)}|\cos[2\pi(\hat{n}_1-k)]\,|\psi_0^{(0)}\rangle_1 \\
&\quad - E_J\,{}_1\langle\psi_1^{(0)}|\cos(\hat{\phi}_1+\varphi)\,|\psi_0^{(0)}\rangle_1 \\
&= -E_Q\int_{-\infty}^{\infty} dn\cos[2\pi(n-k)]\psi_1^{(0)}(n)^*\psi_0^{(0)}(n) \\
&\quad - E_J\int_{\infty}^{\infty} d\phi\cos(\phi+\varphi)\psi_1^{(0)}(\phi)^*\psi_0^{(0)}(\phi) \\
&= e^{-\frac{z}{4}}\sqrt{\frac{z}{2}}E_J\sin(\varphi) - i\pi e^{-\frac{\pi^2}{z}}\sqrt{\frac{2}{z}}E_Q\sin(2\pi k).
\end{aligned}
$$

We substitute the results into Eq. (C1) and, noting that $\hbar\Omega z = 2E_C$, we obtain Eq. (26a).

The computation for ${}_{1,2}\langle\Psi_{0;k,\varphi}|\,\hat{\mathcal{A}}_\phi\,|\Psi_{0;k',\varphi'}\rangle_{1,2}$ is implemented in a similar manner.

APPENDIX D: RESONATOR BASED CHARGE SYNDROME MEASUREMENT AND QUBIT READOUT

We recall that the external charge n_x typically drifts over time, which is a source of noise for the dualmon. It is thus necessary to detect and correct such type of charge noise. A possible way to do so is as follows. First, from Eqs. (23), (27a), and (27b) it follows that one can couple to the system operators

$$
\hat{\mathcal{A}}'_n = 2\pi E'_Q\sin(2\pi\hat{n}_2), \tag{D1a}
$$

$$
\hat{\mathcal{A}}'_\phi = E'_J\sin(\hat{\phi}_2), \tag{D1b}
$$

by capacitively or inductively coupling to the dualmon circuit, respectively. Focusing on an encoding into the ground state $|0,0\rangle$ and one saddle point $|0,\pi\rangle$, the operator $\hat{\mathcal{A}}'_n$ can act as syndrome for charge noise. This follows from the fact that a shift in external charge $n_x \to n_x - \varepsilon$ can equivalently be interpreted as a shift in k. Since $\sin(2\pi\hat{n}_2)\,|\varepsilon,\varphi\rangle = \sin(2\pi\varepsilon)\,|\varepsilon,\varphi\rangle$, a shift with magnitude $|\varepsilon| < 1/4$ can in principle be detected by nondestructively measuring $\hat{\mathcal{A}}'_n$.

Also, a measurement of $\hat{\mathcal{A}}'_\phi$ interestingly can be used to readout the logical qubit state. Particularly, we can set the external flux to $\phi_x = -\pi/2$ such that $\hat{\mathcal{A}}'_\phi \to \hat{\mathcal{A}}'_{\phi+\pi/2} = E'_J\cos(\hat{\phi}_2)$. As $\cos(\hat{\phi}_2)\,|0,0\rangle = |0,0\rangle$ and $\cos(\hat{\phi}_2)\,|0,\pi\rangle = -|0,\pi\rangle$, a measurement of this operator corresponds to a logical basis measurement. Moreover, the $\hat{\mathcal{A}}'_\phi$ measurement is robust to small shifts in φ.

A potential approach to nondestructively measuring the operators $\hat{\mathcal{A}}'_n$ and $\hat{\mathcal{A}}'_\phi$ is to couple the dualmon circuit to a resonator. The resulting coupling is of the similar form to Eq. (23) with the replacements $n_x(t) \to n_x(t) + \hat{n}_r$, $\phi_x(t) \to \phi_x(t) + \hat{\phi}_r$, for capacitive or inductive coupling, respectively. Here $\hat{n}_r \sim \hat{a}_r^\dagger + \hat{a}_r$ is the charge bias and $\hat{\phi}_r \sim i\hat{a}_r^\dagger - i\hat{a}_r$ the flux bias due to the resonator, with $\hat{a}_r$ the resonator annihilation operator. The nondemolition measurement of interest then may be performed by modulating the coupling strength, based on the longitudinal readout scheme proposed in Ref. [42]. A similar scheme might even be employed to enact resonator induced one-qubit and two-qubit phase gates [43]. A more detailed study of resonator based readout and control will be the subject of future work.

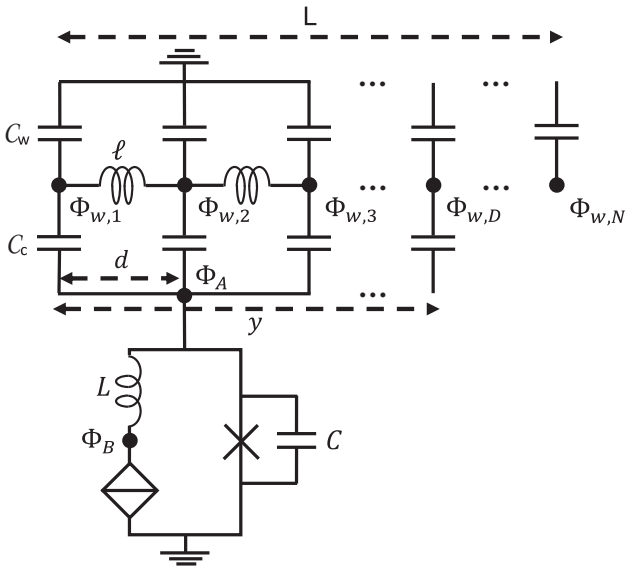

FIG. 7. Microscopic model of the capacitive coupling of the realistic dualmon circuit to the waveguide.

APPENDIX E: COUPLING TO A WAVEGUIDE

1. Hamiltonian derivation

Figure 7 shows the microscopic model of the capacitive coupling between the realistic dualmon circuit and the waveguide. The waveguide of length L is discretely decomposed into unit cells of length d. The number of unit cells is $N = \mathsf{L}/d$, each of which has an inductance ℓ and a ground capacitance $\mathcal{C}_w$; the waveguide inductance and capacitance per unit length are $\bar{\ell} = \mathsf{L}/d$ and $\bar{\mathcal{C}}_w = \mathcal{C}_w/d$. The coupling capacitance is C_c. This capacitance has a length of y across $D = y/d$ unit cells of the waveguide, yielding a distributed coupling capacitance $\mathcal{C}_c = C_c/D$ per unit cell. We also assume that the size of the coupling capacitance is very small compared to that of the waveguide, i.e., $y \ll \mathsf{L}$.

Starting from the classical equations of motion, the Lagrangian of the net circuit is given by

$$\begin{aligned}\mathcal{L}_{\rm tot} &= \dot{\Phi}_B Q_Q(\dot{\Phi}_B) + \frac{2eV_c}{2\pi}\cos\left(\frac{2\pi}{2e}Q_Q(\dot{\Phi}_B)\right) + \frac{C}{2}\dot{\Phi}_A^2 \\ &+ \sum_{j=1}^{D}\frac{\mathcal{C}_c}{2}(\dot{\Phi}_{w,j}-\dot{\Phi}_A)^2 + \sum_{j=1}^{N}\frac{\mathcal{C}_w}{2}\dot{\Phi}_{w,j}^2 \\ &+ \frac{I_c\Phi_0}{2\pi}\cos\left(\frac{2\pi}{\Phi_0}\Phi_A\right) - \frac{1}{2L}(\Phi_A-\Phi_B)^2 \\ &- \sum_{j=1}^{N}\frac{1}{2\ell}(\Phi_{w,j+1}-\Phi_{w,j})^2, \end{aligned} \tag{E1}$$

where

$$Q_Q(\dot{\Phi}_B) = \frac{2e}{2\pi}\arcsin(\dot{\Phi}_B/V_c). \tag{E2}$$

The momenta $Q_A, Q_B, Q_{w,1}, \ldots, Q_{w,N}$ are respectively

$$Q_A = C\dot{\Phi}_A + \sum_{j=1}^{D}\mathcal{C}_c(\dot{\Phi}_A - \dot{\Phi}_{w,j}), \tag{E3}$$

$$Q_B = Q_Q(\dot{\Phi}_B), \tag{E4}$$

$$Q_{w,j} = \mathcal{C}_c(\dot{\Phi}_{w,j}-\dot{\Phi}_A) + \mathcal{C}_w\dot{\Phi}_{w,j}, \quad j = 1,\ldots,D, \tag{E5}$$

$$Q_{w,j} = \mathcal{C}_w\dot{\Phi}_{w,j}, \quad j = D+1,\ldots,N. \tag{E6}$$

The Hamiltonian is then

$$\begin{aligned}\mathcal{H}_{\rm tot} &= -\frac{2eV_c}{2\pi}\cos\left(\frac{2\pi}{2e}Q_Q(\dot{\Phi}_B)\right) - \frac{I_c\Phi_0}{2\pi}\cos\left(\frac{2\pi}{\Phi_0}\Phi_A\right) \\ &+ \frac{1}{2L}(\Phi_A-\Phi_B)^2 + \sum_{j=1}^{N}\frac{1}{2\ell}(\Phi_{w,j+1}-\Phi_{w,j})^2 \\ &+ \frac{C}{2}\dot{\Phi}_A^2 + \sum_{j=1}^{D}\frac{\mathcal{C}_c}{2}(\dot{\Phi}_{w,j}-\dot{\Phi}_A)^2 + \sum_{j=1}^{N}\frac{\mathcal{C}_w}{2}\dot{\Phi}_{w,j}^2. \end{aligned} \tag{E7}$$

Equations (E4) and (E6) show

$$\dot{\Phi}_B = V_c\sin\left(\frac{2\pi}{2e}Q_B\right), \tag{E8}$$

$$\dot{\Phi}_j = Q_{w,j}/\mathcal{C}_w, \quad j = D+1,\ldots,N. \tag{E9}$$

Thus, to express $\mathcal{H}_{tot}$ in terms of coordinates and conjugate momenta requires one to find

$$\dot{\Phi}_A = \dot{\Phi}_A(Q_A, Q_{w,1}, \ldots, Q_{w,D}), \tag{E10}$$

$$\dot{\Phi}_{w,j} = \dot{\Phi}_{w,j}(Q_A, Q_{w,1}, \ldots, Q_{w,D}), \quad j = 1,\ldots,D, \tag{E11}$$

which, from Eqs. (E3) and (E5), are determined by solving the system of equations

$$\begin{aligned} C\dot{\Phi}_A + \sum_{j=1}^{D}\mathcal{C}_c(\dot{\Phi}_A-\dot{\Phi}_{w,j}) &= Q_A, \\ \mathcal{C}_c(\dot{\Phi}_{w,1}-\dot{\Phi}_A) + \mathcal{C}_w\dot{\Phi}_{w,1} &= Q_{w,1}, \\ &\vdots \\ \mathcal{C}_c(\dot{\Phi}_{w,D}-\dot{\Phi}_A) + \mathcal{C}_w\dot{\Phi}_{w,D} &= Q_{w,D}. \end{aligned} \tag{E12}$$

We substitute the solutions of (E12) [and Eqs. (E8) and (E9) as well] into Eq. (E7), keep terms to first order of $\mathcal{C}_c$ only, and get

$$\begin{aligned}\mathcal{H}_{\rm tot} &= -\frac{2eV_c}{2\pi}\cos\left(\frac{2\pi}{2e}Q_B\right) - \frac{I_c\Phi_0}{2\pi}\cos\left(\frac{2\pi}{\Phi_0}\Phi_A\right) \\ &+ \frac{1}{2L}(\Phi_A-\Phi_B)^2 + \frac{C-D\mathcal{C}_c}{2C^2}Q_A^2 \\ &+ \sum_{j=1}^{D}\frac{\mathcal{C}_w-\mathcal{C}_c}{2\mathcal{C}_w^2}Q_{w,j}^2 + \sum_{j=D+1}^{N}\frac{1}{2\mathcal{C}_w}Q_{w,j}^2 \\ &+ \sum_{j=1}^{N}\frac{1}{2\ell}(\Phi_{w,j+1}-\Phi_{w,j})^2 + \sum_{j=1}^{D}\frac{\mathcal{C}_c}{\mathcal{C}_w C}Q_A Q_{w,j}. \end{aligned} \tag{E13}$$

Note that for $\mathcal{C}_c$ very small compared to other capacitances, we have $(C-D\mathcal{C}_c)/(2C^2) \approx 1/(2C)$ and $(\mathcal{C}_w-\mathcal{C}_c)/(2\mathcal{C}_w^2) \approx 1/(2\mathcal{C}_w)$. We then set

$$\begin{aligned} E_{\mathcal{C}_w} &= (2e)^2/(2\mathcal{C}_w), \quad E_\ell = \Phi_0^2/(8\pi^2\ell), \\ E_{\mathcal{C}_c} &= \mathcal{C}_c(2e)^2/(\mathcal{C}_w C), \\ n_{w,j} &= Q_{w,j}/(2e), \quad \phi_{w,j} = 2\pi\Phi_{w,j}/\Phi_0, \end{aligned}$$

use notations defined in Appendix A, and change the coordinates of the dualmon circuit as in Eq. (13) to simplify Eq. (E13) into

$$\hat{\mathcal{H}}_{\rm tot} = \hat{\mathcal{H}}_{\rm sys} + \hat{\mathcal{H}}_{\rm wg} + \hat{\mathcal{H}}_{\rm coup}, \tag{E14}$$

where

$$\begin{aligned}\hat{\mathcal{H}}_{\rm sys} &= E_C\hat{n}_1^2 + E_L\hat{\phi}_1^2 - E_Q\cos[2\pi(\hat{n}_1-\hat{n}_2)] \\ &- E_J\cos(\hat{\phi}_1+\hat{\phi}_2), \end{aligned} \tag{E15}$$

$$\hat{\mathcal{H}}_{\rm wg} = \sum_{j=1}^{N}E_{\mathcal{C}_w}\hat{n}_{w,j}^2 + E_\ell(\hat{\phi}_{w,j+1}-\hat{\phi}_{w,j})^2, \tag{E16}$$

$$\hat{\mathcal{H}}_{\rm coup} = \sum_{j=1}^{D}E_{\mathcal{C}_c}\hat{n}_1\hat{n}_{w,j}. \tag{E17}$$

2. Diagonalization of the waveguide Hamiltonian

We diagonalize the bare Hamiltonian of the waveguide in Eq. (E16). We first define the traveling modes

$$\begin{aligned}\bar{\phi}_s &= \frac{1}{\sqrt{N}}\sum_{j=1}^{N}e^{-2\pi ijk/N}\hat{\phi}_{w,j}, \\ \bar{n}_s &= \frac{1}{\sqrt{N}}\sum_{j=1}^{N}e^{2\pi ijk/N}\hat{n}_{w,j}, \end{aligned} \tag{E18}$$

which have the inverse

$$\begin{aligned}\hat{\phi}_{w,j} &= \frac{1}{\sqrt{N}}\sum_{k=0}^{N-1}e^{2\pi ijk/N}\bar{\phi}_s, \\ \hat{n}_{w,j} &= \frac{1}{\sqrt{N}}\sum_{k=0}^{N-1}e^{-2\pi ijk/N}\bar{n}_s. \end{aligned} \tag{E19}$$

By this, Eq. (E16) becomes

$$\hat{\mathcal{H}}_{\rm wg} = 2\sum_{k=0}^{N/2-1} E_{\mathcal{C}_w}\bar{n}_s\bar{n}_{N-s} + 2E_\ell\left[1-\cos\left(\frac{2\pi k}{N}\right)\right]\bar{\phi}_s\bar{\phi}_{N-s}. \tag{E20}$$

We then introduce symmetric and antisymmetric modes

$$\begin{aligned}
\tilde{n}_{s,+} &= (\bar{n}_s + \bar{n}_{N-s})/\sqrt{2},\\
\tilde{n}_{s,-} &= i(\bar{n}_s - \bar{n}_{N-s})/\sqrt{2},\\
\tilde{\phi}_{s,+} &= (\bar{\phi}_s + \bar{\phi}_{N-s})/\sqrt{2},\\
\tilde{\phi}_{s,-} &= -i(\bar{\phi}_s - \bar{\phi}_{N-s})/\sqrt{2},
\end{aligned} \tag{E21}$$

where $0 < k < N/2-1$. It follows that

$$\begin{aligned}
\hat{\mathcal{H}}_{\rm wg} = &\sum_{s=0}^{N/2-1} E_{\mathcal{C}_w}\left(\tilde{n}_{s,+}^2 + \tilde{n}_{s,-}^2\right)\\
&+2E_\ell\left(1-\cos\frac{2\pi s}{N}\right)\left(\tilde{\phi}_{s,+}^2 + \tilde{\phi}_{s,-}^2\right).
\end{aligned} \tag{E22}$$

We define

$$\begin{aligned}
\tilde{n}_{s,\pm} &= \left(\frac{2E_\ell(1-\cos 2\pi s/N)}{E_{\mathcal{C}_w}}\right)^{1/4}\tilde{\tilde{n}}_{s,\pm},\\
\tilde{\phi}_{s,\pm} &= \left(\frac{E_{\mathcal{C}_w}}{2E_\ell(1-\cos 2\pi s/N)}\right)^{1/4}\tilde{\tilde{\phi}}_{s,\pm},\\
\hat{a}_{s,\pm} &= (-i\tilde{\tilde{\phi}}_{s,\pm} + \tilde{\tilde{n}}_{s,\pm})/\sqrt{2},\\
\hat{a}_{s,\pm}^\dagger &= (i\tilde{\tilde{\phi}}_{s,\pm} + \tilde{\tilde{n}}_{s,\pm})/\sqrt{2},\\
\hbar\omega_s &= \sqrt{2E_{\mathcal{C}_w}E_\ell[1-\cos(2\pi s/N)]},
\end{aligned} \tag{E23}$$

and take the limit $N\to\infty$ to achieve

$$\omega_s = \pi s/(\mathsf{L}\sqrt{\bar{\mathcal{C}}_w\bar{\ell}}), \tag{E24}$$

$$\hat{\mathcal{H}}_{\rm wg} = \sum_{s=0}^{\infty}\hbar\omega_s(\hat{a}_{s,+}^\dagger\hat{a}_{s,+} + \hat{a}_{s,-}^\dagger\hat{a}_{s,-}). \tag{E25}$$

3. The coupling Hamiltonian

We rewrite the coupling Hamiltonian (E17) in terms of $\hat{a}_{s,\pm}$ and $\hat{a}_{s,\pm}^\dagger$. Concretely,

$$\begin{aligned}
\hat{\mathcal{H}}_{\rm coup} &= \sum_{j=1}^{D} E_{\mathcal{C}_c}\hat{n}_1\hat{n}_{w,j} = \sum_{j=1}^{D} E_{\mathcal{C}_c}\hat{n}_1\frac{1}{\sqrt{N}}\sum_{s=0}^{N-1} e^{-2\pi ijs/N}\bar{n}_s = \sum_{j=1}^{D} E_{\mathcal{C}_c}\hat{n}_1\frac{1}{\sqrt{N}}\sum_{s=1}^{N/2-1}(e^{-2\pi ijs/N}\bar{n}_s + e^{2\pi ijs/N}\bar{n}_{N-s})\\
&= \sum_{j=1}^{D} E_{\mathcal{C}_c}\hat{n}_1\frac{1}{\sqrt{N}}\sum_{s=1}^{N/2-1}[e^{-2\pi ijs/N}(\tilde{n}_{s,+} - i\tilde{n}_{s,-})/\sqrt{2} + e^{2\pi ijs/N}(\tilde{n}_{s,+} + i\tilde{n}_{s,-})/\sqrt{2}]\\
&= \sum_{j=1}^{D} E_{\mathcal{C}_c}\hat{n}_1\sqrt{\frac{2}{N}}\sum_{s=1}^{N/2-1}[\cos(2\pi js/N)\tilde{n}_{s,+} - \sin(2\pi js/N)\tilde{n}_{s,-}]\\
&= E_{\mathcal{C}_c}\hat{n}_1\sqrt{\frac{2}{N}}\sum_{s=1}^{N/2-1}\int_0^y\frac{dx}{d}[\cos(2\pi sx/\mathsf{L})\tilde{n}_{s,+} - \sin(2\pi sx/\mathsf{L})\tilde{n}_{s,-}]\quad(x = jd)\\
&= E_{\mathcal{C}_c}\hat{n}_1\sqrt{\frac{2}{N}}\sum_{s=1}^{N/2-1}\left(\frac{\mathsf{L}}{2\pi sd}\sin(2\pi sy/\mathsf{L})\tilde{n}_{s,+} - \frac{\mathsf{L}}{\pi sd}\sin^2(\pi sy/\mathsf{L})\tilde{n}_{s,-}\right)\\
&= E_{\mathcal{C}_c}\hat{n}_1\sqrt{\frac{2}{N}}\sum_{s=1}^{N/2-1}\left(\frac{y}{d}\tilde{n}_{s,+} - \frac{\pi sy^2}{d\mathsf{L}}\tilde{n}_{s,-}\right)\quad\text{(the second term will be dropped in the limit }\mathsf{L}\to\infty)\\
&= \frac{C_c(2e)^2}{\mathcal{C}_wC}\hat{n}_1\sqrt{\frac{2}{N}}\sum_{s=1}^{N/2-1}\tilde{n}_{s,+}\quad[\text{note that } E_{\mathcal{C}_c} = \mathcal{C}_c(2e)^2/(\mathcal{C}_wC)\text{ and }\mathcal{C}_cy/d = \mathcal{C}_cD = C_c]\\
&= \frac{C_c(2e)^2}{\mathcal{C}_wC}\hat{n}_1\sqrt{\frac{2}{N}}\sum_{s=1}^{N/2-1}\left(\frac{2E_\ell[1-\cos(2\pi s/N)]}{E_{\mathcal{C}_w}}\right)^{1/4}\tilde{\tilde{n}}_{s,+} = \frac{C_c(2e)^2}{\mathcal{C}_wC}\hat{n}_1\sqrt{\frac{2}{N}}\sum_{s=1}^{N/2-1}\left(\frac{4E_\ell(\pi sd/\mathsf{L})^2}{E_{\mathcal{C}_w}}\right)^{1/4}\tilde{\tilde{n}}_{s,+}\\
&= \frac{C_c(2e)^2}{\bar{\mathcal{C}}_wC}\hat{n}_1\sqrt{\frac{2}{\mathsf{L}}}\sum_{s=1}^{N/2-1}\left(\frac{E_\ell}{E_{\mathcal{C}_w}}\right)^{1/4}\left(\frac{2\pi s}{\mathsf{L}}\right)^{1/2}\tilde{\tilde{n}}_{s,+} = \sum_{s=0}^{\infty} g_s(\hat{a}_{s,+}^\dagger + \hat{a}_{s,+})\hat{n}_1,
\end{aligned} \tag{E26}$$

where

$$g_s = (2eC_c/C)\sqrt{2\hbar\omega_s/(\bar{\mathcal{C}}_w\mathsf{L})}. \tag{E27}$$

Since $\hat{\mathcal{H}}_{\rm coup}$ couples only modes $(s,+)$ of the waveguide to the dualmon system, in the expression of $\hat{\mathcal{H}}_{\rm wg}$ in Eq. (E25) we can ignore modes $(s,-)$. For brevity we further shorten the subscript $(s,+)$ into s, yielding

$$\hat{\mathcal{H}}_{\rm wg} = \sum_s \hbar\omega_s \hat{a}_s^\dagger \hat{a}_s, \tag{E28}$$

$$\hat{\mathcal{H}}_{\rm coup} = \sum_s g_{\omega_s}(\hat{a}_s^\dagger + \hat{a}_s)\hat{n}_1. \tag{E29}$$

Taking the continuum limit [44], the two above Hamiltonians become

$$\hat{\mathcal{H}}_{\rm wg} = \int_{-\infty}^{\infty} d\omega\, \hbar\omega \hat{a}^\dagger(\omega)\hat{a}(\omega), \tag{E30}$$

$$\hat{\mathcal{H}}_{\rm coup} = \int_{-\infty}^{\infty} d\omega\, g(\omega)[\hat{a}^\dagger(\omega) + \hat{a}(\omega)]\hat{n}_1, \tag{E31}$$

where the lower limit of the frequency ω has been extended to $-\infty$ [31], and

$$g(\omega) = (2eC_c/C)\sqrt{2\hbar\omega Z_{\rm wg}/\pi}, \tag{E32}$$

with $Z_{\rm wg} = \sqrt{\ell/\mathcal{C}_w}$ the waveguide impedance. The spectral density is given by

$$J(\omega) = \frac{1}{\hbar^2}\int_{-\infty}^{\infty} d\omega\, g^2(\omega)\delta(\omega-\omega_s) = \frac{8e^2}{\pi\hbar}\frac{C_c^2}{C^2}Z_{\rm wg}\omega. \tag{E33}$$

We can write $J(\omega) = \nu\hbar\omega$ with

$$\nu = \frac{8e^2}{\pi\hbar^2}\frac{C_c^2}{C^2}Z_{\rm wg}. \tag{E34}$$

APPENDIX F: INPUT-OUTPUT CALCULATIONS

We employ the rotating wave approximation and the Markov approximation [31,32] to simplify the coupling Hamiltonian in Eq. (E31) to

$$\hat{\mathcal{H}}_{\rm coup} = \int_{-\infty}^{\infty} d\omega\hbar\sqrt{\gamma/2\pi}[\hat{a}^\dagger(\omega)\hat{n}_1^- + \hat{a}(\omega)\hat{n}_1^+], \tag{F1}$$

where $\hbar\sqrt{\gamma/2\pi} \equiv g(\omega_D)$ is the coupling strength evaluated at the drive frequency ω_D, and $\hat{n}_1^+$ ($\hat{n}_1^-$) is the lower (upper) triangularized version of $\hat{n}_1$. Note that the Markov approximation is valid in the regime of narrow-band interaction, and the operator $\hat{n}_1^+$ in terms of the eigenbasis $\{|\Psi_{m;k,\varphi}\rangle_{1,2}\}$ is of the form

$$\hat{n}_1^+ = \sum_{m>n}\int_{-1/2}^{1/2}\int_{-\pi}^{\pi} dk\, d\varphi_{1,2}\langle\Psi_{m;k,\varphi}|\hat{n}_1|\Psi_{n;k,\varphi}\rangle_{1,2} \times |\Psi_{m;k,\varphi}\rangle_{1,2}\langle\Psi_{n;k,\varphi}|. \tag{F2}$$

The master equations for the system density operator and the input-output relation are then, using the results in Refs. [31,32], given by Eqs. (31)–(33) in the main text.

The spectrum displayed in Fig. 5 is obtained by assuming the dualmon state initially in the ground state manifold with a specific pair of (k,φ), say, the state $|\Psi_{0;k,\varphi}\rangle_{1,2}$. We then approximate the dualmon as a two-level system with eigensystem

$$|\Psi_{0;k,\varphi}\rangle_{1,2}, \quad E_{0;k,\varphi} = \hbar\Omega/2 - E'_Q\cos(2\pi k) - E'_J\cos(\varphi),$$
$$|\Psi_{1;k,\varphi}\rangle_{1,2}, \quad E_{1;k,\varphi} = 3\hbar\Omega/2 - E''_Q\cos(2\pi k) - E''_J\cos(\varphi),$$

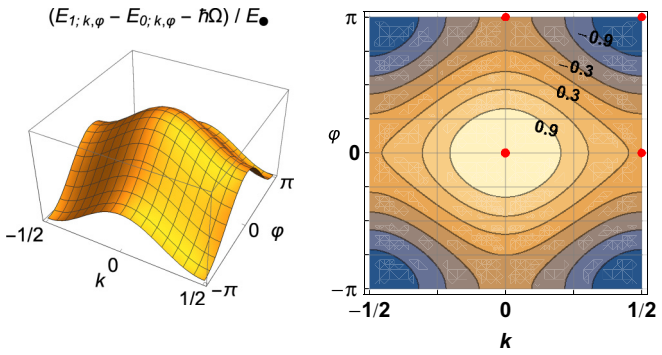

FIG. 8. (Left) and (Right) Three-dimensional and contour plots of the transition frequency between the the ground state and first excited state manifolds relative to the unperturbed harmonic oscillator frequency, $\hbar\Omega^{(1,0)}_{k,\varphi} - \hbar\Omega \equiv E_{1;k,\varphi} - E_{0;k,\varphi} - \hbar\Omega$. The transition at the ground state ($k=0$, $\varphi=0$) and the maximally excited state ($k=1/2$, $\varphi=\pi$) is unique, i.e., maximal and minimal respectively, whereas the transition at each saddle point is degenerate. For illustrative purposes, plots are drawn with $E_Q = E_J \equiv E_\bullet$, $E_C/E_J = 200$, and $E_L/E_J = 10$.

where

$$\begin{aligned} E'_Q &= e^{-\pi^2/z}E_Q, \\ E'_J &= e^{-z/4}E_J, \\ E''_Q &= (1-2\pi^2/z)E'_Q, \\ E''_J &= (1-z/2)E'_J. \end{aligned} \tag{F3}$$

The transition frequency, $\hbar\Omega^{(1,0)}_{k,\varphi} = E_{1;k,\varphi} - E_{0;k,\varphi}$, is

$$\hbar\Omega^{(1,0)}_{k,\varphi} = \hbar\Omega + \frac{2\pi^2}{z}E'_Q\cos(2\pi k) + \frac{z}{2}E'_J\cos(\varphi). \tag{F4}$$

In Fig. 8, we plot the variation of $\Omega^{(1,0)}_{k,\varphi}$ with respect to (k,φ). The transition is unique at the ground state ($k=0$, $\varphi=0$) and the maximally excited state ($k=1/2$, $\varphi=\pi$) only, being maximal and minimal respectively.

We move to the frame rotating at the drive frequency ω_D, making the master equation (31) time independent. We then solve for the steady-state solution of this master equation, and compute the transmission. Relevant parameters for plotting are chosen as $E_Q = E_J$, $\hbar\Omega = 40\sqrt{5}\,E_J$, $z = \sqrt{20}$, $\gamma = 0.01\,\omega_D$, and $\hbar\alpha^2 = 0.1\,E_J$. Interestingly, a time-dependent treatment with higher truncation for the transmission problem yields a considerably similar result.

APPENDIX G: SCANNING OVER BIAS CHARGE AND FLUX

We recall that the spectrum shown in Fig. 3 is computed by numerically solving the eigensystem of mode 1 described by the Hamiltonian $\hat{H}_1(k,\varphi)$ in Eq. (18) in the absence of flux and charge biases. When the two biases are nonzero, the Hamiltonian of mode 1 is

$$\hat{H}_1(k,\varphi;n_x,\phi_x) = E_C(\hat{n}_1+n_x)^2 + E_L(\hat{\phi}_1-\phi_x)^2 - E_Q\cos[2\pi(\hat{n}_1-k)] - E_J\cos(\phi_1+\varphi). \tag{G1}$$

It can be checked that, under the unitary transformation

$$\hat{U}(n_x, \phi_x) = \exp(i\hat{n}_1\phi_x)\exp(i\hat{\phi}_1 n_x), \tag{G2}$$

$\hat{H}_1(k, \varphi; n_x, \phi_x)$ becomes

$$\hat{U}(n_x, \phi_x)\hat{H}_1(k, \varphi; n_x, \phi_x)\hat{U}^\dagger(n_x, \phi_x) = \hat{H}_1(k + n_x, \varphi + \phi_x). \tag{G3}$$

This implies that the spectrum of $\hat{H}_1(k, \varphi; n_x, \phi_x)$ is obtained by shifting the origin of the $\hat{H}_1(k, \varphi)$ spectrum to $(-n_x, -\phi_x)$. After turning on the bias parameters, the system state (initially assumed to be an eigenstate) is changed into a new eigenstate with a new eigenenergy and new transition frequencies. Hence, scanning over the biases $n_x \in [-1/2, 1/2)$ and $\phi_x \in [-\pi, \pi)$ maps the full spectrum of the dualmon system.

APPENDIX H: THERMAL INDUCED DEPHASING RATE

We calculate the dephasing rates due to thermal excitations and relaxations for two different cases, that is, a qubit that is encoded in an ordinary two-level system and a qubit that is encoded in the ground state manifold analogous to the proposed dualmon qubit.

The master equation for the standard two-level-system case is

$$\dot{\rho} = -\frac{i}{\hbar}[\hat{H}, \rho] + \gamma_-\mathcal{D}[\hat{\sigma}_-]\rho + \gamma_+\mathcal{D}[\hat{\sigma}_+]\rho, \tag{H1}$$

where

$$\begin{aligned} \hat{H} &= \tfrac{1}{2}\hbar\omega(|e\rangle\langle e| - |g\rangle\langle g|), \\ \hat{\sigma}_- &= |g\rangle\langle e|, \\ \hat{\sigma}_+ &= |e\rangle\langle g|, \end{aligned} \tag{H2}$$

and γ_- (γ_+) is the relaxation (excitation) rate. From the master equation, we find the evolution equation for the off-diagonal element ρ_{eg} as follows:

$$\dot{\rho}_{eg} = -i\omega\rho_{eg} - \tfrac{1}{2}(\gamma_+ + \gamma_-)\rho_{eg}, \tag{H3}$$

showing the dephasing rate is proportional to the sum of both the relaxation and excitation rates.

With regards to the qubit encoded in the ground state manifold as in the dualmon device, we assume the system possesses a ground state manifold consisting of $|g_1\rangle$ and $|g_2\rangle$ and an excited state manifold with $|e_1\rangle$ and $|e_2\rangle$. By analogy to the coupling operator $\hat{n}_1$ in Sec. IV D, we further assume that the coupling of the system to a heat bath does not induce transitions within each manifold, but allows selected transitions between different manifolds, namely, $|g_j\rangle \leftrightarrow |e_j\rangle$ (not including $|g_j\rangle \leftrightarrow |e_{j'}\rangle$ for $j \neq j'$). In this case, the relevant master equation is

$$\dot{\varrho} = -\frac{i}{\hbar}[\hat{\mathcal{H}}, \varrho] + \sum_{j=1}^{2}(\gamma_-^{(j)}\mathcal{D}[\hat{\sigma}_-^{(j)}]\varrho + \gamma_+^{(j)}\mathcal{D}[\hat{\sigma}_+^{(j)}]\varrho), \tag{H4}$$

where

$$\begin{aligned} \hat{\mathcal{H}} &= \sum_{j=1}^{2}\frac{1}{2}\hbar\omega_j(|e_j\rangle\langle e_j| - |g_j\rangle\langle g_j|), \\ \hat{\sigma}_-^{(j)} &= |g_j\rangle\langle e_j|, \\ \hat{\sigma}_+^{(j)} &= |e_j\rangle\langle g_j|, \end{aligned} \tag{H5}$$

and $\gamma_-^{(j)}$ and $\gamma_+^{(j)}$ are respectively the relaxation and excitation rates between $|g_j\rangle$ and $|e_j\rangle$. The time evolution for the off-diagonal element $\varrho_{g_1g_2}$, which is related to dephasing of the dualmon qubit, is then

$$\dot{\varrho}_{g_1g_2} = \tfrac{1}{2}i(\omega_1 - \omega_2)\varrho_{g_1g_2} - \tfrac{1}{2}(\gamma_+^{(1)} + \gamma_+^{(2)})\varrho_{g_1g_2}. \tag{H6}$$

This result demonstrates that the dephasing rate for the dualmon qubit is determined by the excitation rates out of the ground state manifold only, remarkably differing from the standard two-level-system case.

[1] P. Bonderson and C. Nayak, Phys. Rev. B **87**, 195451 (2013).
[2] A. Kitaev, arXiv:cond-mat/0609441.
[3] P. Brooks, A. Kitaev, and J. Preskill, Phys. Rev. A **87**, 052306 (2013).
[4] J. M. Dempster, B. Fu, D. G. Ferguson, D. I. Schuster, and J. Koch, Phys. Rev. B **90**, 094518 (2014).
[5] P. Groszkowski, A. Di Paolo, A. Grimsmo, A. Blais, D. Schuster, A. Houck, and J. Koch, New J. Phys. **20**, 043053 (2018).
[6] A. D. Paolo, A. L. Grimsmo, P. Groszkowski, J. Koch, and A. Blais, New J. Phys. **21**, 043002 (2019).
[7] J. M. Martinis, M. H. Devoret, and J. Clarke, Phys. Rev. B **35**, 4682 (1987).
[8] J. Mooij and C. Harmans, New J. Phys. **7**, 219 (2005).
[9] J. Mooij and Y. V. Nazarov, Nat. Phys. **2**, 169 (2006).
[10] O. V. Astafiev, L. B. Ioffe, S. Kafanov, Y. A. Pashkin, K. Y. Arutyunov, D. Shahar, O. Cohen, and J. S. Tsai, Nature (London) **484**, 355 (2012).
[11] S. E. de Graaf, S. T. Skacel, T. Hönigl-Decrinis, R. Shaikhaidarov, H. Rotzinger, S. Linzen, M. Ziegler, U. Hübner, H. G. Meyer, V. Antonov, E. Il'ichev, A. V. Ustinov, A. Y. Tzalenchuk, and O. V. Astafiev, Nat. Phys. **14**, 590 (2018).
[12] D. Gottesman, A. Kitaev, and J. Preskill, Phys. Rev. A **64**, 012310 (2001).
[13] B. C. Travaglione and G. J. Milburn, Phys. Rev. A **66**, 052322 (2002).
[14] K. Likharev and A. Zorin, J. Low Temp. Phys. **59**, 347 (1985).
[15] J. Zak, Phys. Rev. Lett. **19**, 1385 (1967).
[16] M. H. Devoret, *Quantum Fluctuations in Electrical Circuits* (EDP Science, Les Ulis, France, 1997).
[17] A. A. Budini, Phys. Rev. A **64**, 052110 (2001).
[18] T. M. Stace and C. H. W. Barnes, Phys. Rev. A **65**, 062308 (2002).
[19] K. A. Matveev, A. I. Larkin, and L. I. Glazman, Phys. Rev. Lett. **89**, 096802 (2002).
[20] S. Ganeshan and M. Levin, Phys. Rev. B **93**, 075118 (2016).
[21] X. You, J. A. Sauls, and J. Koch, Phys. Rev. B **99**, 174512 (2019).
[22] J. Koch, V. Manucharyan, M. H. Devoret, and L. I. Glazman, Phys. Rev. Lett. **103**, 217004 (2009).

[23] V. E. Manucharyan, J. Koch, L. I. Glazman, and M. H. Devoret, Science **326**, 113 (2009).
[24] Y. Aharonov and A. Casher, Phys. Rev. Lett. **53**, 319 (1984).
[25] J. T. Peltonen, O. V. Astafiev, Y. P. Korneeva, B. M. Voronov, A. A. Korneev, I. M. Charaev, A. V. Semenov, G. N. Golt'sman, L. B. Ioffe, T. M. Klapwijk, and J. S. Tsai, Phys. Rev. B **88**, 220506(R) (2013).
[26] I. M. Pop, B. Douçot, L. Ioffe, I. Protopopov, F. Lecocq, I. Matei, O. Buisson, and W. Guichard, Phys. Rev. B **85**, 094503 (2012).
[27] V. E. Manucharyan, N. A. Masluk, A. Kamal, J. Koch, L. I. Glazman, and M. H. Devoret, Phys. Rev. B **85**, 024521 (2012).
[28] N. A. Masluk, I. M. Pop, A. Kamal, Z. K. Minev, and M. H. Devoret, Phys. Rev. Lett. **109**, 137002 (2012).
[29] M. Vanević and Y. V. Nazarov, Phys. Rev. Lett. **108**, 187002 (2012).
[30] J. T. Peltonen, Z. H. Peng, Y. P. Korneeva, B. M. Voronov, A. A. Korneev, A. V. Semenov, G. N. Gol'tsman, J. S. Tsai, and O. V. Astafiev, Phys. Rev. B **94**, 180508(R) (2016).
[31] C. W. Gardiner and M. J. Collett, Phys. Rev. A **31**, 3761 (1985).
[32] J. Combes, J. Kerckhoff, and M. Sarovar, Adv. Phys. X **2**, 784 (2017).
[33] H. P. Breuer and F. Petruccione, *The Theory of Open Quantum Systems* (Oxford University Press, Oxford, 2002).
[34] M. T. Bell, W. Zhang, L. B. Ioffe, and M. E. Gershenson, Phys. Rev. Lett. **116**, 107002 (2016).
[35] S. Gladchenko, D. Olaya, E. Dupont-Ferrier, B. Douçot, L. B. Ioffe, and M. E. Gershenson, Nat. Phys. **5**, 48 (2009).
[36] B. Douçot and L. B. Ioffe, Rep. Prog. Phys. **75**, 072001 (2012).
[37] M. T. Bell, J. Paramanandam, L. B. Ioffe, and M. E. Gershenson, Phys. Rev. Lett. **112**, 167001 (2014).
[38] W. Smith, A. Kou, X. Xiao, U. Vool, and M. Devoret, arXiv:1905.01206.
[39] T. M. Hazard, A. Gyenis, A. Di Paolo, A. T. Asfaw, S. A. Lyon, A. Blais, and A. A. Houck, Phys. Rev. Lett. **122**, 010504 (2019).
[40] V. Bouchiat, D. Vion, P. Joyez, D. Esteve, and M. Devoret, Phys. Scr. **1998**, 165 (1998).
[41] N. G. N. Constantino, M. S. Anwar, O. W. Kennedy, M. Dang, P. A. Warburton, and J. C. Fenton, Nanomaterials **8**, 442 (2018).
[42] N. Didier, J. Bourassa, and A. Blais, Phys. Rev. Lett. **115**, 203601 (2015).
[43] B. Royer, A. L. Grimsmo, N. Didier, and A. Blais, Quantum **1**, 11 (2017).
[44] S. Fan, Ş. E. Kocabaş, and J.-T. Shen, Phys. Rev. A **82**, 063821 (2010).

Building a bigger Hilbert space for superconducting devices, one Bloch state at a time

Dat Thanh Le,[1] Jared H. Cole,[2] and T. M. Stace[1,*]

[1]*ARC Centre for Engineered Quantum System, School of Mathematics and Physics, University of Queensland, Brisbane, QLD 4072, Australia*

[2]*Chemical and Quantum Physics, School of Science, RMIT University, Melbourne VIC 3001, Australia*

(Received 22 October 2019; accepted 4 February 2020; published 3 March 2020)

Superconducting circuits for quantum information processing are often described theoretically in terms of a discrete charge, or equivalently, a compact phase/flux, at each node in the circuit. Here we revisit the consequences of lifting this assumption for transmon and Cooper-pair box circuits, which are constituted from a Josephson junction and a capacitor, treating both the superconducting phase and charge as noncompact variables. The periodic Josephson potential gives rise to a Bloch band structure, characterized by the Bloch quasicharge. We analyze the possibility of creating superpositions of different quasicharge states by transiently shunting inductive elements across the circuit and suggest a choice of eigenstates in the lowest Bloch band of the spectrum that may support an inherently robust qubit encoding.

DOI: 10.1103/PhysRevResearch.2.013245

I. INTRODUCTION

In 1985, Likharev and Zorin [1] addressed the question of whether the superconducting phase at a circuit node, $\hat{\phi} = 2\pi\hat{\Phi}/\Phi_0$, is a compact variable, $\phi \in (-\pi, \pi]$, or whether it is noncompact, $\phi \in \mathbb{R}$? These alternatives represent distinct physics: if the phase is compact, then the spectrum is discrete, while if it is not compact, the spectrum can be a continuum. For some specific applications, these differences are not material, but they do lead to different physical predictions in general. In this paper, we revisit this question and analyze the experimental consequences.

To illustrate the physical differences between the choice of compact or noncompact flux/phase, consider a circuit node within a (quantized) electronic device. The flux associated to the node is Φ, which we nondimensionalize using the flux quantum, $\Phi_0 = h/(2e)$, to define the superconducting phase $\phi = 2\pi\Phi/\Phi_0$. A conjugate charge Q is associated to the node, and defining the dimensionless charge $n = Q/(2e)$, we impose the canonical commutation relation $[\hat{\phi}, \hat{n}] = i$.

If the Hamiltonian for the device is invariant under a subset of phase translations (e.g., the 2π-periodic phase-translation symmetry of a Josephson junction), then it is reasonably common to identify the phase with that of rotor [2], so that it is compact, and the states $|\phi\rangle_{\bar{\phi}}$ and $|\phi + 2\pi\rangle_{\bar{\phi}}$ are identical (the subscript $\bar{\phi}$ denotes the phase basis). It follows that the Hilbert space in the charge representation is discrete.

The converse holds: if the charge operator is assumed to be discrete, then it follows that the phase is compact. For instance, Bouchiat *et al.* [3] write the (dimensionless) charge operator as

$$\hat{n} = \sum\nolimits_{n\in\mathbb{Z}} n|n\rangle_{\bar{n}}\langle n|, \tag{1}$$

where the subscript $\bar{n}$ indicates the charge basis. In this representation, the charge is explicitly quantized: the nondegenerate spectrum of the charge operator is $\mathbb{Z}$. It follows that phase eigenstates are compact, since

$$|\phi\rangle_{\bar{\phi}} \equiv \sum\nolimits_{n\in\mathbb{Z}} e^{in\phi}\,|n\rangle_{\bar{n}} = |\phi + 2\pi\rangle_{\bar{\phi}}\,. \tag{2}$$

That is, $\mathsf{Spect}(\hat{\phi}) = (-\pi, \pi] \Leftrightarrow \mathsf{Spect}(\hat{n}) = \mathbb{Z}$, where $\mathsf{Spect}(\hat{\bullet})$ denotes the spectrum of the operator $\hat{\bullet}$. (In the rest of this paper, we use the convention that the symbol φ denotes a compact phase variable, and the symbol ϕ denotes a noncompact phase variable.)

An important corollary is that the discrete representation of the charge operator in Eq. (1) prohibits analysis of states with $\phi \notin (-\pi, \pi]$. This is important if a non-phase-translation invariant device (such as an inductor) is attached to the node. In this case, it is typical to assert that ϕ is noncompact. For instance, a conventional model for an oscillator (e.g., an *LC* circuit, or fluxonium) treats the phase ϕ as a noncompact, continuous variable, in which $|\phi\rangle_{\bar{\phi}}$ and $|\phi + 2\pi\rangle_{\bar{\phi}}$ are orthogonal [4–6]. Physically, this amounts to the observation that changing the magnetic flux of the circuit by Φ_0 yields a new, physically distinct state of the system. In the phase basis, the charge operator becomes the differential operator ${}_{\bar{\phi}}\langle\phi|\,\hat{n}\,|\psi\rangle = -i\partial_\phi\psi(\phi)$, and it follows that $\mathsf{Spect}(\hat{\phi}) = \mathsf{Spect}(\hat{n}) = \mathbb{R}$.

There are thus two different Hilbert spaces that have been used to describe a circuit node: one that is compact in a canonical variable (phase) and discrete in its conjugate (charge), and another that is noncompact in both conjugate variables. Likharev and Zorin [1] compared the distinction between these inequivalent descriptions to that between a 2π-periodic pendulum and a particle in an extended periodic cosine potential. Formally, the Hamiltonians for the two cases appear identical. However the different Hilbert spaces give

*stace@physics.uq.edu.au

different spectra. The spectrum of the pendulum is discrete. In contrast, the spectrum of a particle in the periodic lattice consists of continuous Bloch energy bands [1,7]. The Bloch bands include the pendulum spectrum as a discrete subset, corresponding to the Bloch eigenvalues at the center of the Brillouin zone (i.e., the Γ point, in band-structure nomenclature). It follows that the noncompact periodic system includes the pendulum as a subspace, but its larger Hilbert space admits richer physics.

The difference between the Hilbert spaces in these two descriptions gives rise to a challenge in describing the addition of an inductive element, with Hamiltonian $E_L\hat{\phi}^2$ to a transmon or Cooper-pair box (CPB) circuit, whose Hamiltonian is $E_C\hat{n}^2 - E_J\cos(\hat{\phi})$ [5]. If the discrete-charge Hilbert space is assumed when $E_L = 0$, then the transition to $E_L > 0$ is beset by a catastrophic growth in the cardinality of the Hilbert space dimension from $|\mathbb{Z}|$ to $|\mathbb{R}|$. As we discuss later, the dimensional explosion is averted by starting with the assumption that $\mathsf{Spect}(\hat{\phi}) = \mathsf{Spect}(\hat{n}) = \mathbb{R}$ regardless of whether there is an inductor present or not. In other words, we will adopt the view in Refs. [1,5] that the superconducting phase and the charge are inherently noncompact operators.

A related mathematical issue that arises in the transition from $E_L = 0$ to $E_L > 0$ is that the problem is an instance of singular perturbation theory: the Bloch eigenbands for $E_L = 0$, cannot be adiabatically connected to the discrete eigenspectrum for small but nonzero E_L [5]. We discuss this in detail in Sec. III A.

In what follows, we review a convenient basis proposed by Zak [8], and use this to reanalyze the circuit for a transmon/CPB. With a noncompact phase, a 2π phase-periodic device will have an eigensystem arranged into Bloch bands, which are labeled by a band index and a "quasicharge". In the lowest Bloch band, eigenstates are comblike periodic functions of the phase, which is reminiscent of the oscillator code states proposed in Gottesman *et al.* [9]. In Sec. III, we describe experiments that would break the 2π periodicity in order to controllably create and observe superpositions of the Bloch quasicharge states in the lowest band. Section IV then addresses the properties of such superpositions, which includes inherent robustness against relaxation, and possible experimental considerations.

II. REVISITING TRANSMON/COOPER-PAIR BOX IN THE ZAK BASIS

A. The modular Zak basis

The Zak basis [8,10] is useful and interesting because it provides a compact 2D representation of a Hilbert space that is noncompact in a 1D coordinate (e.g., the position or phase, or their conjugate variables). The basis set, $\{|k,\varphi\rangle\}$, is labeled by the modular [11] charge $k \in (-\frac{1}{2}, \frac{1}{2}]$ and modular flux $\varphi \in (-\pi, \pi]$. We will show that this resolves some of the technical difficulties when a large inductance (i.e., small E_L) is shunted across a transmon/CPB circuit. Here we give a brief review of this basis.

The Zak basis states can be defined with respect to either the noncompact phase basis, denoted as $\bar{\phi}$, or the noncompact charge basis $\bar{n}$, as

$$|k,\varphi\rangle = \sum_{j=-\infty}^{\infty} e^{i2\pi jk}|\varphi - 2\pi j\rangle_{\bar{\phi}} \tag{3}$$

$$= \frac{e^{ik\varphi}}{\sqrt{2\pi}}\sum_{j=-\infty}^{\infty} e^{-ij\varphi}|j-k\rangle_{\bar{n}}, \tag{4}$$

with $k \in (-\frac{1}{2}, \frac{1}{2}]$ and $\varphi \in (-\pi, \pi]$. These states satisfy orthonormalization $\langle k,\varphi\,|k',\varphi'\rangle = \delta(k-k')\delta(\varphi-\varphi')$, and the generalized periodic boundary identities $|-1/2,\varphi\rangle = |1/2,\varphi\rangle$ and $|k,-\pi\rangle = e^{-i2\pi k}|k,\pi\rangle$.

The Zak basis is convenient for several reasons. Firstly, it is compact in the 2D space of k and φ, which will turn out to be helpful for numerical calculations.

Secondly, it is complete: using Eq. (3), it is straightforward to show that

$$\int_{-\pi}^{\pi} d\varphi \int_{-1/2}^{1/2} dk\,|k,\varphi\rangle\langle k,\varphi| = \int_{-\infty}^{\infty} d\phi|\phi\rangle_{\bar{\phi}}\langle\phi| = \mathbb{1}. \tag{5}$$

A corollary is that two phase states which are offset from one another by an integer multiple of 2π have orthogonal representations in this basis.

Thirdly, polynomial and (some) periodic functions of charge and flux have local representations in the Zak basis. In particular, we have [11]

$$\langle k,\varphi|\,\hat{n}\,|\psi\rangle = -i\frac{\partial}{\partial\varphi}\psi(k,\varphi), \tag{6}$$

$$\langle k,\varphi|\,\hat{\phi}\,|\psi\rangle = \left(-i\frac{\partial}{\partial k} + \varphi\right)\psi(k,\varphi), \tag{7}$$

and

$$\langle k,\varphi|\cos(2\pi\hat{n})\,|\psi\rangle = \cos(2\pi k)\psi(k,\varphi), \tag{8}$$

$$\langle k,\varphi|\cos(\hat{\phi})\,|\psi\rangle = \cos(\varphi)\psi(k,\varphi), \tag{9}$$

where $\psi(k,\varphi) \equiv \langle k,\varphi|\psi\rangle$.

This is in contrast to the flux or charge bases, for which periodic functions have a delocalized representation, e.g.,

$$\cos(\hat{\phi}) = \frac{1}{2}(e^{i\hat{\phi}} + e^{-i\hat{\phi}})$$

$$= \frac{1}{2}\int_{-\infty}^{\infty} dq(|q+1\rangle_{\bar{n}}\langle q| + |q\rangle_{\bar{n}}\langle q+1|), \tag{10}$$

is delocalized in the charge basis.

B. Band structure of the transmon/Cooper-pair box Hamiltonian

Having introduced a convenient basis that has a local representation of both polynomial and periodic functions of $\hat{n}$ and $\hat{\phi}$, we now revisit the well-studied Hamiltonian describing CPBs and transmons, depending on the parameter choices.

The results of this section can be derived straightforwardly in the phase basis using Bloch's theorem. However, the Zak basis is helpful for describing elements that break the dynamical 2π-phase periodicity in the Hamiltonian, which we address later. In this section we therefore rederive the Bloch wave functions in the Zak basis.

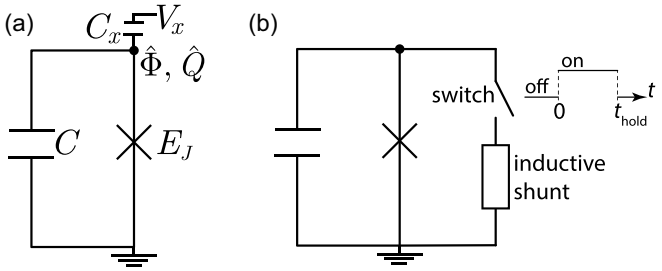

FIG. 1. (a) We use the Zak basis to analyze the circuit for a transmon or Cooper-pair box (CPB), consisting of a Josephson junction and a capacitor, which is characterized by a flux $\hat{\Phi}$ and a conjugate charge $\hat{Q}$. An external voltage source V_x may be capacitively coupled to the node of the circuit. (b) An inductive element (box) is transiently switched into the circuit for the time interval $0 < t < t_{\text{hold}}$. The inductive element may be a linear inductor, which we analyze in Sec. III A or a nonlinear 4π-periodic element, which we analyze in Sec. III B.

We consider the circuit pictured in Fig. 1(a), consisting of a Josephson junction and a capacitor, and subject to an external voltage bias V_x. This circuit is described by the Hamiltonian [2,12]

$$\hat{H}_{\text{tmon}} = E_C(\hat{n} - n_x)^2 - E_J\cos(\hat{\phi}), \tag{11}$$

where $E_C = 2e^2/(C + C_x)$ is the charging energy with C the Josephson junction capacitor and C_x the external capacitor, $n_x = C_x V_x/(2e)$ is the gate voltage referenced to a dimensionless on-site charge shift, and E_J is the junction energy. This Hamiltonian describes a CPB when $E_J \ll E_C$ [3], and a transmon when $E_J \gg E_C$ [2].

Representing states of the system in the Zak basis, $\psi(k,\varphi) = \langle k, \varphi\,|\psi\rangle$, yields the time-independent Schrödinger equation

$$E_C\left(-i\frac{\partial}{\partial\varphi} - n_x\right)^2\psi(k,\varphi) - E_J\cos(\varphi)\psi(k,\varphi) = E\psi(k,\varphi), \tag{12}$$

with generalized, periodic boundary conditions

$$\psi(-1/2,\varphi) = \psi(1/2,\varphi), \tag{13}$$

$$\psi(k,-\pi) = e^{2\pi k i}\psi(k,\pi). \tag{14}$$

Since the only derivatives in Eq. (12) act on φ, the modular charge k is a constant of motion.

We solve Eq. (12) using separation of variables. Substituting $\psi(k,\varphi) = K(k)F(\varphi)$ into Eq. (12), we see that K factorizes out of the resulting expression, yielding

$$E_C\left(-i\frac{\partial}{\partial\varphi} - n_x\right)^2 F(\varphi) - E_J\cos(\varphi)F(\varphi) = E\,F(\varphi). \tag{15}$$

The boundary condition Eq. (14) requires that

$$F(-\pi) = e^{2\pi k i}F(\pi). \tag{16}$$

Since F is supposed to be independent of k, this boundary condition appears to lead to a contradiction in the separability assumption. However, if $K(k) = \delta(k-\kappa)$ for some constant κ, then F may depend parametrically on κ without violating separability [15]. Thus the modular charge is promoted to a quantum number, $k \to \kappa$, which is commonly called the *Bloch wave number*, or alternatively the *quasicharge* in Likharev and Zorin [1].

Thus transmon/CPB eigenstates $|\psi\rangle$ are expressed in the Zak basis as $\psi(k,\varphi) = \delta(k-\kappa)F_\kappa(\varphi)$, where $F_\kappa(-\pi) = e^{2\pi\kappa i}F_\kappa(\pi)$, which follows from Eq. (16). This generalized periodic boundary condition implies that $F_\kappa(\varphi)$ are the Bloch wave functions. This is made clear by defining the periodic function $u_\kappa(\varphi) = e^{i\kappa\varphi}F_\kappa(\varphi)$, which satisfies the Bloch equation

$$E_C\left(-i\frac{\partial}{\partial\varphi} - (n_x+\kappa)\right)^2 u_\kappa(\varphi) - E_J\cos(\varphi)u_\kappa(\varphi) = E u_\kappa(\varphi), \tag{17}$$

with $u_\kappa(\varphi) = u_\kappa(\varphi + 2\pi)$.

As a result, the transmon/CPB eigenenergies $E^{\text{tmon}}_{\kappa,b}$ and eigenstates $|\psi^{\text{tmon}}_{\kappa,b}\rangle$ are labeled by the wave number $\kappa \in (-1/2, 1/2]$ and the band index $b \in \mathbb{N}$, giving rise to the usual Bloch bands. Here, for brevity, we label the eigensystem with the superscript "tmon" for "transmon", but with the understanding that these arguments also apply for CPBs. In the compact Zak basis, the eigenfunctions are

$$\psi^{\text{tmon}}_{\kappa,b}(k,\varphi) \equiv \langle k,\varphi\,|\psi^{\text{tmon}}_{\kappa,b}\rangle = \delta(k-\kappa)F^{\text{tmon}}_{\kappa,b}(\varphi). \tag{18}$$

It also follows from Eq. (17) and Bloch's theorem that in the noncompact phase basis, the transmon/CPB eigenfunctions are

$$\psi^{\text{tmon}}_{\kappa,b}(\phi) \equiv {}_{\vec{\phi}}\langle\phi\,|\psi^{\text{tmon}}_{\kappa,b}\rangle = e^{-i\kappa\phi}u_\kappa(\phi) = F^{\text{tmon}}_{\kappa,b}(\phi), \tag{19}$$

where $\phi \in \mathbb{R}$. That is, F is the eigenfunction in the noncompact phase basis.

Figure 2 depicts the band structure and selected eigenfunctions for the Hamiltonian, Eq. (11), for $E_C/E_J = 1$, with $n_x = 0$. As an aside, we note that n_x just sets the origin of the band-structure, so there is no loss of generality in setting $n_x = 0$. In this regime, the bands are relatively flat, so that the bandwidth of the lowest band is narrow relative to the band gaps. For these parameters, the transition energy at the center of the Brillouin zone is approximately given by the harmonic oscillator energies that would be associated to the linearized system, $\sqrt{2E_JE_C}$, i.e., numerically we find that

$$(E_{\kappa=0,b=1} - E_{0,0})/\sqrt{2E_JE_C} \approx 0.9, \tag{20}$$

is close to unity.

The eigenfunction at the center of the Brillouin zone, $\psi^{\text{tmon}}_{\kappa=0,b}(\phi)$, is 2π-periodic in the noncompact phase basis, while the eigenfunction at the edge of the Brillouin zone, $\psi^{\text{tmon}}_{\kappa=\frac{1}{2},b}(\phi)$, is 4π-periodic. This is illustrated in the insets in Fig. 2. In the lowest band, $b = 0$, the states at the center and at the edge of the Brillouin zone are comblike, similar to the code states of the oscillator GKP code proposed by Gottesman *et al.* [9], which have previously been discussed for stable superconducting qubits [6]. The width of the peaks in the comb scales as $\sqrt{E_C/E_J}$, which sets the dimensionless zero-point modular displacement of the device.

III. TRANSIENT SYMMETRY BREAKING

The previous section rederived standard results from Bloch's theorem for a particle in a periodic potential over

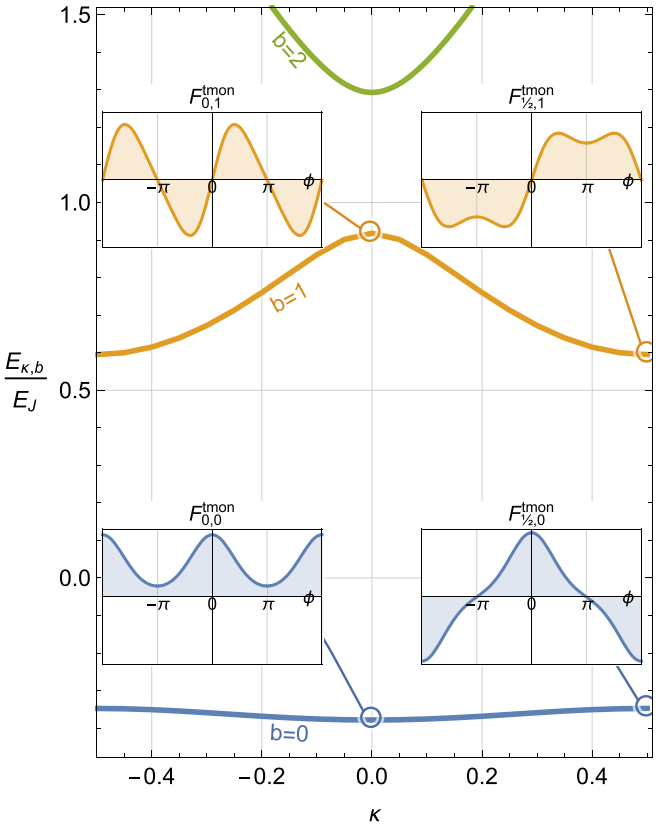

FIG. 2. The spectrum of the Hamiltonian in Eq. (11), as a function of the quasicharge, κ, with $E_C/E_J = 1$, and $n_x = 0$. Note that the regime $E_J/E_C = 1$ is intermediate [13] between the transmon and CPB ones and is used here for illustrative purpose only. Bands are labeled by the band index b. In this regime, the lowest band is quite narrow relative to the gap. Inset figures depict selected Bloch wave functions $F^{\text{tmon}}_{\kappa,b}(\phi)$ in the noncompact phase basis, given in Eq. (19), for the lowest two bands, at the center and at the edge of the Brillouin zone. The vertical axis in the insets is arbitrary, but scaled identically for all. The restriction of $F^{\text{tmon}}_{\kappa,b}$ to the compact domain $(-\pi, \pi]$ yields the form on the RHS of Eq. (18). The inset modes at the center and edge of the lowest Bloch band are comblike states, with periodicity 2π and 4π, respectively.

a noncompact domain. The Zak basis becomes particularly helpful for analyzing the situation of a transmon or CPB that is transiently shunted by an electronic element that breaks the 2π periodicity of the Josephson junction, such as a linear inductor or a (phenomenological) nonlinear 4π-periodic inductive element. This is illustrated in Fig. 1(b), showing the transmon/CPB circuit with a switch that allows a linear or nonlinear inductive shunt element (box) to be transiently shunted across the circuit. This circuit has similarities to the gates proposed for the 0-π qubit [6,14–16], which we touch on later.

In this section we solve the transient evolution for both cases. Since the 2π periodicity of the Josephson junction is broken, the eigenstates of the transmon/CPB Hamiltonian become coupled, and the evolution of the system generates superpositions of the Bloch eigenstates of the bare system. In particular, we will show that it is possible to controllably create coherent superpositions of states at the center and edge of the Brillouin zone in the lowest band, i.e.,

$$|\Psi_{b=0}\rangle = \alpha \left|\psi^{\text{tmon}}_{0,0}\right\rangle + \beta \left|\psi^{\text{tmon}}_{\frac{1}{2},0}\right\rangle. \tag{21}$$

The possibility of producing and measuring such a superposition is the core development in this paper.

A. Transiently shunted linear inductor

Here we suppose that the inductive shunt is a linear inductor, with inductance L. The Hamiltonian describing this system is [5,17]

$$\hat{H} = E_C \hat{n}^2 + E_L(t)\hat{\phi}^2 - E_J \cos(\hat{\phi}), \tag{22}$$

where

$$E_L(t) = \begin{cases} 0, & t < 0 \\ E_L, & 0 < t < t_{\text{hold}} \\ 0, & t > t_{\text{hold}} \end{cases}, \tag{23}$$

for $E_L = \Phi_0^2/(8\pi^2 L)$, and we set the external voltage bias to zero (i.e., $n_x = 0$). For a time-independent inductive term, we note that this Hamiltonian would describe a fluxonium circuit [5,17], up to some choice of flux bias. While the switch is on, the inductor explicitly breaks the 2π periodicity of the junction Hamiltonian, making it very clear that the phase ϕ is not a compact variable. In Appendix A, the fluxonium states in the Zak basis are plotted and compared to the transiently inductor-shunted transmon/CPB states.

The inductive shunt in Eq. (22) breaks the periodic flux-translation symmetry, and is unbounded above, so the spectrum of eigenstates $\{E_{j\in\mathbb{N}}\}$ is discrete. In the Zak basis, the energy eigenfunctions $\langle k, \varphi | \psi^{\text{ind}}_j \rangle \equiv \psi^{\text{ind}}_j(k, \varphi)$ satisfy the time-independent Schrödinger equation

$$-E_C \frac{\partial^2 \psi^{\text{ind}}_j}{\partial \varphi^2} + E_L \left(-i\frac{\partial}{\partial k} + \varphi\right)^2 \psi^{\text{ind}}_j - E_J \cos(\varphi)\psi^{\text{ind}}_j = E_j \psi^{\text{ind}}_j, \tag{24}$$

along with the boundary conditions Eqs. (13) and (14). Here the superscript "ind" labels the eigenmodes of the inductively shunted device.

In the rest of this section, we wish to solve the evolution generated by Eq. (24), assuming the system is initialized in the transmon/CPB ground state, $|\psi^{\text{tmon}}_{0,0}\rangle$, at $t = 0$. In the Zak basis, this is given by Eq. (18):

$$\psi^{\text{tmon}}_{0,0}(k, \varphi) = \delta(k) F^{\text{tmon}}_{0,0}(\varphi). \tag{25}$$

The ground state Bloch wave function, $F^{\text{tmon}}_{0,0}$, is shown as an inset in Fig. 2.

Unfortunately, Eq. (24) presents a technical challenge in dealing with situations where E_L is small. In particular, E_L appears as a coefficient on the highest order derivative with respect to k, so the limit $E_L \to 0^+$ is an instance of singular perturbation theory. Singular perturbation problems are often solved by introducing a small "length" scale, over which the singular perturbation relaxes.[1] Inside the small length scale,

[1]Since the order of a PDE determines the number of boundary conditions that need to be specified, taking $E_L = 0$ results in a

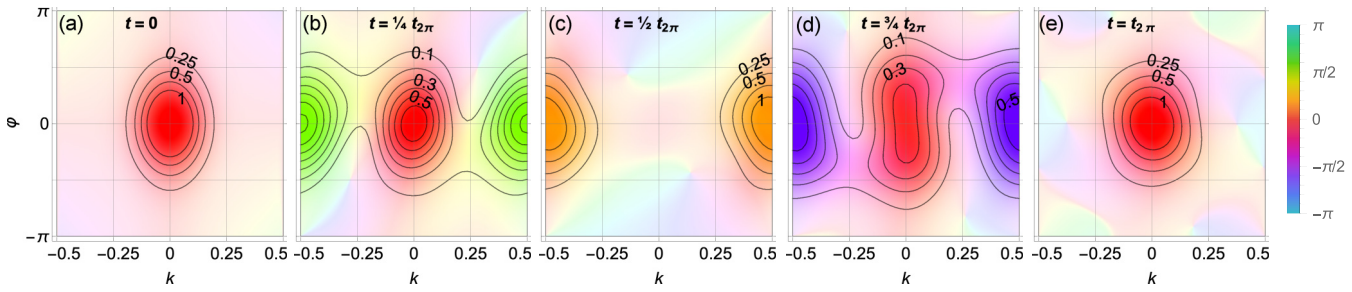

FIG. 3. [(a)–(e)] Snapshots of the time evolution of the wave function probability density, $|\psi^{\text{ind}}(t;k,\varphi)|^2$, of a transmon transiently shunted by an inductor (contours). The hue shows the local phase of the wave function, $\arg(\psi^{\text{ind}})$, relative to the phase at the origin, enumerated in the scale bar. The initial state is a (nearly) separable, Δ-broadened state given in Eq. (28), and we have set the (dimensionless) broadening parameter to $\Delta = 0.2$. For these plots, other parameters are $E_C/E_J = 1$, $E_L/E_J = 1/(2\pi)^2$, and $n_x = 0$. For numerics, we have generated the evolution using the first 100 eigenmodes.

the singular perturbation is significant, outside this scale, it becomes negligible.

In our case, the singular term in Eq. (24) corresponds to a diffusive operator, $-E_L\partial_k^2$, in the Schrödinger equation with a small coefficient. If $E_L = 0$, then the spectrum of the Hamiltonian is the continuum band-structure discussed in the previous section, and shown in Fig. 2. However if $E_L > 0$ is arbitrarily small but nonzero, then the spectrum becomes discrete, so that there is no adiabatic way to connect the spectra as E_L changes from 0. In practice, this means that systems which are initially highly localized in the k coordinate will diffuse rapidly over very short times, but this coherent diffusion becomes insignificant as the wave function spreads out. Physically this corresponds to large, transient currents through the shunting inductor as the modular charge redistributes across the device.

As such we now solve the evolution generated by Eq. (24) as an initial value problem, and regularize the rapid diffusion at short times (arising from the singular perturbation) by replacing the δ function in Eq. (25) with a Δ-broadened Gaussian:

$$\delta(k) \to \delta_\Delta(k,\varphi) \equiv \mathcal{N} e^{-ik\varphi}\left(e^{-(k/\Delta)^2} - e^{-(\frac{1}{2}/\Delta)^2}\right). \tag{26}$$

Here, $\mathcal{N}$ is a normalisation chosen to satisfy $\int_{-\frac{1}{2}}^{\frac{1}{2}} dk|\delta_\Delta(k,\varphi)|^2 = 1$, and we introduce the offset $e^{-(\frac{1}{2}/\Delta)^2}$ and complex phase $e^{-ik\varphi}$ on the right-hand side (RHS) of Eq. (26) to ensure that δ_Δ satisfies the boundary conditions Eqs. (13) and (14), respectively.

We then (implicitly) define broadened transmon eigenmodes $|\psi^{\text{tmon}}_{\kappa,b}\rangle_\Delta$ through

$$\langle k,\varphi\,|\psi^{\text{tmon}}_{\kappa,b}\rangle_\Delta = \delta_\Delta(k,\varphi)F^{\text{tmon}}_{\kappa,b}(\varphi). \tag{27}$$

This allows us to define the Δ-broadened ground state of the transmon with which we initialize the system,

$$|\psi^{\text{ind}}(t=0)\rangle = |\psi^{\text{tmon}}_{0,0}\rangle_\Delta\,. \tag{28}$$

For the rest of this section, we use the parameter values $E_C/E_J = 1$, $E_L/E_J = 1/(2\pi)^2 \ll 1$, and $n_x = 0$. To calculate the time evolution, we decompose the initial state into the eigenmodes of the inductively shunted transmon (i.e., the fluxonium). For reference, some eigenmodes and eigenenergies are plotted in the Zak basis in Appendix A. In spite of the smallness of E_L, the spectrum is discrete, emphasising the effect of the singular perturbation relative to the continuum band-structure when $E_L = 0$.

Snapshots of the time-evolved probability density $|\psi^{\text{ind}}(t;k,\varphi)|^2$ are shown as contours in Fig. 3. The initial state is localized around $k = 0$, and somewhat delocalized in φ (for visualisation, we choose $\Delta = 0.2$). At a later time, $t_{2\pi} = 2\pi/(E_1^{\text{ind}} - E_0^{\text{ind}})$, the system returns to a state that is localized around $k = 0$, and has a large overlap with the initial state. For the parameter choices in Fig. 3, $t_{2\pi} \approx 6.8/E_J$. At intermediate times, the state is delocalized over k. In particular, at $t_{2\pi}/4$ and $3t_{2\pi}/4$, the state is a superposition of approximately localized modes with support around $k = 0$ and $k = \frac{1}{2}$, i.e., it is approximately $(|\psi^{\text{tmon}}_{0,0}\rangle_\Delta + e^{i\theta}\,|\psi^{\text{tmon}}_{\frac{1}{2},0}\rangle_\Delta)/\sqrt{2}$. At time $t_{2\pi}/2$, the state is localized around $k = \frac{1}{2}$.

This evolution is confirmed by computing the return probability, $|_\Delta\langle\psi^{\text{tmon}}_{0,0}|\psi^{\text{ind}}(t)\rangle|^2$, as a function of the switch hold time, t_{hold}, as well as the time-dependent probability for the system to be in the state $|\psi^{\text{tmon}}_{\frac{1}{2},0}\rangle_\Delta$, i.e., $|_\Delta\langle\psi^{\text{tmon}}_{\frac{1}{2},0}|\psi^{\text{ind}}(t)\rangle|^2$. These quantities are plotted in Fig. 4, confirming oscillations between the initial state near $k = 0$ and a state near the edge of the Brillouin zone. We note that the incomplete overlap with $|\psi^{\text{tmon}}_{\frac{1}{2},0}\rangle_\Delta$ at $t_{2\pi}/2$ is a consequence of the anharmonic Schrödinger evolution for this nonlinear system which mildly distorts the localized wave packets at intermediate times – since the evolution is unitary, the state remains pure at all times. The dotted-shaded curve shows the residual probability to be in a state other than these two modes. Specifically, the ideal state $|\psi^{\text{tmon}}_{\frac{1}{2},0}\rangle_\Delta$, similar to $|\psi^{\text{tmon}}_{0,0}\rangle_\Delta$, has a probability distribution $|\langle k,\varphi|\psi^{\text{tmon}}_{\frac{1}{2},0}\rangle_\Delta|^2$ that is symmetric about $\varphi = 0$ and $k = 0$. However, in the middle snapshot of Fig. 3 there is a small asymmetry in the distribution, so the overlap with $|\psi^{\text{tmon}}_{\frac{1}{2},0}\rangle_\Delta$ is not perfect.

This result shows that a transmon which is transiently shunted by an inductor will become delocalized over the

lower order PDE than any value $E_L \to 0^+$. Archetypal singular value problems occur in the Navier-Stokes equation for laminar flow of viscous fluids, where the small parameter is the inverse of the Reynolds number, and the relaxation length scale corresponds to the boundary layer thickness.

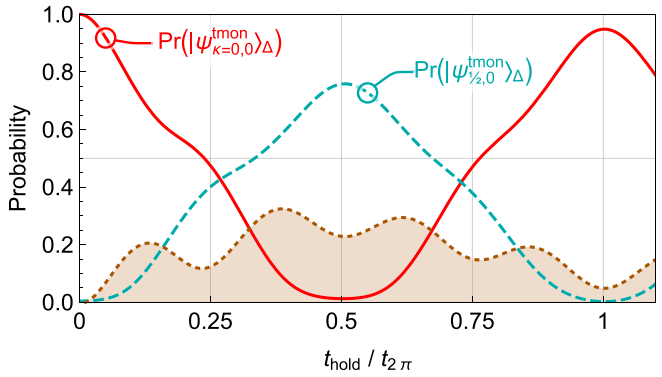

FIG. 4. Time-evolution of the return probability of the inductively shunted transmon (solid-red), initialized in the Δ-broadened state $|\psi^{\rm tmon}_{0,0}\rangle_\Delta$, Eq. (28). Also shown is the probability of the Δ-broadened state localized near the Brillouin zone boundary, $|\psi^{\rm tmon}_{\frac{1}{2},0}\rangle_\Delta$ (dashed-blue), along with the residual probability in other states (dotted-shaded). The parameter values used in the simulation are $E_C/E_J = 1$, $E_L/E_J = 1/(2\pi)^2$, and $\Delta = 0.2$.

modular charge, k. If the inductor is switched out of the circuit at $t_{\rm hold} = t_{2\pi}/4$ or $3t_{2\pi}/4$, the device will be left in a superposition of different transmon/CPB eigenstates which approximate the state given in Eq. (21).

B. Transiently shunted 4π-periodic device

An alternative approach to coupling different k states is to break the 2π-periodic ϕ-translation symmetry by shunting the transmon with a 4π-periodic element [18,19]. For the purposes of this section, we do not describe the implementation of such an element [13,20–22], but begin with a phenomenological Hamiltonian [22]

$$\hat{H} = E_C\hat{n}^2 - E_J\cos(\hat{\phi}) - E_{4\pi}(t)\cos(\hat{\phi}/2), \tag{29}$$

where

$$E_{4\pi}(t) = \begin{cases} 0, & t < 0 \\ E_{4\pi}, & 0 < t < t_{\rm hold} \\ 0, & t > t_{\rm hold} \end{cases}. \tag{30}$$

We note in passing that switching control could be established in this system by forming a SQUID-like configuration of parallel 4π-periodic elements with a flux bias, so that the $E_{4\pi}$ may be controllably tuned by an external bias current, in analogy with the switchable junction in Brooks *et al.* [6].

Along with the transient control in Eq. (30), we assume the system is initialized in the transmon ground state,

$$|\psi^{4\pi}(t=0)\rangle = \left|\psi^{\rm tmon}_{0,0}\right\rangle, \tag{31}$$

which is localized at $k = 0$, as in Eq. (25). Since the Hamiltonian term associated to such a device is bounded, the problems arising from singular perturbations are avoided, and there is no need to invoke Δ broadened initial states.

There are several solution strategies for this problem. Using Eq. (3), it is straightforward to check that $\cos(\hat{\phi}/2)|k,\varphi\rangle = \cos(\varphi/2)|k+\frac{1}{2},\varphi\rangle$, and recalling that $k \in (-\frac{1}{2},\frac{1}{2}]$ compact, so we identify $k+\frac{1}{2} > 1$ with $k-\frac{1}{2}$. Thus we have

$$\cos(\hat{\phi}/2) = \int_{-\frac{1}{2}}^{\frac{1}{2}} dk \int_{-\pi}^{\pi} d\varphi\cos(\varphi/2)\left|k+\frac{1}{2},\varphi\right\rangle\langle k,\varphi|, \tag{32}$$

which couples states that differ in k by $\frac{1}{2}$. In Appendix B, we describe a solution using this decomposition of $\cos(\hat{\phi}/2)$.

However, a more natural approach is to note that because the $\hat{\phi}$-dependent potential in Eq. (29) is 4π-periodic for all values of $E_{4\pi}$, we can define a new 4π-periodic Zak basis that accommodates this reduced symmetry. In particular, we define the orthonormal 4π-Zak basis

$$|\tilde{k},\tilde{\varphi}\rangle = 2\sum_{j\in\mathbb{Z}} e^{i4\pi j\tilde{k}}|\tilde{\varphi}-4\pi j\rangle_{\tilde{\phi}} \tag{33}$$

$$= \frac{1}{2}\frac{e^{i\tilde{k}\tilde{\varphi}}}{\sqrt{2\pi}}\sum_{j\in\mathbb{Z}} e^{-ij\tilde{\varphi}/2}|j/2-\tilde{k}\rangle_{\tilde{n}}, \tag{34}$$

where $\tilde{k} \in (-1/4, 1/4]$ and $\tilde{\varphi} \in (-2\pi, 2\pi]$. The boundary conditions in this basis are

$$\psi(-1/4,\tilde{\varphi}) = \psi(1/4,\tilde{\varphi}), \tag{35}$$

$$\psi(\tilde{k},-2\pi) = e^{4\pi\tilde{k}i}\psi(\tilde{k},2\pi), \tag{36}$$

and the system eigenstates take the form

$$\left\langle\tilde{k},\tilde{\varphi}\middle|\psi^{4\pi}_{\tilde{\kappa},b}\right\rangle \equiv \psi^{4\pi}_{\tilde{\kappa},b}(\tilde{k},\tilde{\varphi}) = \delta(\tilde{k}-\tilde{\kappa})F^{4\pi}_{\tilde{\kappa},b}(\tilde{\varphi}), \tag{37}$$

where $b \in \mathbb{N}$ is a new band index. In this basis, the eigenstates satisfy the eigenvalue problem

$$-E_C\frac{\partial^2\psi^{4\pi}_{\tilde{\kappa},b}}{\partial\tilde{\varphi}^2} - (E_J\cos(\tilde{\varphi}) + E_{4\pi}\cos(\tilde{\varphi}/2))\psi^{4\pi}_{\tilde{\kappa},b} = E^{4\pi}_{\tilde{\kappa},b}\psi^{4\pi}_{\tilde{\kappa},b}, \tag{38}$$

where $E^{4\pi}_{\tilde{\kappa},b}$ is the eigenenergy. The first three eigenfunctions at the center of the Brillouin zone, $F^{4\pi}_{\tilde{\kappa}=0,b}(\tilde{\varphi})$, of the 4π-shunted transmon are shown in the middle panel of Fig. 5.

We now describe the time evolution of the system subject to a transiently shunted 4π-periodic element. The wave function for the initial transmon ground state, $|\psi^{\rm tmon}_{0,0}\rangle$, is plotted in the extended Zak basis in the top panel of Fig. 5 (solid-red). As in the previous section, we decompose the initial state into the eigenmodes of the shunted system, $|\psi^{4\pi}_{\tilde{\kappa},b}\rangle$, and evolve in the usual way. Since $\tilde{k}$ is conserved, the initial state $|\psi^{\rm tmon}_{0,0}\rangle$ only has support on modes with $\tilde{\kappa} = 0$, i.e., those at the center of the Brillouin zone in the 4π-Zak basis. Of these states, the lowest two have large overlap with the initial state, and so dominate the evolution.

For the numerical results here, we assume that $E_C/E_J = 1$ and $E_{4\pi}/E_J = 1/2$. (This choice of parameters makes the 4π-periodic potential in Eq. (29) qualitatively comparable to the aperiodic potential in Eq. (22): the two potential functions have a global minimum at $\varphi = 0$, local minima at or near $\varphi = \pm 2\pi$, and with a potential difference between these local minima and the global minimum $\approx E_J$). We define the time for a coherent oscillation between the lowest and first excited states at the center of the extended Brillouin zone (i.e., at $\tilde{\kappa} = 0$), $t_{2\pi} = 2\pi/(E^{4\pi}_{\tilde{0},1} - E^{4\pi}_{\tilde{0},0})$. For the parameter choices in Fig. 5, $t_{2\pi} \approx 7.04/E_J$.

The time evolution is represented in the bottom panel of Fig. 5, starting with the initial state with 2π periodicity at

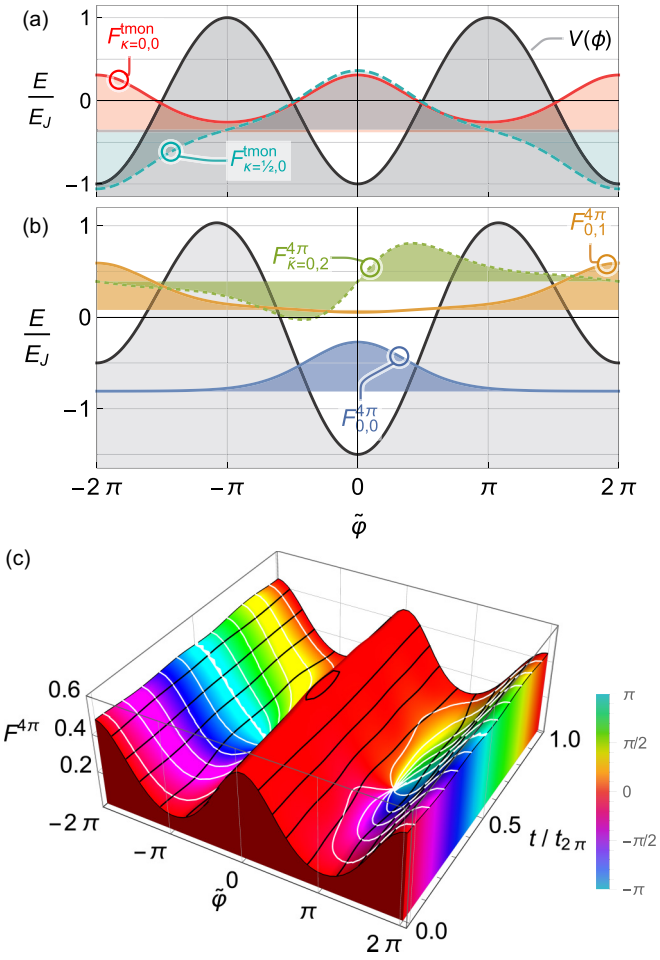

FIG. 5. (a) The lowest band wave functions, $b = 0$, for the unshunted transmon ground state and the Brillouin zone edge (respectively, $\kappa = 0$, solid red and $\kappa = \frac{1}{2}$, dashed blue), shown relative to the cosine potential in the extended Zak basis, Eq. (33). The system is initialized in the ground state of the transmon Hamiltonian, $|\psi^{\text{tmon}}_{\kappa=0,0}\rangle$ (solid red). Parameters are $E_C/E_J = 1$ and $E_{4\pi} = 0$. (b) The lowest three eigenstates of the shunted system with $\tilde{\kappa} = 0$, in the shunted 4π-periodic potential with $E_{4\pi}/E_J = 1/2$. The initial wave function, $F^{\text{tmon}}_{0,0}$, has large and approximately equal overlap with the ground and first excited wave functions of the 4π-periodic system, $F^{4\pi}_{\tilde{\kappa}=0,b=0}$ and $F^{4\pi}_{0,1}$. (c) The system evolves from the 2π-periodic initial state $F^{\text{tmon}}_{\kappa=0,0}$, through to a state at $t = t_{2\pi}/2$ that has very large overlap with the 4π-periodic $F^{\text{tmon}}_{\kappa=\frac{1}{2},0}$ pictured in the top panel (dashed blue). At $t = t_{2\pi}$, the system returns to a state close to the initial state. The scale bar shows the complex phase of the wave function.

$t = 0$. The system evolves to a 4π-periodic state at $t_{2\pi}/2$ with a positive (red) anti-node at $\tilde{\varphi} = 0$, and a negative (cyan) antinode at $\tilde{\varphi} = \pm 2\pi$. This is qualitatively very similar to $|\psi^{\text{tmon}}_{\frac{1}{2},0}\rangle$, as shown in the top panel of Fig. 5 (dashed blue). At $t = t_{2\pi}$, the system returns very close to the initial state.

The probability for the time-evolved state to be in either the initial state, $|\psi^{\text{tmon}}_{0,0}\rangle$, or a state at the Brillouin zone boundary, $|\psi^{\text{tmon}}_{\frac{1}{2},0}\rangle$, is shown in Fig. 6. The evolution occurs almost entirely in the space spanned by these two states, so that nearly perfect coherent oscillation between the initial and intermediate state is observed. The residual probability to

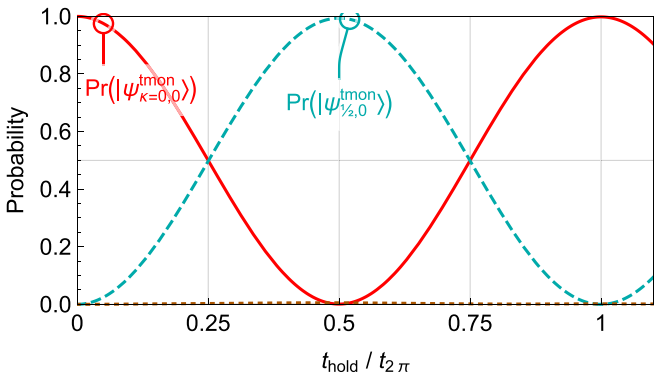

FIG. 6. Time evolution of the return probability of a transmon initialized in the state $|\psi^{\text{tmon}}_{0,0}\rangle$ and then shunted by a the 4π-periodic element (solid red). Also shown is the probability of the state $|\psi^{\text{tmon}}_{\frac{1}{2},0}\rangle$ localized near the Brillouin zone boundary (dashed blue), along with the residual probability in other states (dotted) which is less than 1% for the chosen parameters, $E_C/E_J = 1$ and $E_{4\pi}/E_J = 1/2$.

evolve out of this two-state subspace, shown as a dotted curve, is less than 1% at all t. Since the state evolution is unitary, the very-nearly equal probabilities for the two states at $t = t_{2\pi}/4$ and at $t = 3t_{2\pi}/4$ indicate that the system is very close to the state $(|\psi^{\text{tmon}}_{0,0}\rangle + e^{i\theta}|\psi^{\text{tmon}}_{\frac{1}{2},0}\rangle)/\sqrt{2}$ at these times.

In summary, a 4π-periodic element switched transiently across a 2π-periodic transmon device yields evolution in a two-dimensional (qubitlike) subspace spanned by $\{|\psi^{\text{tmon}}_{0,0}\rangle, |\psi^{\text{tmon}}_{\frac{1}{2},0}\rangle\}$. This is closely analogous to the result that a conventional 2π-periodic Josephson junction switched transiently across a π-periodic device (i.e., the circuit for the 0-π qubit) yields a computational gate in the 0-π encoded subspace [6,14]. Comparisons between the 0-π qubit and the qubit proposed here will be given in more detail in the next section.

IV. DISCUSSION

The description of the complete spectrum of superconducting devices in terms of band structure, which is a consequence of Bloch's theorem, was identified by Likharev and Zorin [1]. However, it is an atypical approach to theoretical modeling of such systems, and it leads to somewhat surprising conclusions.

There are several natural questions that arise from the analysis above. (1) Given that the Bloch spectrum is a continuum, why does experimental spectroscopy of transmons yield apparently discrete spectra? (2) Given that $|\psi^{\text{tmon}}_{0,0}\rangle$ is the unique ground state, what is the lifetime of another state $|\psi^{\text{tmon}}_{\kappa,0}\rangle$, in the lowest Bloch band? (3) How do we interpret superpositions of Bloch eigenstates? (4) What are the coherence properties of such superpositions? Here we address these questions.

Firstly, our analysis shows that transmons and CPBs do not have discrete spectra, and so should not be thought of as "artificial atoms." Instead their spectrum is arranged in bands, with densely packed eigenstates. However, intraband transitions can only occur when the device is subject to symmetry-breaking perturbations, and so cannot be induced

by external driving or other perturbations that respect the dynamical 2π-phase periodicity in the Hamiltonian. An example of such symmetry-breaking perturbations is a shunted inductor that we have presented in Sec. III A or a shunted 4π-periodic junction as in Sec. III B. Also, quasiparticle tunneling introduces an environmental term $\propto \sin(\hat{\phi}/2)$ [23], which breaks the symmetry of concern. It follows that spectroscopic measurements will yield discrete spectra corresponding to direct (i.e., κ-conserving) interband transitions, as observed in numerous experiments.

Secondly, any perturbation that preserves the dynamical 2π-phase periodicity cannot couple states $|\psi^{\text{tmon}}_{\kappa,b}\rangle$ and $|\psi^{\text{tmon}}_{\kappa',b'}\rangle$ with different values of the Bloch wave number, i.e., $\kappa \neq \kappa'$.[2] It follows that any state, $|\psi^{\text{tmon}}_{\kappa',0}\rangle$, in the lowest band cannot relax to the true ground state $|\psi^{\text{tmon}}_{0,0}\rangle$, unless the symmetry is broken.

Thirdly, our analysis indicates that superpositions of eigenstates with different wave numbers within the same band are also possible states of the system. In particular, the state $|\Psi_b\rangle = \alpha|\psi^{\text{tmon}}_{\kappa,b}\rangle + \beta|\psi^{\text{tmon}}_{\kappa',b}\rangle$, introduced in Eq. (21), should be physically admissible (just as superpositions of different band indices, b, are currently used to define qubit states of transmons and CPBs). A physical interpretation can be given to certain such superpositions. For example, the state $|\psi^{4\pi}_{\tilde{\kappa}=0,0}\rangle \approx |\psi^{\text{tmon}}_{0,0}\rangle + |\psi^{\text{tmon}}_{\frac{1}{2},0}\rangle$ is the ground state of the 4π-periodic shunted Hamiltonian Eq. (29), pictured as the lowest mode in the middle panel of Fig. 5, so is a state with 4π-periodicity in the superconducting phase. In the charge basis, the state will have $1e$ charge periodicity.

Finally, as shown in Ref. [10], dephasing of a coherent superposition of energy eigenstates due to perturbative, stochastic charge noise depends on the gradient of the band, $\Gamma \propto |\partial_\kappa E_{\kappa,b}|^2$. Since the energy bands are extremal at both the center and the edge of the Brillouin zone (i.e., the gradient vanishes), we anticipate that the coherent superposition $\alpha|\psi^{\text{tmon}}_{0,0}\rangle + \beta|\psi^{\text{tmon}}_{\frac{1}{2},0}\rangle$ in Eq. (21) should have extremely long coherence times in the presence of perturbative charge noise. Deep in the transmon regime, where the lowest band is almost flat, this result will hold even for charge fluctuations of order $|\delta n_x| \lesssim 1/2$.

A. A possible qubit encoding

As a consequence of these facts, we expect that any state of the form $|\Psi_{b=0}\rangle$ will have extremely long T_1 and T_2 times. Further, the two states $|\psi^{\text{tmon}}_{0,0}\rangle$ and $|\psi^{\text{tmon}}_{\frac{1}{2},0}\rangle$, pictured in the lowest band of Fig. 2, are approximations to the comblike states proposed for encoding a qubit in an oscillator [9], and so may inherit some of the robustness of such comb states as qubit encodings.

We therefore speculate that the subspace spanned by these states in the lowest band provides an attractive home for a qubit, with computational states $|0\rangle = |\psi^{\text{tmon}}_{0,0}\rangle$ and $|1\rangle = |\psi^{\text{tmon}}_{\frac{1}{2},0}\rangle$. This choice contrasts with the conventional transmon qubit encoding in which the logical "1" state is encoded in the first excited band, i.e., $|\bar{1}\rangle \equiv |\psi^{\text{tmon}}_{0,1}\rangle$. We outline here possible single-qubit gates and spectroscopic readout.

High-quality Pauli-X rotations in this encoding could be generated by transiently switching a 4π-periodic element across the circuit, for a well controlled hold time, as shown in Fig. 6. If $E_J \gg E_C$ (the transmon regime), the computational states are nearly degenerate, but this near-degeneracy can be controllably lifted by tuning E_J dynamically into the regime where $E_J \sim E_C$, which will result in a Pauli-Z rotation in the computational space. Experimentally, control over E_J may be achieved by replacing the junction in Fig. 1 with a flux-tunable SQUID. We note these operations would not be natively robust against fluctuations in the control parameters, however some of the ideas in Ref. [6] for constructing robust gates for the 0-π qubit might be adapted to the encoding suggested here.

Readout in the computational basis can be achieved using spectroscopic methods: Fig. 2 shows that the transition energy from the computational states $|0\rangle$ and $|1\rangle$ to the $b = 1$ band will have different energies depending on the computational state. A reflectometry experiment with a probe field tuned to the $|\psi^{\text{tmon}}_{\kappa=0,b=0}\rangle \leftrightarrow |\psi^{\text{tmon}}_{\kappa=0,b=1}\rangle$ transition will show strong response if the system were in the state $|0\rangle = |\psi^{\text{tmon}}_{0,0}\rangle$, and very little response if the system were in the state $|1\rangle = |\psi^{\text{tmon}}_{\frac{1}{2},0}\rangle$. Thus the observation (or not) of significant reflected power would project the system into the corresponding computational state, facilitating computational readout.

Finally, the fact that the proposed qubit states have comblike representations akin to the GKP encoding of a qubit in an oscillator [9], suggest that active error correction against charge noise could be implemented based on the structure of that code. To do so would require (i) that the comb peaks to be narrow, i.e., $\sqrt{E_C/E_J} \ll 1$, where the device is in the transmon regime, (ii) a mechanism to nondestructively measure the displacement of the modular phase arising from charge noise, and (iii) an actuator to act back on the system to correct for drifts in the modular phase. A protocol to achieve (ii) using spectroscopically resolved transitions to the first excited band in a related system was briefly mentioned in Ref. [10], however a complete analysis of such a protocol in the presence of realistic noise models will be the subject of future research.

1. Comparisons with the 0-π qubit

Table I shows comparisons between the 0-π qubit [6,14] and the noncompact transmon/CPB proposed here. The circuit element required to construct the 0-π qubit is an effective π-periodic Josephson junction ladder [6,24]. The relevant gate operations on the 0-π qubit need an ordinary 2π Josephson junction. The 0-π qubit has been studied in various theoretical works [6,14–16,24] and recently has been realized in experiment [25].

By contrast, the circuit for the noncompact transmon/CPB qubit has been well developed experimentally [26–28], but gate operations, as shown in Sec. III B, would be ideally performed by a 4π-periodic Josephson junction. This element is a current experimental challenge and is being investigated in the context of the Majorana qubit [13,20–22]. A proposal for a 4π-periodic element has been put forward by Bell *et al.* [29].

[2]That is, the quasicharge is a conserved quantum number under symmetry preserving perturbations.

TABLE I. Comparisons between the 0-π qubit and the noncompact transmon/Cooper-pair box. The qubit encoding proposed here is based on a transmon/Cooper-pair box using a conventional 2π Josephson junction, but using states only in the lowest band. To perform gates, a device with a lower symmetry is required. The 0-π qubit is based on a high-symmetry junction (π periodic), but uses a conventional 2π junction for gates.

	Qubit potential periodicity	Gate potential periodicity
The 0-π qubit [6,14]	π	2π
The noncompact transmon/Cooper-pair box	2π	4π

B. Experimental considerations

To our knowledge, superpositions such as Eq. (21) have not been experimentally reported. One reason for this is that it is technically challenging to prepare and measure such a state. To do so, it is necessary to controllably break the dynamical 2π-phase periodicity of the JJ element. As described in Sec. III, a transiently switched inductive element achieves this.

This discussion suggests specific experiments that might be developed to demonstrate the possibility of producing and measuring superpositions of Bloch eigenstates. For example, a device that is intermediate between a transmon and a CPB, with $E_J \lesssim E_C$ will have spectrally resolvable transitions at different values of κ. Repeatedly preparing the ground state of such a system, then shunting a symmetry breaking inductive element across it for different hold times, $t_{\rm hold}$, and then spectroscopically measuring the state via reflectometry should map out coherent oscillations as shown in Figs. 4 and 6. This would constitute evidence for the noncompact description of the charge and flux discussed here.

One of the key experimental hurdles to such a demonstration is the requirement of a fast, dissipation-free switch. This element, depicted in Fig. 1, is required to transiently shunt the inductive element across the circuit. One common approach to building switched devices in superconducting systems is to use a flux-tunable SQUID, in which $E_J(\Phi_x)$ can be switched from large to small values quickly. For small fluctuations of the modular phase, φ, this can be treated as a modulation of a linearized inductance. However SQUIDs are natively 2π-periodic devices, so they are not suitable for switching devices that break this symmetry. Instead, the switch should ideally present infinite (linear) impedance when it is open, and zero impedance when closed, so that the circuit sees only the additional load due to the switched inductive shunt element. One approach to this is to use nanomechanical metallic plates that can be forced in-or-out of contact with one another using electrostatic control fields [30] to build a fast, nano-scale mechanical switch. Another approach is to build a hybrid superconducting device, using, e.g., a gated superconducting-normal-superconducting junction [31], or semiconducting hybrids [32–34] which might enable a controllable superconducting switch [35,36].

In the short term, the general principles discussed here could be demonstrated with a switched linear inductor. However comparison of the solid-red curves in Figs. 4 and 6 shows that for producing well-controlled superpositions of Bloch states, the (phenomenological) 4π-periodic nonlinear inductive element is likely to result in better control of the system. Thus a secondary hurdle in future experiments is the development of robust 4π-periodic elements. While we have adopted a purely phenomenological description of such an element, realistic implementations are the subject of recent theoretical and experimental attention [13,18–22]. Understanding the performance of the switched system using realistic models for practical 4π-periodic elements will be the subject of future research.

V. CONCLUSIONS

We have revisited the question of the complete Hilbert space required to describe superconducting circuits such as transmons and CPBs. Lifting the assumption that charge is discrete (or flux is compact) yields a Bloch band structure arising from the dynamical 2π periodicity in the Josephson junction phase. We have shown that Bloch eigenstates can be coupled using elements that break the dynamical 2π periodicity, including linear and nonlinear inductive elements transiently switched across the circuit. The resulting evolution generates states that are superpositions of the Bloch eigenstates. We speculate that certain eigenmodes in the lowest Bloch band would be naturally stable qubit states with extremely long lived population lifetimes, and we anticipate that they will have native robustness against charge noise. Finally, we have suggested a class of experiments that could test the results in this paper.

ACKNOWLEDGMENTS

This research was supported by the Australian Research Council Centres of Excellence for Engineered Quantum Systems (EQUS, CE170100009), and Future Low-Energy Electronics Technologies (FLEET, CE170100039). TMS acknowledges visitor support from the Pauli Center for Theoretical Studies, ETH Zurich. We thank Clemens Müller, Samuel Wilkinson, Victor Albert, and Arne Grimsmo for useful comments.

APPENDIX A: MODE FUNCTIONS FOR THE INDUCTIVELY SHUNTED TRANSMON (THE FLUXONIUM) IN THE ZAK BASIS

In this Appendix we show the first seven eigenfunctions, which are labeled by the corresponding eigenenergies $E_j^{\rm ind}$ of the inductively shunted transmon, i.e., the fluxonium, arrayed in Fig. 7, in the Zak basis, for the parameter values $E_C/E_J = 1$ and $E_L/E_J = 1/(2\pi)^2$. The eigenfunctions are found by solving the Schrödinger equation Eq. (24) subject to the two boundary conditions defined in Eqs. (13) and (14).

There is an approximate degeneracy between $E_1^{\rm ind}$ and $E_2^{\rm ind}$, for which the corresponding eigenmodes are localized around $\varphi = 0$. The eigenfunctions exhibit qualitative features of the boundary conditions Eqs. (13) and (14). Notably, they are generally delocalized in the modular charge k. This is different from the transiently inductor-shunted transmon/CPB

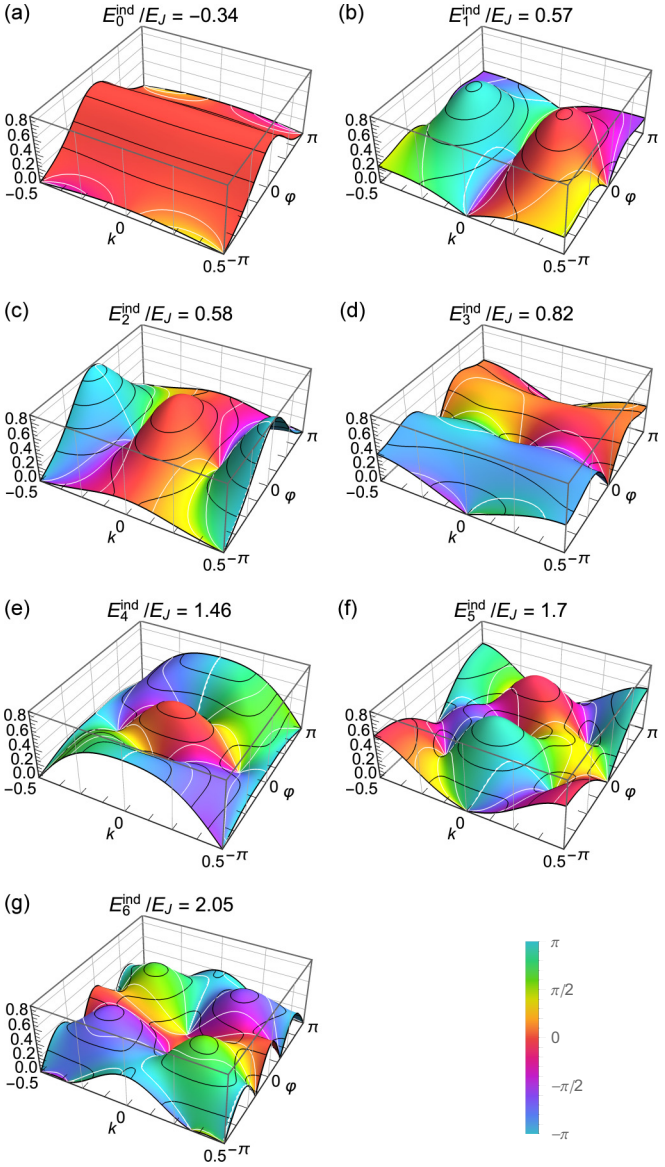

FIG. 7. [(a)–(g)] The first seven complex-valued eigenmodes of the inductively shunted transmon (i.e., the fluxonium), in the Zak basis, $\psi_j^{\text{ind}}(k,\varphi)$. The corresponding, calculated eigenenergies E_j^{ind}/E_J are shown above each plot, for the parameter values $E_C/E_J = 1$ and $E_L/E_J = 1/(2\pi)^2$. For the time evolution shown in Fig. 3, modes $j = 0$ and 2 have large overlap with the initial state (shown at the left of Fig. 3). Colors indicate the phase of the wave function at each point, as specified in the legend (bottom right).

logical states $|\psi_{0,0}^{\text{tmon}}\rangle$ and $|\psi_{\frac{1}{2},0}^{\text{tmon}}\rangle$, which as shown in the first and middle snapshots of Fig. 3 are localized around $k = 0$ and $k = 1/2$, respectively. The eigenfunctions, additionally, are symmetric about the modular phase φ, which is similar to the case of $|\psi_{0,0}^{\text{tmon}}\rangle$ and $|\psi_{\frac{1}{2},0}^{\text{tmon}}\rangle$.

In the limit of large j, we expect the modes to be dominated by the harmonic terms, so that $\lim_{j\to\infty} E_{j+1}^{\text{ind}} - E_j^{\text{ind}} = E_{\text{HO}} = 2\sqrt{E_C E_L}$. For the choice of parameters here, $E_{\text{HO}} = E_J/\pi$, and we confirm that this holds numerically for $j \gtrsim 30$.

For these parameter values, and the initial state Eq. (28), the mode probabilities are plotted in Fig. 8, $|p_j^{\text{ind}}|^2 = |\langle\psi_j^{\text{ind}}|\psi_{0,0}^{\text{tmon}}\rangle_\Delta|^2$. The initial state has no support on odd numbered eigenmodes, and the majority of the probability density has support on the ground and second excited states, accounting for about 95% of the total probability density. Thus the system could be approximated by a two level system, consisting of these two modes. For numerical simulations of temporal evolution, we retain the first 100 such modes, which accounts for $>1–10^{-5}$ of the total probability.

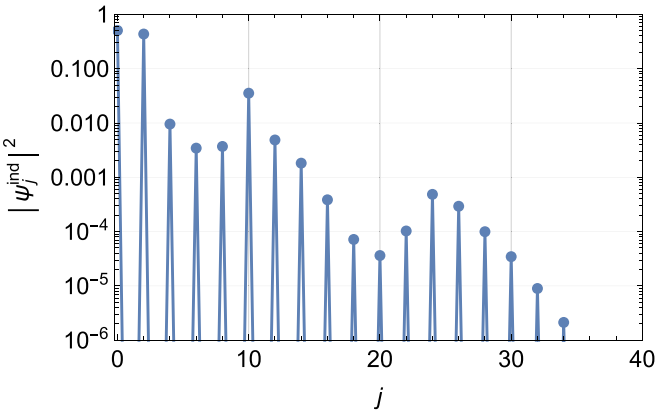

FIG. 8. Probabilities for each mode in the inductively shunted transmon used to calculate the time evolution in Fig. 3. Odd-numbered modes have zero amplitude. The initial state has overwhelming support on the ground and second excited state, making the evolution approximately that of a two-level system.

APPENDIX B: SOLUTION FOR 4π-PERIODIC HAMILTONIAN IN THE ZAK BASIS

The 4π-periodic element conserves $\tilde{k} \equiv (k \bmod \frac{1}{2}) \in (-1/4, 1/4]$, and couples states separated by $\delta k = \frac{1}{2}$. The time evolved state will therefore be of the form

$$|\psi^{4\pi}(t)\rangle = \left|\psi^{4\pi}_{\kappa=0}(t)\right\rangle + \left|\psi^{4\pi}_{\frac{1}{2}}(t)\right\rangle, \tag{B1}$$

where the two (unnormalized) states on the RHS of Eq. (B1) are localized around $\kappa = 0$ and $\frac{1}{2}$, respectively. In the Zak basis the corresponding wave functions $f_\kappa^{4\pi}(t;\varphi)$ are defined implicitly by

$$\psi_\kappa^{4\pi}(t;k,\varphi) \equiv \left\langle k,\varphi\middle|\psi_\kappa^{4\pi}(t)\right\rangle = \delta(k-\kappa) f_\kappa^{4\pi}(t;\varphi). \tag{B2}$$

The wave functions satisfy the coupled Schrödinger equations (for brevity, we have suppressed the argument to $f_\kappa^{4\pi}(t;\varphi)$)

$$\begin{aligned} i\frac{\partial}{\partial t} f_0^{4\pi} &= -E_C \frac{\partial^2}{\partial\varphi^2} f_0^{4\pi} - E_J\cos(\varphi) f_0^{4\pi} - E_{4\pi}\cos\left(\frac{\varphi}{2}\right) f_{\frac{1}{2}}^{4\pi}, \\ i\frac{\partial}{\partial t} f_{\frac{1}{2}}^{4\pi} &= -E_C \frac{\partial^2}{\partial\varphi^2} f_{\frac{1}{2}}^{4\pi} - E_J\cos(\varphi) f_{\frac{1}{2}}^{4\pi} - E_{4\pi}\cos\left(\frac{\varphi}{2}\right) f_0^{4\pi}, \end{aligned} \tag{B3}$$

and boundary conditions $f_\kappa^{4\pi}(t;-\pi) = e^{2i\pi\kappa} f_\kappa^{4\pi}(t;\pi)$, consistent with the boundary condition Eq. (14).

In the usual way, the linear system, Eq. (B3), can be turned into an eigenvalue problem that is characterized by pairs of functions $\{f_0^{4\pi}(\varphi), f_{\frac{1}{2}}^{4\pi}(\varphi)\}_j$, associated to each eigenenergy E_j. We have confirmed that this approach gives the same results as the method described in the main text.

[1] K. Likharev and A. Zorin, J. Low Temp. Phys. **59**, 347 (1985).

[2] J. Koch, T. M. Yu, J. Gambetta, A. A. Houck, D. I. Schuster, J. Majer, A. Blais, M. H. Devoret, S. M. Girvin, and R. J. Schoelkopf, Phys. Rev. A **76**, 042319 (2007).

[3] V. Bouchiat, D. Vion, P. Joyez, D. Esteve, and M. Devoret, Phys. Scr. **1998**, 165 (1998).

[4] T. P. Orlando, J. E. Mooij, L. Tian, C. H. van der Wal, L. S. Levitov, S. Lloyd, and J. J. Mazo, Phys. Rev. B **60**, 15398 (1999).

[5] J. Koch, V. Manucharyan, M. H. Devoret, and L. I. Glazman, Phys. Rev. Lett. **103**, 217004 (2009).

[6] P. Brooks, A. Kitaev, and J. Preskill, Phys. Rev. A **87**, 052306 (2013).

[7] C. Kittel, *Introduction to Solid State Physics*, 8th ed. (Wiley, New York, 2004).

[8] J. Zak, Phys. Rev. Lett. **19**, 1385 (1967).

[9] D. Gottesman, A. Kitaev, and J. Preskill, Phys. Rev. A **64**, 012310 (2001).

[10] D. T. Le, A. Grimsmo, C. Müller, and T. M. Stace, Phys. Rev. A **100**, 062321 (2019).

[11] S. Ganeshan and M. Levin, Phys. Rev. B **93**, 075118 (2016).

[12] T. P. Spiller, T. D. Clark, R. J. Prance, H. Prance, and D. A. Poulton, Il Nuovo Cimento B (1971-1996) **105**, 43 (1990).

[13] D. Aasen, M. Hell, R. V. Mishmash, A. Higginbotham, J. Danon, M. Leijnse, T. S. Jespersen, J. A. Folk, C. M. Marcus, K. Flensberg, and J. Alicea, Phys. Rev. X **6**, 031016 (2016).

[14] A. Kitaev, arXiv:cond-mat/0609441.

[15] A. D. Paolo, A. L. Grimsmo, P. Groszkowski, J. Koch, and A. Blais, New J. Phys. **21**, 043002 (2019).

[16] P. Groszkowski, A. Di Paolo, A. Grimsmo, A. Blais, D. Schuster, A. Houck, and J. Koch, New J. Phys. **20**, 043053 (2018).

[17] V. E. Manucharyan, J. Koch, L. I. Glazman, and M. H. Devoret, Science **326**, 113 (2009).

[18] J. Michelsen, V. S. Shumeiko, and G. Wendin, Phys. Rev. B **77**, 184506 (2008).

[19] L. Fu and C. L. Kane, Phys. Rev. B **79**, 161408(R) (2009).

[20] E. Ginossar and E. Grosfeld, Nat. Commun. **5**, 4772 (2014).

[21] D. Laroche, D. Bouman, D. J. van Woerkom, A. Proutski, C. Murthy, D. I. Pikulin, C. Nayak, R. J. J. van Gulik, J. Nygård, P. Krogstrup, L. P. Kouwenhoven, and A. Geresdi, Nat. Commun. **10**, 245 (2019).

[22] R. Rodríguez-Mota, S. Vishveshwara, and T. Pereg-Barnea, Phys. Rev. B **99**, 024517 (2019).

[23] G. Catelani, J. Koch, L. Frunzio, R. J. Schoelkopf, M. H. Devoret, and L. I. Glazman, Phys. Rev. Lett. **106**, 077002 (2011).

[24] J. M. Dempster, B. Fu, D. G. Ferguson, D. I. Schuster, and J. Koch, Phys. Rev. B **90**, 094518 (2014).

[25] A. Gyenis, P. S. Mundada, A. D. Paolo, T. M. Hazard, X. You, D. I. Schuster, J. Koch, A. Blais, and A. A. Houck, arXiv:1910.07542.

[26] Y. Nakamura, Y. A. Pashkin, and J. S. Tsai, Nature (London) **398**, 786 (1999).

[27] J. A. Schreier, A. A. Houck, J. Koch, D. I. Schuster, B. R. Johnson, J. M. Chow, J. M. Gambetta, J. Majer, L. Frunzio, M. H. Devoret, S. M. Girvin, and R. J. Schoelkopf, Phys. Rev. B **77**, 180502(R) (2008).

[28] F. Arute, K. Arya, R. Babbush, D. Bacon, J. C. Bardin, R. Barends, R. Biswas, S. Boixo, F. G. S. L. Brandao, D. A. Buell, B. Burkett, Y. Chen, Z. Chen, B. Chiaro, R. Collins, W. Courtney, A. Dunsworth, E. Farhi, B. Foxen, A. Fowler, C. Gidney, M. Giustina, R. Graff, K. Guerin, S. Habegger, M. P. Harrigan, M. J. Hartmann, A. Ho, M. Hoffmann, T. Huang, T. S. Humble, S. V. Isakov, E. Jeffrey, Z. Jiang, D. Kafri, K. Kechedzhi, J. Kelly, P. V. Klimov, S. Knysh, A. Korotkov, F. Kostritsa, D. Landhuis, M. Lindmark, E. Lucero, D. Lyakh, S. Mandrà, J. R. McClean, M. McEwen, A. Megrant, X. Mi, K. Michielsen, M. Mohseni, J. Mutus, O. Naaman, M. Neeley, C. Neill, M. Y. Niu, E. Ostby, A. Petukhov, J. C. Platt, C. Quintana, E. G. Rieffel, P. Roushan, N. C. Rubin, D. Sank, K. J. Satzinger, V. Smelyanskiy, K. J. Sung, M. D. Trevithick, A. Vainsencher, B. Villalonga, T. White, Z. J. Yao, P. Yeh, A. Zalcman, H. Neven, and J. M. Martinis, Nature (London) **574**, 505 (2019).

[29] M. T. Bell, W. Zhang, L. B. Ioffe, and M. E. Gershenson, Phys. Rev. Lett. **116**, 107002 (2016).

[30] D. A. Czaplewski, G. A. Patrizi, G. M. Kraus, J. R. Wendt, C. D. Nordquist, S. L. Wolfley, M. S. Baker, and M. P. de Boer, J. Micromech. Microeng. **19**, 085003 (2009).

[31] F. K. Wilhelm, G. Schön, and A. D. Zaikin, Phys. Rev. Lett. **81**, 1682 (1998).

[32] E. Bustarret, C. Marcenat, P. Achatz, J. Kačmarčik, F. Lévy, A. Huxley, L. Ortéga, E. Bourgeois, X. Blase, D. Débarre, and J. Boulmer, Nature (London) **444**, 465 (2006).

[33] J. Ridderbos, M. Brauns, J. Shen, F. K. de Vries, A. Li, S. Kölling, M. A. Verheijen, A. Brinkman, W. G. van der Wiel, E. P. Bakkers *et al.*, arXiv:1907.05510.

[34] S. Gill, J. Damasco, D. Car, E. Bakkers, and N. Mason, Appl. Phys. Lett. **109**, 233502 (2016).

[35] A. Dienst, M. C. Hoffmann, D. Fausti, J. C. Petersen, S. Pyon, T. Takayama, H. Takagi, and A. Cavalleri, Nat. Photonics **5**, 485 (2011).

[36] H. Thierschmann, E. Mulazimoglu, N. Manca, S. Goswami, T. M. Klapwijk, and A. D. Caviglia, Nat. Commun. **9**, 2276 (2018).

MAJORANA CHAINS WITH A JOSEPHSON JUNCTION FOR SUPERCONDUCTING CIRCUITS

DENIZ STIEGEMANN, ABHIJEET ALASE, AND TOM STACE

1. Fock Space and Fermionic Operators

1.1. **Fock Space.** Let $\mathfrak{h}$ be the Hilbert space for the state of each particle. $\mathfrak{H} = \mathfrak{F}-(\mathfrak{h})$ denotes the fermionic Fock space. We will assume that $\mathfrak{h}$ is of finite dimension N. Then $\dim \mathfrak{H} = 2^N$.

In the case of a tight-binding model, $\mathfrak{h}$ is spanned by an orthonormal basis of position states. For a one-dimensional chain with N sites, we have

$$\mathfrak{h} = \mathbb{C}^N = \operatorname{span}\{|j\rangle : j = 1, \ldots, N\}.$$

The annihilation and creation operators $a(|j\rangle)$, $a^\dagger(|j\rangle)$ for a single-particle state $|j\rangle$ are abbreviated as a_j, $a_j^\dagger$. They are operators on $\mathfrak{H}$, acting on anti-symmetrised states, and they satisfy the canonical anti-commutation relations

$$\{a_i, a_j\} = 0 = \{a_i^\dagger, a_j^\dagger\},$$
$$\{a_i, a_j^\dagger\} = \langle i|j\rangle\, I = \delta_{ij} I.$$

We will usually drop the identity I, writing $\{a_i, a_j^\dagger\} = \delta_{ij}$ for example.

Number bases are always defined with respect to a particular choice of annihilation and creation operators. We use the following convenient notation for the number basis. Write

$$\boldsymbol{\alpha} = \alpha_1 \cdots \alpha_N \in \{0,1\}^N$$

for a bit-vector of length N. Then we set

$$|\boldsymbol{\alpha}\rangle = |\alpha_1 \cdots \alpha_N\rangle = (a_1^\dagger)^{\alpha_1} \cdots (a_N^\dagger)^{\alpha_N} |\Omega\rangle \tag{1}$$

where $|\Omega\rangle = |0 \cdots 0\rangle$ denotes the vacuum, and it is understood that $(a_j^\dagger)^0 = I$, that is, a particle in the state $|j\rangle$ is created if and only if the j-th bit is set. There is no further normalisation prefactor, see Bratteli–Robinson, Prop. 5.2.2 (2).

Since $a_i^\dagger a_j^\dagger |\boldsymbol{\alpha}\rangle = -a_j^\dagger a_i^\dagger |\boldsymbol{\alpha}\rangle$ for all i, j, $\boldsymbol{\alpha}$, it matters in which order the fermionic particles are created. With Eq. (1) we fix one choice for our notation. If we associate the bit-vector $\boldsymbol{\alpha} = \alpha_1 \cdots \alpha_N$ with the integer $n = (\alpha_N \cdots \alpha_1)_2$ given in binary digits, then we can enumerate the 2^N basis vectors $|\boldsymbol{\alpha}\rangle$, $\boldsymbol{\alpha} \in \{0,1\}^N$, as the states $|F_n\rangle$, $n = 0, \ldots, 2^N - 1$, defined by

$$|F_n\rangle = |F_{(\alpha_N \cdots \alpha_1)_2}\rangle = |\alpha_1 \cdots \alpha_N\rangle\,.$$

The important thing to note here is the reversed order of the digits since we want to use the more sensible convention of starting at zero with the vacuum, so that $|F_0\rangle = |\Omega\rangle$.

2. Conventions for Majorana Operators

There are two common conventions for normalisation when defining the Bogoliubov operators in terms of annihilation and creation operators. We will refer to them as Convention 1 and 2. They occur in the literature as follows.

Convention 1: Bratteli–Robinson (Vol. 2), Ginossar–Grosfeld
Convention 2: Kitaev, Bravyi–Gosset

The corresponding identities are listed in Table 2. For comparison, we also recall some properties of the unaffected annihilation and creation operators in Table 1.

3. Diagonalising a Quadratic Fermionic Hamiltonian

The goal of this subsection is to take a generic Hamiltonian

$$H = \sum_{i,j=1}^{N} (A_{ij} a_i^\dagger a_j + B_{ij} a_i^\dagger a_j^\dagger + C_{ij} a_i a_j + D_{ij} a_i a_j^\dagger) \tag{2}$$

which is quadratic in the Dirac-fermionic creation and annihilation operators $a_i^\dagger$ and a_i, and bring it into the form

$$H = \sum_{i=1}^{N} 2\omega_i b_i^\dagger b_i + cI = \sum_{i=1}^{N} \omega_i (b_i^\dagger b_i - b_i b_i^\dagger) + c'I \tag{3}$$

which is quadratic and 'diagonal' in some new Dirac-fermionic operators b_i, $b_i^\dagger$, called the **diagonal modes**, up to an additive constant proportional to the identity. We will commonly omit such constants.

To proceed, we will assume without loss of generality that H already has the form

$$H = \sum_{i,j=1}^{N} (A_{ij} a_i^\dagger a_j + B_{ij} a_i^\dagger a_j^\dagger + B_{ji}^* a_i a_j - A_{ji} a_i a_j^\dagger) \tag{4}$$

with

$$A = A^\dagger, \quad B = -B^t. \tag{5}$$

Remark 3.1. We can make these assumptions for the following two reasons. First, the fact that H is hermitian implies that

$$A = A^\dagger, \quad B = C^\dagger, \quad D = D^\dagger, \tag{6}$$

which can easily be seen by taking the adjoint of Eq. (2). Second, using the anti-commutation relations, we can calculate that

$$A_{ij} a_i^\dagger a_j + D_{ji} a_j a_i^\dagger = \frac{1}{2}(A_{ij} - D_{ji}) a_i^\dagger a_j - \frac{1}{2}(A_{ij} - D_{ji}) a_j a_i^\dagger + \frac{1}{2}(A_{ij} + D_{ji})\delta_{ij} \tag{7}$$

Note that the terms on the left-hand side *do* occur together in Eq. (2), albeit grouped differently; $A_{ij} a_i^\dagger a_j$ and $D_{ji} a_j a_i^\dagger$ appear in different terms of the summation $\sum_{i,j=1}^{N}$ on the right-hand side of Eq. (2), namely those with the index variables i and j exchanged. The identity Eq. (7) thus shows that we may substitute A and D by matrices A' and D', respectively, according to

$$A' = \frac{1}{2}(A - D^t), \quad D' = \frac{1}{2}(D - A^t)$$

and will only change the overall Hamiltonian by an additive constant, namely the sum over the last term in Eq. (7). This shows that we can just suppose that

$$D = -A^t \tag{8}$$

in Eq. (2). By a related calculation,

$$B_{ij}a_i^\dagger a_j^\dagger + B_{ji}a_j^\dagger a_i^\dagger = \frac{1}{2}(B_{ij} - B_{ji})a_i^\dagger a_j^\dagger - \frac{1}{2}(B_{ij} - B_{ji})a_j^\dagger a_i^\dagger$$

allows us to make the substitution $B' = \frac{1}{2}(B - B^t)$ if need be, to ensure that we can assume

$$B = -B^t. \tag{9}$$

A similar calculation allows us to suppose

$$C = -C^t. \tag{10}$$

In conclusion, combining Eq. (6) with Eq. (8), Eq. (9), and Eq. (10) gives the form Eq. (4) with Eq. (5).

The Hamiltonian Eq. (4) can also be written in the more compact form

$$H = \alpha^\dagger M \alpha = (a^\dagger, a)\begin{pmatrix} A & B \\ -B^* & -A^* \end{pmatrix}\begin{pmatrix} a \\ a^\dagger \end{pmatrix}.$$

The matrix $M \in M_{2N}(\mathbb{C})$ is called the **mode matrix** of H. The key to finding the diagonal form Eq. (3) lies in constructing a particular diagonalisation of M. Any diagonalisation of M will give a formula of the form Eq. (3) with *some* operators b_i, $b_i^\dagger$; the whole point of the following procedure is to ensure that these new 'diagonal modes' also satisfy the canonical anti-commutation relations.

Remark 3.2. It is worth noting at this point that while the mode matrix corresponds to a linear map on the $2N$-dimensional vector space $\mathbb{C}^{2N}$ and the operator vectors $\alpha, \alpha^\dagger$ each have $2N$ entries, the system really only possesses N fermionic degrees of freedom. For a given index i, the operators a_i and $a_i^\dagger$ do not represent different modes, but one operator is the hermitian conjugate of the other. The artificial doubling implicit in the definition of α and $\alpha^\dagger$ will become even more obvious when we investigate the spectrum and eigen-decomposition of M, and it will sometimes seem as if there were twice the number of modes, when this is really just an artifact of the convenient mathematical treatment of the modes. For example, if $\ker(M)$ is 4-dimensional, this corresponds to 2 zero modes.

We define an anti-unitary operator J on $\mathbb{C}^{2N}$ as

$$J\begin{pmatrix} u \\ v \end{pmatrix} = \begin{pmatrix} v^* \\ u^* \end{pmatrix}, \quad u, v \in \mathbb{C}^N.$$

Observe that $\{M, J\} = 0$. As a consequence, if $x \in \mathbb{C}^{2N}$ is an eigenvector of M with eigenvalue ω, then since

$$MJx = -JMx = -\omega Jx,$$

the vector Jx will be an eigenvector of M with eigenvalue $-\omega$ (as an anti-unitary, J has trivial kernel). This means that the non-zero eigenvalues of M come in positive–negative pairs, and therefore also that the kernel of M has even dimension.

Consequently, we can easily construct an orthonormal basis for $\ker(M)^\perp$, the orthogonal complement of the kernel of M in $\mathbb{C}^{2N}$. Set $K = N - \dim\ker(M)/2$.

We take the normalised eigenvectors $x_1, \ldots, x_K$ of the, say, positive eigenvalues $\omega_1, \ldots, \omega_K$ of M. As discussed, $Jx_1, \ldots, Jx_K$ will be the eigenvectors for the remaining non-zero, that is, negative eigenvalues $-\omega_1, \ldots, -\omega_K$. Therefore,

$$\{\omega_1, \ldots, \omega_K, J\omega_1, \ldots, J\omega_K\}$$

is an orthonormal basis for $\ker(M)^\perp$, and conjugation by the unitary matrix

$$T = (\omega_1, \ldots, \omega_K, J\omega_1, \ldots, J\omega_K)$$

brings M into the particular diagonal form

$$\Omega = T^\dagger M T = \mathrm{diag}(\omega_1, \ldots, \omega_K, -\omega_1, \ldots, -\omega_K).$$

4. Coupling a Transmon with Kitaev's Chain

Our toy model Hamiltonian is the linear operator on the Hilbert space

$$\mathcal{H}_{\mathrm{tmon}} \otimes \mathcal{H}_{\mathrm{chain}}$$

defined by

$$\hat{H} = \hat{H}_{\mathrm{tmon}} \otimes \hat{I} + \hat{I} \otimes \hat{H}_{\mathrm{metal}} + \hat{H}_{\mathrm{couple}},$$

where

$$\begin{aligned}
\hat{H}_{\mathrm{tmon}} &= E_C \hat{n}^2 - E_J \cos\hat{\phi}, \\
\hat{H}_{\mathrm{metal}} &= \sum_{j=1}^{N} \Big(-w_j \Big(\hat{a}_j^\dagger \hat{a}_{j+1} + \hat{a}_{j+1}^\dagger \hat{a}_j \Big) - \mu \Big(\hat{a}_j^\dagger \hat{a}_j - \frac{1}{2} \Big) \Big), \\
\hat{H}_{\mathrm{couple}} &= e^{i\hat{\phi}} \otimes \hat{S} + e^{-i\hat{\phi}} \otimes \hat{S}^\dagger, \\
\hat{S} &= \sum_{j=1}^{N} \Delta_j \hat{a}_j \hat{a}_{j+1}, \qquad \hat{S}^\dagger = \sum_{j=1}^{N} \Delta_j \hat{a}_{j+1}^\dagger \hat{a}_j^\dagger,
\end{aligned}$$

and

$$w_j = \begin{cases} w_{\mathrm{junction}} & \text{if } j = J, \\ w & \text{otherwise,} \end{cases}$$

$$\Delta_j = \begin{cases} 0 & \text{if } j = J, \\ \Delta & \text{otherwise.} \end{cases}$$

Here $1 < J < N$; usually we will assume that N is even and set $J = N/2$. The parameter w_{junction} quantifies a possible reduction in the magnitude of electron hopping across the junction compared to w, and Δ_j vanishes at the junction where there is only non-superconducting metal. Also note that $\Delta \in \mathbb{R}$ with our notation.

4.1. The Transmon.

The differential equation (Bloch equation) for the $\psi_{\kappa,b}$ eigenfunctions is $\mathcal{D}\psi = E\psi$, with

$$\begin{aligned}
\mathcal{D}\psi(\phi) &= \big(E_C(-i\partial_\phi - n_x)^2 - E_J \cos(\phi) \big) \psi(\phi) \\
&= \big(E_C(-\partial_\phi^2 + 2in_x\partial_\phi + n_x^2) - E_J \cos(\phi) \big) \psi(\phi)
\end{aligned}$$

and the boundary condition $\psi(-\pi) = e^{2\pi\kappa i}\psi(\pi)$. We will usually assume $n_x = 0$, in which case the differential operator takes the simple form

$$\mathcal{D} = -E_C \partial_\phi^2 - E_J \cos(\phi).$$

This results in real-valued wavefunctions for $\kappa = 0, \frac{1}{2}$, which simplifies certain calculations.

The functions $\psi_{\kappa,b}$ form a overcomplete basis for the infinite-dimensional Hilbert space $\mathcal{H}_{\text{tmon}}$. They are indexed by the Bloch wavenumber $\kappa \in (-\frac{1}{2}, \frac{1}{2}]$ and the band index $b \in \mathbb{N}$. They have energies $E_{\kappa,b}$, so that $H_{\text{tmon}}|\psi_{\kappa,b}\rangle = E_{\kappa,b}|\psi_{\kappa,b}\rangle$. Matrix elements of the $e^{\pm i\hat{\phi}}$ operators with respect to the $\{\psi_{\kappa,b}\}$ basis can be calculated as

$$\begin{aligned}\langle\psi_{\kappa_1,b_1}|e^{\pm i\hat{\phi}}|\psi_{\kappa_2,b_2}\rangle &= \int_{-\infty}^{\infty}\langle\psi_{\kappa_1,b_1}|e^{\pm i\hat{\phi}}|\phi\rangle\langle\phi|\psi_{\kappa_2,b_2}\rangle d\phi \\ &= \int_{-\infty}^{\infty} e^{\pm i\phi}\,\overline{\psi_{\kappa_1,b_1}(\phi)}\psi_{\kappa_2,b_2}(\phi)d\phi.\end{aligned} \tag{11}$$

4.2. **The Kitaev Chain.** A basis for the 2^N-dimensional Hilbert space $\mathcal{H}_{\text{chain}}$ is given by the Fock eigenstates of the operator $\hat{H}_{\text{junction}}(\phi)$, where

$$\hat{H}_{\text{junction}}(\Delta,\phi) = \hat{H}_{\text{metal}} + \sum_{j=1}^{N}\Delta_j\left(e^{i\phi}\hat{a}_j\hat{a}_{j+1} + e^{-i\phi}\hat{a}_{j+1}^\dagger\hat{a}_j^\dagger\right),$$

with a particular choice for Δ and ϕ that we postpone at this point. The eigenstates $\chi_{\vec{\alpha}}$ are indexed by bit vectors $\vec{\alpha} \in \{0,1\}^N$, such that

$$|\chi_{\vec{\alpha}}\rangle = (\hat{c}_1^\dagger)^{\alpha_1}(\hat{c}_2^\dagger)^{\alpha_2}\cdots(\hat{c}_N^\dagger)^{\alpha_N}|\Omega\rangle.$$

Here the $\hat{c}_k^\dagger$, $\hat{c}_k$ and Ω are defined as follows: The $\hat{c}_k^\dagger$, $\hat{c}_k$ are quasi-particle creation and annihilation operators with respect to which the Hamiltonian $\hat{H}_{\text{junction}}(\Delta_0,\phi_0)$ assumes the diagonal form

$$\hat{H}_{\text{junction}}(\Delta,\phi) = \sum_{k=1}^{N}\hbar\omega_k(\hat{c}_k^\dagger\hat{c}_k - \hat{c}_k\hat{c}_k^\dagger) = \sum_{k=1}^{N}2\hbar\omega_k\hat{c}_k^\dagger\hat{c}_k - \sum_{k=1}^{N}\hbar\omega_k.$$

Ω is the state with $\hat{c}_k|\Omega\rangle = 0$ for all $k = 1,\ldots,N$; in other words, $\Omega = \chi_{\vec{0}}$. For $j = 1,\ldots,N$, the energy of the state $\hat{c}_j^\dagger|\Omega\rangle$ is $E_j = 2\hbar\omega_j - \sum_k\hbar\omega_k$, and we will assume that the creation and annihilation operators are ordered from lowest to highest energy of the state $\hat{c}_j^\dagger|\Omega\rangle$. The Kitaev chain has a degenerate ground state space spanned by two orthogonal states, one of which is $|\Omega\rangle$ and the other $\hat{c}_1^\dagger|\Omega\rangle$.

We refrain from explicitly indicating the dependence of Ω and the $\hat{c}_k^\dagger$ and $\hat{c}_k$ on Δ and ϕ since we will later fix particular initial parameter values throughout.

4.3. **The Coupled System.** We assume that up until $t = 0$, the Kitaev chain has evolved to the ground state of the usual Hamiltonian $\hat{H}_{\text{junction}}(\Delta_0,\phi_0 0)$, where Δ_0 takes a material-specific value and $\phi_0 = 0$ as long as the chain can evolve away from any external magnetic fields. We can later change ϕ_0 to simulate different initial conditions.

Our goal is to initialise the system in the state $\psi_{\kappa_0,b_0}\otimes\Omega$, e.g. with $\kappa_0 = b_0 = 0$, and then see how the dynamics develops. Since Ω depends on κ_0 and b_0 through ϕ_0, we implicitly make the physical assumption that up until $t = 0$, the composite yet uncoupled system has developed according to the dynamics of the Hamiltonian

$$\hat{H}_{\text{uncoupled}} = \hat{H}_{\text{tmon}}\otimes\hat{H}_{\text{junction}}(\Delta_0,\phi_0),$$

which leads to the system being in the product state $\psi_{\kappa_0,b_0} \otimes \Omega$ at $t = 0$ when the coupling is switched on.

To study the time evolution $e^{i\hat{H}t/\hbar}|\psi_{\kappa_0,b_0} \otimes \Omega\rangle$ for $t \geq 0$, we have to compute the matrix elements of $\hat{H}$ with respect to the tensor product basis

$$\left\{\psi_{\kappa,b} \otimes \chi_{\vec{\alpha}} \,\middle|\, \kappa \in (-\tfrac{1}{2}, \tfrac{1}{2}],\, b \in \mathbb{N},\, \vec{\alpha} \in \{0,1\}^N\right\}.$$

We get

$$\begin{aligned}\langle \psi_{\kappa_1,b_1} \otimes \chi_{\vec{\alpha}_1}|\hat{H}|\psi_{\kappa_2,b_2} \otimes \chi_{\vec{\alpha}_2}\rangle = {} & \langle \psi_{\kappa_1,b_1}|\hat{H}_{\text{tmon}}|\psi_{\kappa_2,b_2}\rangle \\ & + \langle \chi_{\vec{\alpha}_1}|\hat{H}_{\text{metal}}|\chi_{\vec{\alpha}_2}\rangle \\ & + \langle \psi_{\kappa_1,b_1}|e^{i\hat{\phi}}|\psi_{\kappa_2,b_2}\rangle\langle \chi_{\vec{\alpha}_1}|\hat{S}|\chi_{\vec{\alpha}_2}\rangle \\ & + \langle \psi_{\kappa_1,b_1}|e^{-i\hat{\phi}}|\psi_{\kappa_2,b_2}\rangle\langle \chi_{\vec{\alpha}_1}|\hat{S}^\dagger|\chi_{\vec{\alpha}_2}\rangle.\end{aligned}$$

The first term is simply

$$\langle \psi_{\kappa_1,b_1}|\hat{H}_{\text{tmon}}|\psi_{\kappa_2,b_2}\rangle = E_{\kappa_1,b_1}\delta_{\kappa_1\kappa_2}\delta_{b_1b_2}.$$

The three terms $\langle \chi_{\vec{\alpha}_1}|\hat{H}_{\text{metal}}|\chi_{\vec{\alpha}_2}\rangle$, $\langle \chi_{\vec{\alpha}_1}|\hat{S}|\chi_{\vec{\alpha}_2}\rangle$ and $\langle \chi_{\vec{\alpha}_1}|\hat{S}^\dagger|\chi_{\vec{\alpha}_2}\rangle$ can be computed by rewriting $\hat{H}_{\text{metal}}$ and $\hat{S}$ in terms of the $\hat{c}_k^\dagger$ and $\hat{c}_k$ operators ($k = 1, \ldots, N$). Finally, we can compute the matrix elements of $e^{\pm i\hat{\phi}}$ using Eq. (11).

We summarise all steps necessary to compute $\langle \psi_{\kappa_1,b_1} \otimes \chi_{\vec{\alpha}_1}|\hat{H}|\psi_{\kappa_2,b_2} \otimes \chi_{\vec{\alpha}_2}\rangle$:

1. Diagonalise $\hat{H}_{\text{tmon}}$ to obtain the energies $E_{\kappa,b}$ and the functions $u_{\kappa,b}$ for the relevant values of κ and b.
2. Calculate Δ_0 as well as $\langle \psi_{\kappa_1,b_1}|e^{i\hat{\phi}}|\psi_{\kappa_2,b_2}\rangle$ and $\langle \psi_{\kappa_1,b_1}|e^{-i\hat{\phi}}|\psi_{\kappa_2,b_2}\rangle$ for all relevant κ, b.
3. Bring $\hat{H}_{\text{junction}}(\Delta_0, \phi_0 = 0)$ into diagonal form, so as to express the $\hat{a}_k^\dagger$, $\hat{a}_k$ in terms of the $\hat{c}_k^\dagger$, $\hat{c}_k$ ($k = 1, \ldots, N$).
4. Transform $\hat{H}_{\text{metal}}$, $\hat{S}$ and $\hat{S}^\dagger$ into the $\{\chi_{\vec{\alpha}}\}$ basis.
5. Pick out the relevant $(\vec{\alpha}_1, \vec{\alpha}_2)$ matrix elements of $\hat{H}_{\text{metal}}$, $\hat{S}$ and $\hat{S}^\dagger$ in the $\{\chi_{\vec{\alpha}}\}$ basis.

We speak of 'relevant values of κ and b' since at least on the infinite-dimensional $\mathcal{H}_{\text{tmon}}$, we have to restrict ourselves to a cut-off Hilbert space (in practice a low-energy cutoff and restriction to a certain finite selection of states in the Brillouin zone) in order to perform actual calculations. In comparison, $\mathcal{H}_{\text{chain}}$ is finite-dimensional, but the dimension grows exponentially in N, so that in practice a cutoff might be necessary here as well, restricting the number of indices $\vec{\alpha}$.

4.4. **Calculations.** We choose to compute results in the regime $E_C = E_J = 1$. The bands and eigenfunctions in the low bands for $\kappa = 0, \frac{1}{2}$ are shown in the LCS paper. For now, we choose a basis of four eigenfunctions, corresponding to the two lowest energies each at $\kappa = 0$ and $\kappa = \frac{1}{2}$. In the 4-dimensional subspace $\mathcal{K}$, we order the basis as

$$\psi_{0,0}, \psi_{0,1}, \psi_{\frac{1}{2},0}, \psi_{\frac{1}{2},1}.$$

In this basis, the phase operators $e^{\pm i\hat{\phi}}$ have the matrix representations

$$(e^{+i\hat{\phi}})_{\mathcal{K}} \approx \begin{pmatrix} 0.612 & 0.626\,i & 0 & 0 \\ 0.626\,i & 0.161 & 0 & 0 \\ 0 & 0 & 0.672 & -0.523\,i \\ 0 & 0 & -0.523\,i & -0.166 \end{pmatrix}$$

and $(e^{-i\hat{\phi}})_{\mathcal{K}} = (e^{+i\hat{\phi}})^*_{\mathcal{K}}$, where the star indicates complex conjugation.

Now we set $\Delta_0 = \langle \psi_{\kappa_1,b_1} | e^{\pm i\hat{\phi}} | \psi_{\kappa_2,b_2} \rangle$ and $\phi_0 = 0$ as discussed before, and write down the Hamiltonian $\hat{H}_{\text{junction}}(\Delta_0, \phi_0)$. We can represent it as an operator on Fock space or merely in terms of the creation–annihilation algebra. The second choice is desirable since it does not involve matrices that grow exponentially with the number of sites in the chain.

5. Kitaev's Fermion Chain with Junction

5.1. **The Physical Hamiltonian.** We consider a chain of a total of N sites, with annihilation and creation operators as explained above. The full Hamiltonian of Kitaev's chain with a junction between sites k and $k+1$ is

$$H = \sum_j \Big(-w_j (a_j^\dagger a_{j+1} + a_{j+1}^\dagger a_j) - \mu \Big(a_j^\dagger a_j - \frac{1}{2} \Big) + \Delta_j a_j a_{j+1} + \Delta_j^* a_{j+1}^\dagger a_j^\dagger \Big)$$

and

$$w_j = \begin{cases} tw & \text{if } j = k, \\ w & \text{otherwise,} \end{cases} \qquad \Delta_j = \begin{cases} \Delta & \text{for } j < k, \\ 0 & \text{for } j = k, \\ \Delta e^{i\phi} & \text{for } j > k. \end{cases}$$

Now we define Majorana operators as follows,

$$\begin{aligned} c_{2j-1} &= a_j^\dagger + a_j, \\ c_{2j} &= i(a_j^\dagger - a_j). \end{aligned}$$

Correspondingly, we replace the creation and annihilation operators as follows,

$$\begin{aligned} a_j &= \frac{1}{2}(c_{2j-1} + i c_{2j}), \\ a_j^\dagger &= \frac{1}{2}(c_{2j-1} + i c_{2j}). \end{aligned}$$

The Hamiltonian then takes the form

$$\begin{aligned} H = -\frac{i}{2} \sum_j \mu c_{2j-1} c_{2j} + \frac{i}{2} \sum_{j<k} \big((\Delta - w) c_{2j-1} c_{2j+2} + (\Delta + w) c_{2j} c_{2j+1} \big) \\ + \frac{i}{2} \sum_{j>k} \big((\Delta \cos(\phi) - w) c_{2j-1} c_{2j+2} + (\Delta \cos(\phi) + w) c_{2j} c_{2j+1} \\ + \Delta \sin(\phi) (c_{2j-1} c_{2j+1} - c_{2j} c_{2j+2}) \big) \\ - \frac{i}{2} w_k (c_{2k-1} c_{2k+2} - c_{2k} c_{2k+1}). \end{aligned}$$

Note that when representing the Hamiltonian on the computer, it is most efficient to separate it into three parts, such that

$$H = H_{\text{static}} + \cos(\phi) H_{\cos} + \sin(\phi) H_{\sin},$$

where H_{static}, $H_{\cos}$ and $H_{\sin}$ are independent of ϕ. Note that the terms with prefactors $-w$ and w in the $j > k$ sum above belong to H_{static}.

5.2. **The Phase-Localised Hamiltonian.** To obtain the phase-localised Hamiltonian, we perform a canonical transformation of the annihilation and creation operators. The new operators $\tilde{a}_j, \tilde{a}_j^\dagger$ are unchanged on the $j \leq k$ half of the system, and

$$\begin{aligned}\tilde{a}_j &= e^{i\phi/2} a_j, \\ \tilde{a}_j^\dagger &= e^{-i\phi/2} a_j^\dagger\end{aligned}$$

for $j > k$. The phase-localised Hamiltonian is then

$$\tilde{H} = \sum_j \Big(-w_j (p_j \tilde{a}_j^\dagger \tilde{a}_{j+1} + p_j^* \tilde{a}_{j+1}^\dagger \tilde{a}_j) - \mu \Big(\tilde{a}_j^\dagger \tilde{a}_j - \frac{1}{2} \Big) + \tilde{\Delta}_j \tilde{a}_j \tilde{a}_{j+1} + \tilde{\Delta}_j^* \tilde{a}_{j+1}^\dagger \tilde{a}_j^\dagger \Big),$$

where

$$p_j = \begin{cases} e^{-i\phi/2} & \text{if } j = k, \\ 1 & \text{otherwise,} \end{cases} \qquad \tilde{\Delta}_j = \begin{cases} \Delta & \text{for } j \neq k, \\ 0 & \text{for } j = k. \end{cases}$$

Again we write this Hamiltonian in terms of Majorana operators, so that

$$\begin{aligned}\tilde{H} = \frac{i}{2} \sum_{j \neq k} \big(-\mu \tilde{c}_{2j-1} \tilde{c}_{2j} + (\Delta - w) \tilde{c}_{2j-1} \tilde{c}_{2j+2} + (\Delta + w) \tilde{c}_{2j} \tilde{c}_{2j+1} \big) \\ - \frac{i}{2} w_k \Big(\cos\Big(\frac{\phi}{2}\Big) (\tilde{c}_{2k-1} \tilde{c}_{2k+2} - \tilde{c}_{2k} \tilde{c}_{2k+1}) \\ - \sin\Big(\frac{\phi}{2}\Big) (\tilde{c}_{2k-1} \tilde{c}_{2k+1} + \tilde{c}_{2k} \tilde{c}_{2k+2}) \Big).\end{aligned}$$

Observe that almost the entire Hamiltonian is now independent of ϕ except for the terms at the junction $j = k$.

6. The Covariance Matrix Approach

6.1. **Inner Product Formulas.** Following Bravyi–Gosset, the covariance matrix for a state $|\psi\rangle \in \mathcal{H}$ is the $2N \times 2N$ matrix defined as

$$\Gamma(\psi)_{p,q} = -\frac{i}{2} \langle \psi | c_p c_q - c_q c_p | \psi \rangle. \tag{12}$$

Given two states $|\psi_1\rangle, |\psi_2\rangle \in \mathcal{H}$ with the same parity σ, we can then easily compute the magnitude of the inner product $\langle \psi_1 | \psi_2 \rangle$ as

$$|\langle \psi_1 | \psi_2 \rangle|^2 = \frac{\sigma}{2^N} \operatorname{Pf}\big(\Gamma(\psi_1) + \Gamma(\psi_2) \big).$$

Since we are not interested in the sign of the Pfaffian, $\operatorname{Pf}(A)^2 = \det(A)$, and Pfaffian and determinant have a comparable computational hardness, it is enough to calculate

$$|\langle \psi_1 | \psi_2 \rangle|^2 = \frac{1}{2^N} \sqrt{\big| \det\big(\Gamma(\psi_1) + \Gamma(\psi_2) \big) \big|}.$$

6.2. **Covariance Matrices for Kitaev's Model.** We will change back and forth between Majorana and Dirac fermions because of how the template from Bravyi–Gosset is formulated. The Hamiltonian is given in terms of Majoranas c_p, but the diagonal modes are Dirac fermions b_i, $b_j^\dagger$. They are obtained from the original Majoranas through a canonical unitary transformation, which means that

$$c_k = \sqrt{2}\sum_{i=1}^{N}\big((u_i^*)_k b_i + (u_i)_k b_i^\dagger\big).$$

We calculate

$$c_p c_q - c_q c_p = -2\delta_{pq} + 4\sum_{i,j=1}^{N}\big((u_i^*)_p(u_j^*)_q b_i b_j + (u_i^*)_p(u_j)_q b_i b_j^\dagger \\ + (u_i)_p(u_j^*)_q b_i^\dagger b_j + (u_i)_p(u_j)_q b_i^\dagger b_j^\dagger\big)$$

If $|\psi\rangle$ is any state in Fock space, we want to calculate the covariance matrix of $|\psi\rangle$ with respect to the unchanged operators c_i, $i = 1,\dots,2N$, since they are independent of the phase parameter ϕ of the Hamiltonian. However, $|\psi\rangle$ is given in a simple form with respect to the diagonal modes b_i, $b_j^\dagger$, which are ϕ-dependent. Therefore, we need to convert the covariance matrix expression Eq. (12) into a form where the Majorana operators are expressed in terms of the diagonal modes, in terms of which the state $|\psi\rangle$ will have a simple form.

Writing

$$B_{ij}^{\circ\circ} = \langle\psi|b_i b_j|\psi\rangle, \qquad B_{ij}^{\circ\dagger} = \langle\psi|b_i b_j^\dagger|\psi\rangle,$$
$$B_{ij}^{\dagger\circ} = \langle\psi|b_i^\dagger b_j|\psi\rangle, \qquad B_{ij}^{\dagger\dagger} = \langle\psi|b_i^\dagger b_j^\dagger|\psi\rangle,$$

and

$$V = (u_1,\dots,u_N),$$

we can write

$$\Gamma(|\psi\rangle) = -2i\big((V^*)^t B^{\circ\circ} V^* + (V^*)^t B^{\circ\dagger} V + V^t B^{\dagger\circ} V^* + V^t B^{\dagger\dagger} V\big) \\ - i\big((V^*)^t V + V^t V^*\big).$$

If $|\psi\rangle = (b^\dagger)^{\mathbf{x}}|\Omega\rangle$ for some N-bitstring $\mathbf{x} \in \{0,1\}^N$, that is, ψ is *not* a superposition of different eigenmode configurations, then $B^{\circ\circ} = B^{\dagger\dagger} = 0$ and

$$B^{\circ\dagger} = \mathrm{diag}(\mathbf{x}), \qquad B^{\dagger\circ} = \mathrm{diag}(\mathrm{not}(\mathbf{x})).$$

Note that all calculations so far scale at most quadratically in N, whereas calculations directly on Fock space commonly grow exponentially in N.

There is also a calculation where we calculate $t_2(\phi) = \mathrm{tr}(P_{0,\pi}P_\phi)$. One needs to apply Gram–Schmidt to the four vectors to construct the first projection; this is easy in Fock space. The computation is then straightforward in Fock space. However, this is again very costly. If we want to use covariance matrices, then we need to decompose the entire calculation, including the Gram–Schmidt orthonormalisation, into known inner products between the known states.

7. The Variability of the Low-Energy Subspace

7.1. **Calculating Phase-Dependant Traces.** For the moment we leave unspecified whether we are dealing with the physical or the phase-localised Hamiltonian, and we denote the ϕ-dependent ground state of either of them by $|\Omega_\phi\rangle$. The choice of $|\Omega_\phi\rangle$ and $b_1^\dagger|\Omega_\phi\rangle$ is completely arbitrary within the degenerate ground state subspace of the Hamiltonian, as long as they are orthonormal to each other.

We are going to call the states in the low-energy subspace

$$\begin{aligned}|\alpha_\phi\rangle &= |\Omega_\phi\rangle,\\ |\beta_\phi\rangle &= b_{\phi,1}^\dagger|\Omega_\phi\rangle,\\ |\mu_\phi\rangle &= b_{\phi,2}^\dagger|\Omega_\phi\rangle,\\ |\nu_\phi\rangle &= b_{\phi,1}^\dagger b_{\phi,2}^\dagger|\Omega_\phi\rangle,\end{aligned}$$

To numerically quantify the movement of the low-energy subspace of the Hamiltonian through Fock space as ϕ varies, we consider its projector

$$P_\phi = |\alpha_\phi\rangle\langle\alpha_\phi| + |\beta_\phi\rangle\langle\beta_\phi| + |\mu_\phi\rangle\langle\mu_\phi| + |\nu_\phi\rangle\langle\nu_\phi|.$$

The quantity we want to compute is the trace

$$t(\phi) = \mathrm{tr}(P_0 P_\phi).$$

For the physical Hamiltonian, we have $t(0) = t(2\pi) = 2$, and for the phase-localised Hamiltonian, we have $t(0) = t(4\pi) = 2$. Plugging in expressions for the states, we can calculate

$$t(\phi) = \sum_{x,y\in\{\alpha,\beta,\mu,\nu\}} |\langle x_0|y_\phi\rangle|^2.$$

It follows that $0 \leq t(\phi) \leq 2$ for all ϕ.

The magnitude of the inner products $|\langle x_0|y_\phi\rangle|^2$ can be calculated directly in Fock space, but such calculations are very costly for larger system sizes. Instead we can use the formula from the previous subsection that only requires the covariance matrices of the involved states.

TABLE 1. CAR algebra and common identities.

Canonical anti-commutation relations
$\{a_i(f), a_i(g)\} = 0$
$\{a_i(f), a_i(g)^\dagger\} = \langle f, g\rangle I$
Nilpotence
$a(f)^2 = a^\dagger(f)^2 = 0$
Norm
$\|a(f)\| = \|a^\dagger(f)\| = \|f\|$

TABLE 2. Conversion between Bogoliubov operators and annihilation and creation operators, as well as some basic identities of the Bogoliubov operators, under the two common conventions for normalisation.

Convention 1	Convention 2
From annihilation & creation to Bogoliubov	
$B(f) = \frac{1}{\sqrt{2}}(a(f) + a^\dagger(f))$	$B(f) = a(f) + a^\dagger(f)$
$B(if) = \frac{-i}{\sqrt{2}}(a(f) - a^\dagger(f))$	$B(if) = -i(a(f) - a^\dagger(f))$
From Bogoliubov to annihilation & creation	
$a(f) = \frac{1}{\sqrt{2}}(B(f) + iB(if))$	$a(f) = \frac{1}{2}(B(f) + iB(if))$
$a^\dagger(f) = \frac{1}{\sqrt{2}}(B(f) - iB(if))$	$a^\dagger(f) = \frac{1}{2}(B(f) - iB(if))$
Selfadjointness	
$B(f) = B(f)^\dagger$	
$B(if) = B(if)^\dagger$	
Anti-commutation relations	
$\{B(f), B(g)\} = \mathrm{Re}\langle f, g\rangle$	$\{B(f), B(g)\} = 2\,\mathrm{Re}\langle f, g\rangle$
Involution, and invertibility for $f \neq 0$	
$B(f)^2 = B(if)^2 = \frac{1}{2}\|f\|^2 I$	$B(f)^2 = B(if)^2 = \|f\|^2 I$
$B(f)^{-1} = 2\|f\|^{-2} B(f)$	$B(f)^{-1} = \|f\|^{-2} B(f)$
Norm	
$\|B(f)\| = \frac{1}{\sqrt{2}}\|f\|$	$\|B(f)\| = \|f\|$

Project Narrative: Cluster-State Quantum Error-Correction Based on AdS/CFT Codes

Project Info:

- **Prof. Thomas Stace (PI)**,
  University of Queensland, Brisbane, Australia
- FY18-21 funding: $100,000 /yr

Goals:

- To develop the theory of holographic codes (inspired by AdS/CFT).
- To formulate a description in terms of 'cluster states', which are universal quantum states suitable for hosting quantum processing tasks.
- To compute performance metrics of holographic codes.
- To generalize the construction of holographic codes to more general tensor network codes.

Questions:

- Holographic codes have desirable properties so may have applications in real quantum computing platforms. How well do holographic codes perform relative to other codes?
- The construction of holographic codes lends itself to cluster state construction. How well does a cluster-state model of holographic codes perform?
- Does the holograph code construction generalize to other codes?

Payoff:

- High performance quantum error correcting codes for quantum processing.
- A pathway to construct large codes from elementary codes, with the possibility for code optimization tailored to specific physical architectures.

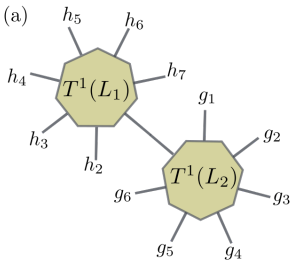

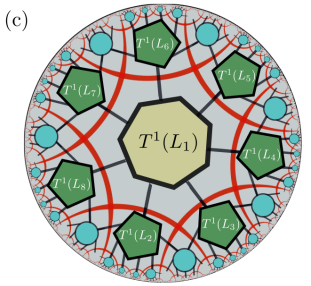

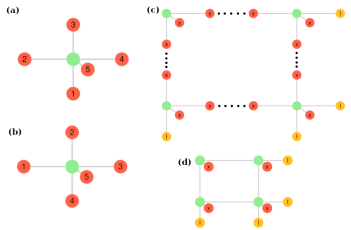

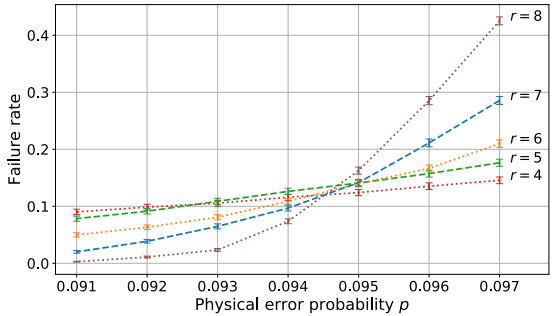

Top left: the elementary connections of holographic and other tensor network codes.
Top right: the structure of holographic tensor network codes.
Bottom left: a planar tensor network code related to the surface code.
Bottom right: performance threshold of a holograph code encoding multiple logical qubits.